TUNABLE POLYMERSOMES: TOWARDS ENZYME REPLACEMENT THERAPY THROUGH THE BLOOD-BRAIN BARRIER

by

Jessica Kelly

A dissertation submitted to the Graduate Faculty of
Auburn University
in partial fulfillment of the
requirements for the Degree of
Doctor of Philosophy

Auburn, Alabama
May 6, 2017

Keywords: Nanomedicine, polymersomes, blood-brain barrier delivery

Approved by

Dr. Mark Byrne, Co-chair, Professor
Dr. Douglas Martin, Co-chair, Professor
Dr. Elizabeth Lipke, committee member, Sanders Associate Professor
Dr. Allan David, committee member, Assistant Professor
Dr. Tatiana Samoylova, committee member, Research Professor

Abstract

Delivery of therapeutics to the brain through non-invasive administration is a difficult task due to the blood-brain barrier (BBB), which prevents the transport of 98% of therapeutics. In GM1 gangliosidosis, patients are missing β-galactosidase (βgal), an enzyme necessary for cellular digestion, with major central nervous system (CNS) manifestation. GM1 gangliosidosis is fatal in infancy with no clinically available treatment. **We have designed and characterized the first nanoparticle-mediated treatment of GM1 gangliosidosis using self-assembled polymersomes for IV enzyme delivery.** When coupled with apolipoprotein, delivery through the BBB and to the lysosome of neural cells will occur, treating patients without invasive surgery.

Poly(ethylene glycol)-b-Poly(lactic acid) (PEG-b-PLA) polymersome formed via passive mixing in water at average polymersome diameters of 237.2 ± 66.5 nm over 150 minutes. Empty polymersomes increased to 4.63 ± 0.01 times their size after lyophilization, showing lack of long-term stability. The use of lyoprotectants, mannitol and inulin, to maintain particle size distribution (PSD) was studied. The incorporation of both molecules was confirmed. Differences in moisture content were found after lyophilization between samples incorporating inulin and mannitol. It was hypothesized that lyoprotectants replaced water, maintaining polymersome structure under stressful processing conditions. The ability to reconstitute polymersome drug delivery carriers without altering size distribution is paramount to the creation of effective and efficient drug delivery systems.

PEG-b-PLA polymersomes also formed via solvent injection with 2 wt%/v mannitol at an average diameter of 145 ± 21 nm. PEG-b-PLA polymersomes encapsulate βgal at 72.0 ± 12.2% efficiency and demonstrate simultaneous encapsulation and ligand attachment at 86.7 ± 11.6% efficiency. Amine-reactive PEG facilitated the attachment of CF 350 Amine, a blue fluorescent ligand, for fluorescent imaging, and apolipoprotein E (ApoE), a target to the low density lipoprotein family of receptors, for BBB delivery, to the polymersome surface. In vitro, PEG-b-PLA polymersomes demonstrate limited release in physiologic environment, pH 7.4, with a burst release upon membrane poration in lysosomal environment, pH 4.8. Cellular studies, using GM1 gangliosidosis-diseased fibroblasts, confirm that βgal-loaded polymersomes increase enzyme activity to normal levels with doses as low as 0.7 mg/cm^2 and the use of an ApoE-tag increases enzyme activity to normal levels with doses as low as 0.175 mg/cm^2. **Results are promising towards the goal of creating the first clinical treatment for GM1 gangliosidosis, using a combination of enzyme replacement therapy and nanotechnology methods to cross the BBB.**

Abbreviation List

AAV: adeno-associated virus/viral

AF: Alexa Fluor

ApoB: Apolipoprotein B

ApoE: Apolipoprotein E

ARSA: arylsulfatase A

ARSB: arylsulfatase B

ATR FT-IR: attenuated total reflection coupled with Fourier transform-infrared spectroscopy

BBB: Blood brain barrier

βgal: β-galactosidase

BSA: Bovine Serum Albumin

CED: Convection-enhanced delivery

CNS: Central Nervous System

CSF: cerebrospinal fluid

DLS: Dynamic Light Scattering

DMSO: dimethyl sulfoxide

DNAse I: deoxyribonuclease I

ERT: enzyme replacement therapy

FDA: Food and Drug Administration

GAG: glycosaminoglycan

GALC: galactocerebrosidase

GLD: globoid cell leukodystrophy

GUSB: β-glucuronidase

HLA: human leukocyte antigen

HSCT: Hematopoietic stem cell transplantation

ICAM-1: Intercellular Adhesion Molecule 1

ICV: Intracerebroventricular

ID: injected dose

IDUA: α- L- iduronidase

IGF II: Insulin-like growth factor II

IgG: Immunoglobulin G

LINCL: late-infantile neuronal ceroid lipofuscinosis

LDLR: low density lipoprotein receptor

LSD: Lysosomal Storage Disease

MAb: monoclonal antibody

MLD: metachromatic leukodystrophy

MLNC: multi-wall lipid-core nanocapsules

MPS: Mucopolysaccharidosis

MW: molecular weight

MWCO: molecular weight cut off

NPD: Niemann-Pick Disease

ORMOSIL: organically modified silica nanoparticles

ORN: olfactory receptor neuron

PBCA: Poly(butyl cyanoacrylate)

PEG: polyethylene glycol

PEG-b-PLA: poly(ethylene glycol)-b-poly(lactic acid)

PLA: poly(lactic acid)

PLGA: poly(d,l-lactide-co-glycolide)

PS: polystyrene

PSD: particle size distribution

RMT: receptor-mediated transcytosis

SDS: sodium lauryl sulfate

SLN: solid lipid nanoparticle

TEM: Transmission electron microscopy

TNF-α: Tumor necrosis factor-α

TPP1: tripeptidyl peptidase 1

vg: vector genome

Table of Contents

Acknowledgements

This research was funded by both the US Department of Education GAANN Graduate Fellowship Program in Biological & Pharmaceutical Engineering Award No. P200A120244 from January 2013 to September 2016. From October 2016 to the end of this dissertation, the Auburn University Research Initiatives in Cancer provided funding. JMK is a GAANN Fellow.

I would like to thank both Dr. Mark Byrne and Dr. Douglas Martin for their continual support and guidance throughout the course of this work and my graduate studies. I would like to thank my committee members, Dr. Elizabeth Lipke, Dr. Allan David, and Dr. Tatiana Samoylova, for their knowledge and time in the critical review and preparation of this manuscript. I would also like to thank Elizabeth Pearce, Ricky Whitener, Liana Wuchte, Stephen DiPasquale, Laura Osorno, Dr. Brandie Brunson, Dr. Ashley Randle, Dr. Heather Gray-Edwards, Amanda Gross, Taylor Voss, Lauren Ellis, Dr. Elise Diffie, and Dr. Emily Graff for their assistance with many aspects of this work. I would also like to thank Alan Hanley, Andre Hansford, Chelsea Harris, David Roe, Matthew Hilliard, Kyle Stone, Morgan Ellis, Nicole Habbit, Pranav Vengsarkar, Richard Cullum, Stephen Montgomery, William Hand, and Alexander Haywood for being an invaluable support system. Personal gratitude is also extended to Dr. Mario Eden, Dr. Brian Thurow, and Dr. Jeffrey Fergus for their guidance unrelated to research.

I would like to thank Allan David in the department of Chemical Engineering in the Samuel Ginn College of Engineering at Auburn University for use of the ZetaSizer

Nano for polymersome diameter analysis. I would like to thank Virginia Davis in the department of Chemical Engineering in the Samuel Ginn College of Engineering at Auburn University for use of ATR FT-IR. I would like to thank Dr. Vitaly Vodyanoy and Oleg Pustovyy in the Department of Anatomy, Physiology, and Pharmacology in the College of Veterinary Medicine at Auburn University for their use of CytoViva hyperspectral microscopy to visualize our polymersomes with both fluorescent ligand attachment and fluorescent encapsulant. I would like to thank Allison Church Bird of the Flow Cytometry and High-Speed Cell Sorting Laboratory in the College of Veterinary Medicine at Auburn University for her assistance in flow cytometry for both fluorescent ligand attachment and fluorescent encapsulant analysis of polymersomes. I would like to thank John Dennis in the College of Veterinary Medicine at Auburn University for use of and assistance with confocal microscopy.

Finally, this would not have been possible without the support of my family. Thank you to my mother, Amy Larsen, for being an incredible listener during the challenging times and an incredible supporter of all of my accomplishments. I would like to thank my siblings, James, Christina, and Mary Larsen and Kyle Kelly, for always trying to understand my research and being as proud of my accomplishments as they are of their own. Thank you to my in-laws, Thomas and Mary Ann Kelly, for their constant support. Finally, I would like to acknowledge and thank my husband and true partner in life, Alexander Kelly.

List of Tables

List of Figures

Chapter 1: Introduction and Motivation

According to the World Health Organization, neurological diseases account for 6.3% of global burden of disease, greater than the burden of HIV/AIDs, respiratory disease, and some cancers [*13*]. This burden is brought on by more than 600 disorders that exhibit symptoms in the central nervous system (CNS) [*14*] including a variety of conditions related to disease, infection, and trauma. In this category, there are a number of fatal and untreatable CNS disorders caused by improper enzyme production, called neuropathic lysosomal storage diseases (LSDs) [*15*]. This work focuses on one specific disease in this category, GM1 gangliosidosis.

Although the global burden of neurological disease is so high, the brain remains untreatable. Because of the central importance of the brain and its limited ability to self-regenerate [*16*], obstacles are in place to prevent potentially harmful substances from entering. The two main methods of protection utilized by organisms with a CNS are the blood-brain barrier (BBB) and the blood-cerebrospinal fluid (blood-CSF) barrier.

The current methods of treatment used to overcome these barriers include intracerebral, intrathecal, and intranasal delivery. Both intracerebral and intrathecal delivery have been extensively explored in the treatment of neuropathic lysosomal storage diseases. Although these treatment methods have demonstrated some success in vivo [*15*], they require invasive procedures that can lead to complications. Although, intranasal delivery is a non-invasive means of delivery to the CNS [*17*], there are many pathways that therapeutic agents can take depending on the size of the particle [*11*, *18*].

Therefore, efficiency of brain penetration may be suboptimal for intranasally delivered drugs.

Each delivery method has demonstrated clinical success, though all have limitations that call for the development of less invasive and more efficient delivery methods through the BBB using the vascular system. Ideal treatment would involve intravenous treatment that could cross the BBB, as the diffusion distance between capillaries and neurons is very small [*10*, *19*], which would allow for universal treatment of the brain via non-invasive means. The use of injectable, targeted carriers could significantly benefit treatment of numerous brain maladies on a large scale. In the past ten years, three categories of nanocarriers have been used in research studies, clinical trials, and some currently FDA- approved pharmaceutical therapies: liposomes, metal based nanoparticles, and polymersomes. Nanocarriers may be paired with moieties for receptor-mediated transport through the BBB, or they may exploit a disruption mechanism that achieves passage into the brain by temporarily compromising the BBB.

The work presented in this dissertation focuses on the creation of polymersomes for delivery of high molecular weight enzymes, due to a multitude of properties that are beneficial over the other delivery options. Polymersomes, or polymeric vesicles, are made up of two or more amphiphilic block copolymers that can encapsulate hydrophilic molecules within their interior and hydrophobic molecules in their membrane [*6*]. Polymersomes, by nature, are tunable on the molecular level [*5*] and may take advantage of many different release mechanisms. They also show increased stability and half-life over liposomes [*4*], which have formulations available on the market.

Approximately 1 in 5,000 to 8,000 children are born annually with a LSD in which one or more enzymes necessary for cellular function are not produced [*20–23*]. Lack of enzyme production leads to the accumulation of substrates that are normally cleaved by these enzymes, the formation of large vacuoles within cells, and ultimate cell death. Current treatment of LSDs has fallen short of treating the brain due to the presence of the BBB, which prevents passage of 98% of small molecule drugs, including enzymes, from the blood into the brain. Patients with neuropathic LSDs, including GM1 gangliosidosis, present with severe CNS degeneration, ataxia, and premature death, with no treatment available on the market and no hope for parents of young diagnosed patients. The brain is a vital organ that controls the majority of functions in the body including movement, communication, decision-making, and emotions. The current standard of care for non-neuropathic LSDs is enzyme replacement therapy (ERT), in which the exogenous enzyme is infused into the patient in IV infusions that can occur as frequently as weekly or as infrequently as bimonthly depending on the enzyme being infused [*24*].

This project combines the knowledge of ERT, which has successfully treated patients with non-neuropathic lysosomal storage diseases, with nanotechnology to develop a carrier that has the potential to facilitate the transport of β-galactosidase (βgal) through the BBB in the treatment of GM1 gangliosidosis. This polymeric carrier may be able to eradicate this one horrific and fatal juvenile disease. Its development also has the potential to create a paradigm shift in the treatment of all CNS disease, providing a

universal platform that can easily be manipulated in its size, therapeutic payload, release mechanisms, and targeting ligands.

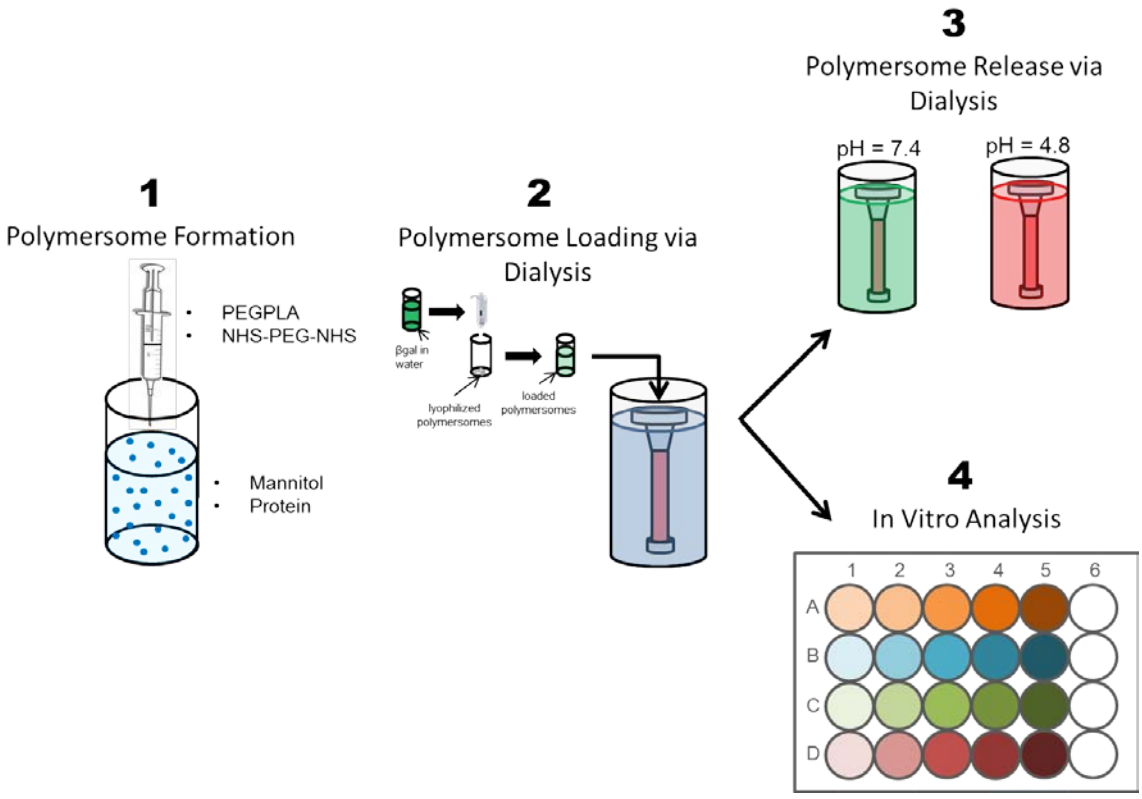

Figure 1.1. Process of PEGPLA polymersome creation and analysis. *This diagram depicts overall nanoparticle creation and analysis in four very basic steps. (1) Polymersomes are formed via the injection method, in which PEGPLA and NHS-PEG(2000)-NHS are dissolved in DMSO prior to injection into water with mannitol and protein (ApoE) for ligand attachment. (2) After formation, lyophilized polymersomes are loaded with 1 mg/ml of βgal in water. Loaded polymersomes are placed into a dialysis device to monitor βgal loading. After polymersomes are loaded, either release in buffer (3) or in a cellular model (4). (3) Release of βgal is monitored in pH 7.4 (physiologic) and pH 4.8 (lysosomal) to mimic in vivo conditions. (4) Four different treatments, free βgal, empty polymersomes, polymersomes loaded with βgal and untagged, as well as polymersomes loaded with βgal and tagged with ApoE are incubated with GM1SV3 cells at five different concentrations. After incubation, cell lysates are monitored for βgal activity.*

Chapter 2: Explored Methods of Treatment for Lysosomal Storage Disease and other Neuropathic Disorders

2.1. Lysosomal Storage Diseases

LSDs are inherited metabolic disorders that impact the biological function of lysosomes. Lysosomes are cytoplasmic, membrane-bound organelles that possess hydrolytic enzymes to break down macromolecules such as glycosaminoglycans (GAGs), oligosaccharides, sphingolipids, and other lipids [*25, 26*]. LSDs result from a mutation in genes that code for lysosomal enzymes, transport proteins, activator proteins, or other gene products necessary for proper lysosomal function [*27*], leading to substrate accumulation, or storage, within the cell. Storage causes lysosomal distension, cellular dysfunction, and, in turn, systemic clinical symptoms [*27*]. In the majority of LSDs, more than one storage compound accumulates within the lysosome causing various symptoms based upon the affected system. For example, in Pompe disease, there is one deficient protein, α-glucosidase, and only one storage product, glycogen. However, in GM1 gangliosidosis, there is one deficient protein, β-galactosidase, but a multitude of storage materials including gangliosides GM1, GA1 and lyso-GM1, oligosaccharides, and keratan sulfate [*28*].

There are over 50 known LSDs, and although individual LSDs are considered orphan diseases, collectively the incidence is high at 1 in 5,000-8,000 live births [*22, 29*]. The heterogeneity in clinical presentation and disease progression makes individual LSDs difficult to identify and diagnose [*26*]. Diagnosis typically occurs post-symptomatically, as patients begin to show developmental decline after a period of normal development.

LSDs affect multiple organs, with central nervous system (CNS) involvement occurring in approximately 50%-70% of diseases in this category [*22*, *30*]. Symptomatology of these so-called "neuropathic" LSDs is often similar, and peripheral disease may remain subclinical because CNS deterioration is more progressive and severe than in peripheral organs. Patients typically present with delayed development, spasticity in movement, hypotonia, macular cherry red spots, and seizures[*26*, *31*]. A summary of the symptoms and incidence of discussed neuropathic LSDs can be found in Table 2.1.

Even more difficult than the diagnosis of LSDs is the prognosis. As these diseases are progressive, the majority of patients with the most severe, or infantile, phenotype will die before they reach school age. LSDs cause high morbidity and early mortality [*30*]. For patients affected with LSDs without CNS involvement, the advent of ERT and substrate reduction therapy have greatly improved the quality of life. However, there are no current treatments available for patients with neuropathic LSDs largely due to the inability of systemic treatments to bypass the BBB, and the inherent risk associated with direct brain injection. Although the BBB and blood-CSF barrier may minimize the number of therapeutic options, even a small increase in enzyme activity in the CNS (to ~10% of normal) can be therapeutic for patients [*27*], with at least 15-20% of normal levels being highly effective [*32*].

It is clear that the BBB presents a large hurdle for delivery of therapeutic molecules for neuropathic LSDs. However, potential treatments that bypass the BBB or even exploit its properties to enhance delivery have shown promise in pre-clinical and clinical trials, including *in vivo* gene therapy and *ex vivo* transfection of cells for

transplantation. Whether a therapeutic approach to treat neuropathic LSDs is direct (targeting neural cells) or indirect (using non-neural cells to produce functional enzyme), its success depends to a large degree on the phenomenon of cross-correction. Most lysosomal enzymes can be secreted by donor cells for uptake by neighboring enzyme-deficient cells such as neurons, and overexpression of the enzyme increases its rate of secretion. For example, *ex vivo* gene therapy is used to overexpress a lysosomal enzyme in patient-derived hematopoietic cells, which are re-injected into the patient, migrate into the CNS and serve as enzyme donors for adjacent neurons. Cells corrected by *ex vivo* gene therapy also have a survival advantage over native cells, allowing them to multiply and further enhance their potency.

The goal of *in vivo* gene therapy is to introduce a functional gene into the patient by direct transfection of neural cells or by targeting other cell types that can cross-correct neural cells. The majority of gene therapy methods circumvent the BBB via intracranial injections, though more recently, others have shown preclinical success using various viral vectors and routes of administration, e.g. intravascular injection, to penetrate the BBB.

Although gene therapy has had success in reaching clinical trials, other treatments are already approved by the United States Food and Drug Administration (FDA) and do not require invasive injections or immunogenic viral vectors. ERT has long been the standard of care for LSDs without CNS involvement and involves intravenous infusions of either the wild-type or a modified version of the deficient enzyme. Through cross-correction of enzyme-deficient cells, storage products are cleared and disease is

ameliorated. ERT has shown clinical success by restoring enzymatic activity to patients, addressing peripheral pathology, and improving quality of life and survival. Perhaps the best-known ERT for a non-neuropathic LSD is Cerezyme®, a recombinant form of glucocerebrosidase for type I Gaucher disease (see www.cerezyme.com). However, no ERT is yet available that can cross the BBB to treat the primary CNS burden in the majority of LSDs. Developments have been made towards the use of intracerebroventricular (ICV)-based ERT, focused on targeting treatment to the CSF in the brain, in an attempt to circumvent the BBB and deliver enzyme. Although this route of administration has the potential to treat the CNS indirectly, it is not without inherent, surgical complications.

Recently, nanoparticle-mediated delivery of enzyme (ERT) or viral vector (gene therapy) has been explored for the treatment of LSDs with CNS involvement. The use of nanoparticles has been shown to prolong drug circulation, allow for extended, sustained levels of therapeutic release, and decrease the frequency of drug administration [*23*] in various disease models. Nanoparticles may aid in the transport of enzymes or viral vectors across the BBB while protecting their function. This dissertation will focus on the promise of ERT in the treatment of LSDs. Other treatment methods are extensively reviewed in Progress in Neurobiology [*33*].

2.1.1. GM1 Gangliosidosis

The LSD of focus for this dissertation is GM1 Gangliosidosis. GM1 gangliosidosis results from a mutation in the GLB1 gene that encodes for the enzyme β-galactosidase [*34–37*]. Because β-galactosidase is not present within the lysosome, GM1

ganglioside is not properly catabolized. GM1 ganglioside, along with keratan sulfate and some specific oligosaccharides which are also substrates of β-galactosidase, are stored in the lysosomes of cells [*37*], causing ultimate apoptosis of neural cells. This alteration in ganglioside catabolism and neural cell death causes severe CNS symptoms (Table 2.1) which are dependent on the intensity of disease.

There are three types of GM1 gangliosidosis. The first is infantile GM1 gangliosidosis, which has an early onset and severely premature death, typically by age 2-4. The second is juvenile GM1 gangliosidosis with an onset in early childhood and a slow disease progression compared to the most severe, infantile form. The third is adult GM1 gangliosidosis, which can present itself anytime during late childhood or early adulthood and is the least severe of the types [*38*]. Ultimately, regardless of the age of onset of disease, GM1 gangliosidosis remains untreatable by any form of therapy.

2.2. Barriers to Intravenous Delivery

Although intravenous treatment shows promise in curing neuropathic LSDs, transport from the blood to the brain remains difficult due to a biological barrier in the capillaries of the brain. Capillaries comprise the microcirculation of the body and may be lined with sinusoidal, fenestrated or continuous endothelium. For example, within skeletal muscle, heart, and dermis, transport is common because the porosity of fenestrated or sinusoidal capillaries in these organs permits passage of many molecules. Continuous endothelium is found within the brain, iris, retina, and inner ear [*1*] and forms a much less permissive barrier for passage of molecules. The continuous brain

endothelium acts as a one-way-barrier, allowing only certain proteins, ions, and amino acids [*39*] to transport through the blood into the brain parenchyma and CSF.

Endothelial cells may be connected by different types of junctions, whose general role is to mediate cell to cell interactions or connect cells to the extracellular matrix [*40*], and may be classified as occluding, anchoring, or communicating [*2*, *41*]. Occluding junctions limit transport and create a semi-permeable membrane, regulating movement of water and solutes[*2*]. Anchoring junctions form connections involving the endothelial cells and cytoskeletal proteins[*40*]. Communicating junctions aid in the transmission of chemical information from cell to cell throughout the vasculature[*42*]. Junctions may be further categorized based on width between endothelial cells and include spot junctions (~100 Angstroms)[*1*] and tight junctions ($\leq$ 12 Angstroms)[*1*]. More data regarding the type of endothelial cells and junctions present in the body is summarized in Table 2.2. At its most basic, the BBB is a capillary endothelial membrane serving as the first level of defense for the brain. To understand the possible mechanisms of drug transport through the BBB, it is important to understand the anatomy of this system with respect to transport regulation. A traditional schematic of the BBB, with endothelial cells and tight junctions, is shown in Figure 2.1.

However, a more comprehensive view (Figure 2.2a) may include at least two additional constituents, pericytes and astrocytes (i.e., astrocyte foot processes) [*10*, *43*, *44*]. Pericytes wrap around endothelial cells, helping to regulate capillary blood flow and growth [*45*] and to provide structural stability [*43*]. Research has shown that pericytes also contribute to the barrier function of the capillary endothelium. In a 2010 study using

pericyte-deficient mouse mutants, it is shown that pericyte-deficiency causes the BBB to become leaky [*46*]. The passage of Evans blue dye into the brain, in correlation with brain capillary diameter and density, was highest among mice with the lowest amount of pericyte-capillary coverage (26%). Transmission electron microscopy imaging showed irregular junctions between endothelial cells in pericyte-deficient mice [*46*], confirming the importance of pericytes to barrier integrity. Astrocytes are characteristically shaped glial cells, taking on different morphologies based upon their location[*10*], that are present in both the brain and the spinal cord[*47*]. Though astrocytes provide structural stability for brain endothelial cells[*43*], their role in BBB function is under debate[*48*].

The luminal surface area of the BBB is 7.4 - 8.4 mm^2 per mm^3 of tissue[*49*], varying with the section of brain being studied. The BBB has an overall surface area of about 20 m^2 per average adult or 1.3 kg brain [*10*, *50*] and is located throughout the majority of the brain vasculature. The BBB restricts transport of molecules through the brain based upon the physiochemical nature of the materials that are attempting to pass through. In order for uninhibited transport through the BBB, a material needs to have a molecular weight less than 400-600 Da and possess less than eight hydrogen bonds [*51*]. Lipid soluble materials can more easily penetrate the BBB [*1*] and carrier-mediated transport is used to facilitate passage of nutrients through the BBB [*51*]. However, since most drugs exceed the physicochemical constraints for unlimited diffusion through the BBB, it constitutes the main limitation for intravenous treatment of the CNS.

Transport of some molecules and ions, like Ca^{2+}, into the brain is facilitated by the blood-CSF barrier. At the choroid plexus, epithelial cells connected by tight junctions

secrete CSF at a rate of 0.3 to 0.4 mL/minute, with a daily production between 280 and 1,000 mL[*52–54*]. Based upon production rates and the volume of CSF in the human brain (100 to 150 mL in adults), the CSF has a turnover rate of around 3.7 to 4 times per day[*55*], allowing waste to be removed from the brain[*56*]. It circulates through the central canal of the spinal cord, the subarachnoid space, and the ventricles of the brain to cushion and protect the CNS[*53*]. Relative to drug delivery to the brain, an important property of CSF is its sink action. Its goal is to minimize the concentration of high molecular weight substances in the brain[*54*], and its effect increases with increasing molecular radii[*55*]. Since CSF ultimately is absorbed into the blood stream, sink action may also hinder the delivery of lipid-insoluble, large molecular weight therapeutic carriers.

2.3. Introduction to Currently Explored Routes of CNS Drug Delivery

Three current routes of drug delivery to the brain are intracerebral, intrathecal, and intranasal. By injection directly into the brain parenchyma, intracerebral administration circumvents the need to traverse the BBB. Intrathecal administration delivers the drug to CSF in the intrathecal space around the spinal cord, while intranasal administration exploits the easy access to the olfactory pathway for brain delivery.

2.3.1. Intracerebral Delivery

Intracerebral delivery of drugs or viral vectors directly into the brain is performed through a craniotomy site in the skull[*17*] and has demonstrated profound success in animal models of LSD[*27, 57–59*]. Disadvantages of intracerebral injection include a lack of distribution throughout the brain[*17*] due to slow diffusion in the brain tissue[*18,*

60]. A modified form of intracerebral administration, convection-enhanced delivery (CED) is thought to improve distribution by maintaining a constant pressure gradient during infusion[*61*]. Even if improvements in drug distribution are achieved, intracerebral injections are invasive and can lead to surgical complications such as hemorrhage, infection, blood clots or leaking of CSF. Therefore, other methods of drug delivery to the brain are needed.

2.3.2. Intrathecal and Intracerebroventricular Delivery

Intrathecal administration often utilizes a pump placed underneath the skin of the abdomen to deliver drug through a catheter inserted in the intrathecal space around the spinal cord. A multitude of studies have been done to test the safety and efficacy of the intrathecal pump[*62–64*] for the delivery of pain medication[*63*]. Medtronic has the only system approved by the United States FDA, and therefore its system was studied in all cases. Of 102 patients reported in 1995, 42 (41%) had between 1 and 5 catheter complications, with the average time to first complication at 19.6 months[*63*]. In a later study of 209 patients, 20 to 25% of the systems experienced catheter related complications, including catheter dislodgement or migration[*64*]. Though invasive surgery accounts for the majority of the complications associated with intrathecal delivery, including infections and leakage of CSF[*62*], the system itself may also cause issues[*63*, *64*]. Intrathecal pumps require regular refill procedures which increase the opportunity for bacterial infections in the subarachnoid space [*62*]. If the refill is done too quickly, an increase in pressure can cause malfunctions, or air may be injected into the system. While intrathecal pumps generally are less invasive than intracerebral methods,

intrathecal delivery does not treat deep brain structures very well[*65*]. A less invasive procedure with more uniform drug distribution is needed for treatment of brain diseases.

Intracerebroventricular treatment involves transport to the brain through the CSF via strategically placed catheters into the lateral ventricle. In some studies this treatment appears efficacious over intravenous treatment, as less antibodies are produced up to 4 weeks post treatment[*66*], suggesting that targeting the CNS may circumvent potentially deleterious immune response against the recombinant protein. In one study it was shown that the half-life of treatment in the blood stream was very small, with enzyme levels in the brain reduced to 10% of normal after 24 hours, demonstrating lack of sustained activity and the necessity of repeated infusions. [*67*].

In one study done on dogs with an LSD [*68*], ICV injections were able to treat the brain, but the treatment regimen remained as burdensome as traditional IV ERT, as infusions were given every other week over a period of 2 to 4 hours. Also, a multitude of complications arose from ICV infusions. Dogs developed surgical complications during ICV implantation, such as meningitis and obstructive hydrocephalus from a foreign body reaction to the catheter. At 4 months, ICV catheters ceased to be used for infusions as they became occluded or migrated into the brain parenchyma.

Together, these studies demonstrate the possibility of using intracerebroventricular ERT to directly target the brain through the CSF, as neurological function and lifespan were improved in all three cases. However, the requirement of invasive surgeries, the complications associated with catheter implantation, and the

necessity of frequent hospital visits are burdens of intracerebroventricular ERT as a treatment method. More studies of intracerebroventricular ERT are needed to correct these issues prior to reaching clinical trials.

2.3.3. Intranasal Delivery

Compared to intracerebral and intrathecal methods of delivery, intranasal administration is noninvasive[*17*] and has the ability to transport drugs quickly to the CNS through the nasal mucosa. The olfactory pathway is made up of olfactory receptor neurons (ORNs) [*18*], which are regenerated by the body about once a month, making the nasal barrier to the CNS naturally leaky[*18*]. Also, ORNs lead to the olfactory bulb and therefore provide direct access to the brain. Molecules with a molecular weight over 400-600 Da have been transported through the nasal mucosa into the brain[*11*]. However, the efficiency of intranasal delivery may be altered by many factors, including head position, volume inhaled, administration technique, and formulation of the therapeutic. Also, with relatively non-specific modes of administration (including drops, flexible tubing and spray [*18*]), intranasally delivered drugs may follow several paths that result in different ultimate destinations (Figure 2.3). For example, an intranasally administered therapeutic may end up in the olfactory bulbs, circulation, lymph nodes, CSF, or a cranial compartment[*11*]. Therefore, efficiency and accuracy of brain delivery may be suboptimal.

2.4. Currently Explored Treatment Methods for Neuropathic LSDs

Explored treatments for LSDs take advantage of some of these routes of administration to bypass the BBB through application of either *ex vivo* or *in vivo* gene

therapy or a form of ERT. As ERT is the method of treatment applied in this dissertation, it will be the method most extensively discussed. Other treatment methods are reviewed more thoroughly elsewhere [*15*].

2.4.1. Ex Vivo Gene Therapy

Initial efforts to treat LSDs relied on allogenic bone marrow transplantation. The requisite human leukocyte antigen (HLA) compatibility of the donor and bone marrow ablation of the recipient produced an undesirable safety profile, and transplantation of unmodified donor marrow had little effect on most neuropathic LSDs. Nevertheless, long-term engraftment of transplanted marrow was demonstrated, an advantage that recently has been merged with enhanced expression and cross-correction of lysosomal enzymes through *ex vivo* cell-mediated gene therapy. Cells are harvested from donors or autologously, transduced by a viral vector to overexpress the therapeutic enzyme, then transplanted into enzyme deficient recipients. Transplanted cells with supraphysiologic enzymatic activity engraft in the host and through cross-correction, deficient cells have a source of the therapeutic enzyme. As with all therapies, many options need to be tested to develop effective *ex vivo* gene therapy, including donor cell type, viral vector, mode of transplantation for transduced cells and immunosuppression regimen. Numerous studies have been conducted to optimize the various parameters in LSDs with CNS deficits, and they have been extensively reviewed elsewhere [*27, 69–77*].

Hematopoietic stem cell transplantation (HSCT) from donor umbilical cord blood or bone marrow is the standard of care for some neuropathic LSDs such as globoid cell leukodystrophy (GLD, also known as Krabbe disease)[*78, 79*], though the treatment is

not curative. Following HSCT, healthy donor cells infiltrate systemic organs and also cross the BBB as microglia precursor cells. Once established, donor cells then secrete the therapeutic enzyme, which is taken up by surrounding cells via cross correction. The premise of *ex vivo* gene therapy in this case is that genetically engineered HSC progeny will overexpress the therapeutic enzyme, facilitating enhanced cross-correction and improved treatment of the CNS. Collection and transduction of the patient's own cells minimizes immune rejection after transplantation, a serious complication in previous bone marrow procedures.

Ex vivo gene therapy is the basis of at least 3 human clinical trials: NCT00004454, completed in 2005, in which lymphocytes were infused to treat Mucopolysaccharidosis (MPS) II; NCT00001234, completed in 2008, in which transduced bone marrow stem cells were used to treat Gaucher disease and Fabry disease[*80*]; and NCT01560182, using HSCs to treat late infantile MLD.

Though the potential of *ex vivo* gene therapy has been demonstrated dramatically by the MLD clinical trial NCT01560182, obstacles to its routine use remain. For example, the success of *ex vivo* gene therapy depends on the efficiency with which systemically delivered donor cells pass through the BBB. While treating neonatal mice intravenously on day 1 or 2 of life clearly allowed donor cells to reach the brain parenchyma [*81*], the mouse BBB is not fully formed in neonates. Most human patients with LSDs are diagnosed months after birth, and though the exact time of BBB closure in infants has been largely debated, the latest studies suggest that it is fully functional prior to birth[*82*]. Despite the success of *ex vivo* gene therapy for the late-infantile form of

MLD, earlier-onset infantile phenotypes are more aggressive and may not be amenable to such an approach. Relative to disease severity, a critical dosing threshold may need to be established for each phenotype. Additionally, if above normal levels of enzyme are required for therapeutic benefit, toxicity must be considered. Exceeding endogenous levels may prove harmful to cells, overwhelm subcellular protein processing and/or initiate an apoptotic cascade. For example, overexpression of galactocerebrosidase (GALC), the defective enzyme in Krabbe disease, is toxic to HSCs [*83*].

2.4.2. In Vivo CNS Directed Gene Therapy

To bypass the BBB and avoid myeloablation often required for transplantation of human stem cells, viral gene transfer vectors can be directly injected into the brain parenchyma via intracranial routes. As with *ex vivo* gene therapy, there are many decisions to be made regarding the ideal viral vector, injection route, immunosuppression regimen, and animal model. Early studies were conducted with retroviral and herpes viral vectors; however, enduring safety concerns compelled the field to develop more innocuous alternatives. The use of adenoviral vectors circumvented many previous concerns, but presented a new set of immunogenicity and toxicity challenges. In the last decade adeno-associated viral (AAV) vectors have emerged as the safest and most effective vehicle of gene delivery, and success in studies utilizing murine models of LSDs has led to the establishment of numerous pre-clinical studies in large animal models and initiation of 5 human clinical trials (Table 2.3). *In vivo* gene therapy treatment can be found in various clinical trials, summarized in Table 2.3 [*80*]. The challenges and recent advances to gene therapy in LSDs have been extensively reviewed

elsewhere in the past 3 years[*69–77*].

An obstacle of *in vivo* gene therapy is the associated immune response with direct injection of viral vectors. Compared to their early viral vector counterparts, the AAV delivery vehicle has little to no acute toxicity[*57*], shown with decreased antibody responses to the various serotypes in mouse models of LSDs [*84*]. However, in large animals immunosuppression may be required to deliver efficacious amounts of enzyme to various LSD models [*85, 86*]. Although immunosuppression can lead to increased effects of *in vivo* gene therapy necessary to treat the manifestations of LSDs, there are a number of associated side effects making co-treatment less than ideal.

A second hurdle of *in vivo* gene therapy is reaching therapeutically beneficial levels of enzyme activity homogenously throughout the entire brain. Studies in both small and large animal models have demonstrated a decrease in enzyme activity as distance from the injection site increases [*87–90*], creating a gradient of therapeutic effect in the brain. The lack of uniform enzyme levels in the brain post-intracranial treatment of AAVs warrants exploration of other therapy methods or delivery routes in the treatment of LSDs.

2.4.3. In Vivo Systemic Gene Therapy

Certain AAV serotypes have recently been found to cross the BBB and thus mitigate the risks associated with intracranial gene therapy, yet preserve the advantages of the vector delivery system. Also, AAVs that cross the BBB can be used to exploit the brain's rich capillary network for homogenous and widespread deliver of therapy. Most

extensively explored for systemic treatment of the CNS is AAV9. AAV9 has been used via intraparenchymal, intravenous, intrathecal, and intrauterine routes of administration, and neuronal transduction efficiency seems to decrease with age. After intravenous injections, neuronal transduction was greater in neonatal animals versus adults, in which AAV9 transduced primarily endothelial cells and astrocytes. It has been hypothesized that this is due to developmental changes in the BBB. Nevertheless, the ability of most lysosomal enzymes to cross-correct neurons makes intravenous injection of AAV9 a promising therapeutic approach [*91*].

Systemic delivery of AAV9 to adult GM1 gangliosidosis mice at $1x10^{11}$ vector genomes (vg) (low dose) or $3x10^{11}$ vg (high dose) resulted in dose dependent partial restoration of β-galactosidase activity in the CNS and overexpression in peripheral organs, namely liver, heart, muscle, and serum. Low dose systemic delivery of AAV9 resulted in minimal reduction of storage product while the high dose significantly reduced ganglioside content and number of reactive astrocytes. There was also a dose dependent improvement on behavioral performance tests and survival, although both doses resulted in significant extension in lifespan compared to untreated GM1 mice[*35*].

Mice with Sandhoff disease (GM2 gangliosidosis) were treated with a single intravenous injection of AAV9 expressing hexosaminidase as either neonates at a dose of $2.5\ x10^{14}$ vg/kg or 6-week-old adults at a dose of $3.5x10^{13}$ vg/kg. Neonatal treatment led to improved motor function and significantly improved survival while adult treatment had little effect on motor activity or life span. Sandhoff mice treated systemically as neonates had elevated hexosaminidase activity, decreased ganglioside storage, and

attenuated neuroinflammation in the brain while adult-treated Sandhoff mice did not. Interestingly, at 43 weeks of age, 8 out of 10 neonatally injected Sandhoff and control mice developed liver (n=7) or lung (n=1) tumors, which were not present in mice that reached endpoint at an earlier age or in adult-treated mice. It is important to note that neonatal treatment of metachromatic leukodystrophy (MLD) mice with a similarly high dose did not generate tumors after a 15-month follow-up. The potential for tumorigenesis after systemic delivery of AAV must be thoroughly investigated before human clinical trials are initiated [*92*].

Though AAV9 is the current gold standard for CNS gene therapy delivered through the vasculature, other serotypes demonstrate equivalent or even superior brain transduction, such as AAVrh8 and AAVrh10[*93*]. More studies with novel capsids will further inform the utility of systemic gene therapy for neuropathic LSDs. Still, some general conclusions can be drawn from the growing body of work with AAV9 in mouse models. AAV9 has the ability to cross the BBB and has achieved persistent and widespread activity of several lysosomal enzymes in the brain of small animal models of LSDs after systemic administration [*94*, *95*]. Enzyme levels in the CNS increased in a dose-dependent manner and the age of treatment proved to be an important factor in efficacy, as it is with other therapeutic approaches. Supraphysiologic levels of enzyme in peripheral organs, namely the liver and spleen, could have toxic effects and furthermore, tumors resulted from intravenous administration of high-dose AAV9 in neonatal Sandhoff mice, revealing a serious safety concern. It remains unclear if the risk of oncogenesis is limited to neonatal administration of very high doses and/or the murine

species. Preclinical studies using larger animal models are needed to analyze the safety and efficacy of systemic gene delivery and to identify the optimal serotype for CNS treatment.

2.4.4. Enzyme Replacement Therapy

2.4.4.1. Introduction and Mechanism of Delivery

Although there is not yet a cure for LSDs, there is a current FDA approved method of treating peripheral organs: ERT. ERT does not correct the innate defect of the storage disease, i.e., patient cells remain incapable of producing the lysosomal enzyme de novo. Rather, ERT delivers a purified, functional enzyme that cross-corrects diseased cells and transiently increases enzymatic activity. ERT has been conducted since the 1970s with purified enzymes [*30*]. However, purified enzymes are not always preferentially delivered into the cells or trafficked to the lysosome, and may require modifications for optimal function. Naturally produced lysosomal enzymes in the endoplasmic reticulum are transported to the Golgi apparatus where a mannose-6-phosphate tag is added for selective transport to lysosomes. Though a portion of the newly synthesized enzymes is transported to the lysosome to recycle appropriate substrates, another fraction is secreted into the extracellular space and is endocytosed by neighboring cells, defining the cross-correction mechanism upon which most lysosomal disease therapies depend [*96, 97*]. The role of mannose-6-phosphate in the brain uptake of lysosomal enzymes through cross-correction is discussed further throughout the literature [*19, 98–100*]. A variety of clinical trials are underway to increase the

application of ERT to neuropathic LSDs, to lessen the financial burden and time commitment of ERT patients, and to improve delivery through the IV route (Table 2.4).

2.4.4.2. Enzyme Modification

Although clinical therapies have shown success in mitigating the symptoms found in peripheral organs, ERT is not yet able to treat the CNS component of LSDs. Protein-based drugs are ineffective due to degradation by proteolytic enzymes, rapid clearance by the kidneys or reticuloendothelial system, immunogenicity [*101*] and/or inability to penetrate the BBB. Methods of enzyme modification have been explored that may allow intravenously-infused enzyme therapeutics to cross the BBB.

With regards to chemical modification of the lysosomal enzymes, deglycosylation has been the most explored as a method of increasing the serum half-life and therefore the therapeutic efficacy of lysosomal enzymes [*102*]. This treatment removes, or inactivates, the terminal sugar moieties found on the enzyme, in turn eliminating carbohydrate-dependent clearance and destroying mannose-6-phosphate recognition [*102*, *103*]. Sly, *et al.*, have extensively explored the treatment of MPS type VII mice with its missing enzyme β- glucuronidase **(**GUSB**)** in various ERT methods[*103–106*]. Histologically, some improvement was shown by quantifiable reduction of lysosomal storage vesicles in neocortical neurons. Secondary elevation of α-galactosidase and β-hexosaminidase was significantly decreased in the brain after delivery of deglycosylated GUSB when compared to control and native GUSB [*103*]. However, deglycosylated GUSB was 38 fold higher in serum than brain, which had an increase in GUSB activity to

only ~ 1.5% above control, or well below the therapeutic window. Therefore, translating this approach to human clinical trials is unlikely.

Late-infantile neuronal ceroid lipofuscinosis (LINCL) is caused by a deficiency in tripeptidyl peptidase 1 (TPP1). Delivery of unmodified TPP1, periodate treated TPP1, and deglycosylated TPP1 via tail vein injections to TPP1 (-/-) mice was explored. Both methods of modification effectively destroyed mannose-6-phosphate recognition. Moderate increase in half-life of modified enzymes occurred from 12 minutes in unmodified to 30 minutes in deglycosylated and 70 minutes in periodate treated TPP1. Unmodified TPP1 at a dose of 2 mg, led to the greatest brain enzyme activity, approximately 10% of normal [*102*]. Contrasting data indicates the sensitivity of different enzymes to different methods of modification due to different transcytosis pathways, highlighting the fact that deglycosylation is not a widely applicable method of enzyme modification allowing passage through the BBB after intravenous infusion.

It is suggested that the addition of polyethylene glycol (PEG) grafts on the enzymes may decrease their uptake by the reticuloendothelial system, allowing them to reach therapeutic levels in areas other than the liver and spleen [*30*]. Covalent attachment of PEG, also called PEGylation, can modify some undesirable properties for delivery of enzymes, while allowing the enzyme to maintain its activity [*107*]. PEG increases the size of the enzyme, its aqueous solubility, and significantly increases serum half-life [*101*]. The PEGylation of enzymes has led to clinically available treatments for some systemic disorders through parenteral administration. First generation PEGylation, involving linear PEG molecules, led to the creation of pegademase (Adagen), for the

treatment of severe combined immunodeficiency, and pegasparase (Oncaspar), for the treatment of various types of leukemia. Second generation PEGylation, attachment of branched PEG molecules, led to greatly increased half-lives of enzymes and therefore increased efficacy. Most success in this area has been in treating hepatitis C through PEGinterferon α2b (PEGIntron), which increases the percentage of patients showing loss of viral DNA by 9% at the lowest explored dose (0.5 μg/kg) and 25% at the highest explored dose (1.5 μg/kg) [*101*].

Although the availability of PEGylated enzymes as therapeutics may suggest this method of treatment as promising, this technique has not yet been reported for lysosomal enzymes. When using the method of PEGylation, it is important to measure enzyme activity, as activity may be reduced due to conjugation of PEG close to potential active sites. PEG molecules need to attach far enough away from the binding site, so as not to impact the binding efficacy of the enzyme to the lysosome. This method of treatment would need to be further explored to allow for applications with lysosomal enzymes when CNS symptoms are involved, as reaching the brain is already difficult without the complication of limiting enzymatic activity.

Most promising for expanding the treatment of ERT to neuropathic LSDs through increased brain delivery is the fusion of lysosomal enzymes with targeting peptides, which involves addition of ligands to the enzyme itself. Fusion of the recombinant enzyme to peptides specific to BBB endothelial cell surface receptors increases cellular uptake. This has been done using (a) derivatives of insulin-like growth factor- II (IGF II) and mannose-6-phosphate to target to the IGF II/mannose-6 phosphate receptor, (b)

receptor associated proteins to target to the low density lipoprotein family of receptors, and (c) monoclonal antibodies to either the human insulin or transferrin receptors [*30*]. These receptors, as well as the leptin receptor, have been shown to aid lysosomal enzyme transport through BBB to treat CNS storage. A detailed review of BBB targeting moieties and how they can be exploited to deliver therapeutics to the brain has been published recently[*108*].

In the past ten years, creation of either fusion proteins or conjugates with lysosomal enzymes has demonstrated variable *in vivo* success in treating CNS manifestations of LSDs. In 2005, bacterial β-galactosidase, used as a model enzyme, was conjugated to a monoclonal antibody to the transferrin receptor via streptavidin-biotin linkage. This chemically modified enzyme was injected in the jugular vein of BALB/c mice at doses of 150 and 50 µg. Conjugated enzymes showed a 10-fold improvement in brain uptake of both high and low dosed mice when compared to unconjugated enzyme and the capillary depletion technique showed that greater than 90% of the conjugated enzyme was passing through the capillary membrane to reach the brain parenchyma[*109*]. Although the enzyme explored in the previous study was bacterial, it demonstrated that an enzyme conjugate could retain function and be delivered through the BBB. Isolating receptors specific to brain capillary endothelial cells may be difficult, but early data suggested that this method of enzyme delivery could make noninvasive brain delivery possible.

Recently, research done by Pardridge *et. al.* has employed a more conventional fusion peptide approach to treat MPS IIIA, also known as Sanfilippo syndrome type A,

through the creation of a sulfamidase fusion protein targeting the human insulin receptor. Affinity to the human insulin receptor and activity of sulfamidase were maintained by the fusion protein. After a 6 hour incubation with MPS IIIA fibroblasts, the fusion protein was located in the lysosomal compartment and caused a dose dependent reduction in lysosomal GAGs. Radioactively labeled IgG-sulfamidase fusion protein was injected intravenously into one male Rhesus monkey at a dose of 19 µg/kg. High amounts of fusion protein were found in the total brain homogenate 140 minutes after injection, with the majority found in the post vascular supernatant indicating passage through the BBB. The fusion protein had a brain uptake of ~ 0.8 % injected dose (ID)/100 g brain [*110*]. The authors determined that a much higher dose of fusion protein, 3 mg/kg, should be sufficient to increase brain sulfamidase activity to endogenous levels. However, the behavior of the fusion protein at higher concentrations and higher doses is unknown. Increasing doses will change the rate of clearance and uptake, potentially leading to toxic effects.

To increase brain enzyme activity of intravenously infused human α- L-iduronidase (IDUA), the missing enzyme in MPS I, a fusion protein of IDUA and an antibody to the human insulin receptor was created. Purified fusion protein had a specific activity comparable to that of recombinant IDUA. The fused enzyme was taken up into lysosomes and decreased GAG accumulation by 70% in MPS I fibroblasts. Co-localization of antibodies to the fusion protein and lysosomes suggested effective trafficking of the enzyme. After intravenous injection of 957 µCi of iodine tagged fusion protein in a Rhesus monkey, the monoclonal antibody fusion protein was detectible in

small quantities (~1% of ID /100 g) in cerebrum gray and white matter as well as cerebellum gray and white matter [*111*]. In both the liver and spleen ~12% ID/100 g was detected, with fusion protein also found in larger quantities than the brain in lung, kidney, heart, and fat. Fusion of targeting molecules in this manner allows for maintenance of enzymatic activity, proven by MPS I fibroblast experiments. However, limited enzyme activity in the brain suggests that targeting the insulin receptor is not be the best option for delivering IDUA across the BBB, although it may aid in treatment of peripheral disease.

In the past three years, the attachment of apolipoproteins to enzymes has been shown to facilitate transport of intravenously injected enzymes through the BBB and into the brain. Apolipoproteins bind to receptors in the low density lipoprotein receptor family, which facilitate transport of their payload to the lysosome[*112*, *113*]. Fusion of proteins to the C terminus of IDUA was determined to not interfere with the activity, folding, or processing of the enzyme. Therefore, in order to evaluate the effectiveness of the fusion protein, liver-specific IDUA-ApoE constructs were injected in to the tail vein of MPSI mice for hepatocyte-mediated delivery into the circulation. Plasma IDUA activity reached 55 to 112 fold of normal levels 2 days post injection, and brains of injected mice exhibited 10-30 fold higher IDUA levels than when treated with an IDUA-Myc control. The IDUA-ApoE fusion protein localized to neurons and reduced GAG storage in the brain of MPSI treated mice. IDUA-ApoE was visualized in the abluminal side of the BBB-forming capillary endothelial cells, suggesting that astrocyte end-feet and/or pericytes are involved in the uptake of the transcytosed fusion protein. Co-

localization of IDUA-ApoE and neurons was observed [*114*]. Though IDUA-ApoE had clearly increased brain delivery compared to an IDUA-Myc control, brain activity was only 5% of normal IDUA activity. Further studies demonstrating the possibility of long term hepatic production of enzyme and its effect on symptom progression would provide more insight on the efficacy of IDUA-ApoE fusion proteins to treat children with MPSI.

TPP1-ApoE fusion proteins were created to treat CNS involvement in LINCL. When the ApoE-receptor binding sequence was inserted at the N-terminus, between the signal sequence and pro-domain of TPP1, the fusion protein was not expressed. An attempt to then fuse ApoE to the C-terminus of the pre-proprotein resulted in an expressed but inactive form of TPP1. Since the engineered fusion proteins interfered with TPP1 folding or processing, a peptide that can act in trans to mediate delivery of TPP1 was evaluated. Intravenous co-injection of peptide K16ApoE and TPP1 into LINCL mice resulted in ~800% of wild-type levels of TPP1 in the brain, compared to only ~20% with TPP1 alone. ApoE mediated delivery of TPP1 reached neurons, and the protein reduced storage material in these cells. Delivery of TPP1 and ApoE also improved sensory motor function and significantly prolonged lifespan compared to untreated and TPP-only treated LINCL mice. Efficacy of brain delivery was comparable when K16ApoE was premixed with TPP1 or injected either immediately prior to or after TPP1 administration. The functional half-life of K16ApoE was found to be ~20 minutes, suggesting that K16ApoE may transiently open the BBB. This study highlights an efficient and effective “mix and inject” strategy that does not necessitate the creation of fusion proteins [*115*].

To evaluate modification of arylsulfatase A (ARSA) for better CNS distribution for MLD, constructs were created with ARSA fused to human immunodeficiency virus TAT protein (Tat), an Angiopep peptide (Ang-2), the receptor-binding domains of human apolipoprotein B (ApoB), and apolipoprotein E (ApoE). ARSA-ApoE, but none of the other constructs, prolonged the ARSA serum half-life by 2-fold when injected intravenously into ARSA knock out mice. Furthermore, brain levels of ARSA-ApoE were increased 54% over wild-type levels. When endogenously expressed ApoE was controlled for in ApoE-knockout mice, treatment with ARSA-ApoE resulted in further increased brain levels to 62% higher than that of wild-type ARSA due to the lack of competition for receptor binding. The ARSA-ApoE construct was functional and cleared 1.7-fold more sulfatide storage from the brain and kidney than wild-type ARSA [*116*].

These studies demonstrate the ability of ApoE to mediate delivery through the BBB, increasing enzymatic activity and decreasing storage in the brain when IDUA and ARSA enzymes were delivered intravenously. However, 5% of normal activity (as in the case of IDUA) may not be sufficient to reverse storage occurring in neural cells of MPSI patients [*114*]. Also, not all enzymes maintained function upon ApoE fusion, and fusion proteins will not be applicable for the treatment of all neuropathic LSDs. The co-injection of K16ApoE with TPP1 led to high TPP1 brain activity and may be more widely applicable for treatment of neuropathic LSDs, as it may not cause losses of activity. It is important to note that this treatment method does not directly target the brain.

2.4.4.3. Clinical Therapies

In 1991, The first FDA approved ERT product became available to treat Gaucher disease, a non-neurologic LSD [*26*]. Now, there are six LSDs in which ERT has been used as a form of clinical treatment: Gaucher's disease in 1991, Fabry disease in 2003, Hurler disease in 2003, MPS VI in 2005, and most recently Hunter and Pompe disease[*24*, *27*, *117–119*]. It is important to note that all of the LSDs stated have little to no CNS involvement. The most successful example of ERT involves Gaucher's disease, a deficiency of glucocerebrosidase causing accumulation of sphingolipids and glucosylceramide. The first enzyme product for treatment was alglucerase, licensed approximately 20 years ago. Alglucerase was subsequently replaced with a recombinant version, imiglucerase [*117*], removing algucerase from the market[*24*]. Table 2.5 lists ERT drugs available to treat the systemic symptoms of patients with specific, non-neurologic LSDs.

Although historically ERT has demonstrated therapeutic success, no ERT available on the market has shown transport through the BBB. The efficacy of clinical ERT is limited in its ability to correct both bone and brain manifestations [*99*], which are present in the majority of LSDs. However, current research shows the possibility of enhancing CNS access using either intracerebroventricular injection or implanted intrathecal delivery system to transport the enzyme through the CSF [*26*]. With this route of administration comes risk of infection and fibrosis with long term catheter implantation [*120*].

Despite FDA approval for some LSDs, ERT does not come without burden to the patient, the medical system, and society. The life-long requirement of weekly to monthly infusions of ERT is of substantial encumbrance to the patient [*26*]. For example, imiglucerase as a treatment for Gaucher's disease requires approximately 3 treatments a week administered over 1 to 2 hours per treatment. Treatment with velaglucerase alfa can decrease injection frequency to once every other week with 1 hour infusions[*24*]. Additionally, long-term injection of enzymes may lead to immune responses and over-time, limited efficacy of the treatment or even anaphylaxis. Along with the physical burden of routine infusions, the expense to the patient can be prohibitive, with an annual cost of approximately $318,000 per 70 kg patient [*32*]. Expansion of ERT to treat the CNS is expected to come with the same patient burdens, while allowing for increase in life span of patients with brain involvement. Although this treatment regimen is not ideal, currently ERT is the most viable treatment for LSDs.

With the Orphan Drug Act of 1983, 22% of drugs treating orphan diseases and only 19% of drugs treating other diseases are approved in the clinical trial process [*121*]. The first protein replacement therapy approved under the orphan drug act was to treat LSDs [*122*], probably due to the fact that one of the three spaces in which these types of drugs have had the most success involves pediatrics. As of November 2011, the probability of approval for ERTs that reach clinical trials is 88% [*121*]. Also, biologic drugs have an overall approval rate much higher than small molecule drugs, at 32% versus 13% [*122*]. These high rates of approval should be encouraging to researchers looking toward ERT as a treatment for neuropathic LSDs. Because of these statements,

the goal of this project was to extend the use of ERT to the brain through the application of nanoparticles.

2.5. Nanoparticle Mediated CNS Drug Delivery

2.5.1. Introduction

The development of nanotechnology may allow for passage of enzyme and vector through the BBB in the treatment of the CNS. Nanotechnology involves materials less than 100 nm in size that may be able to interact with and stimulate systems on the molecular level[*123*]. Nanotechnology may also be able to overcome the disadvantages of ERT and gene therapy, as both can stimulate immune responses and can lead to high costs to patients[*32*].

Nanoparticles can provide protection of the therapeutic from biological activity, namely degradation. They also facilitate attachment of tissue specific targets and their large surface area to volume ratio allows for high therapeutic payloads. The small size of nanoparticles has been shown to improve cellular uptake, with 100 nm poly(d,l-lactide-co-glycolide) (PLGA) particles showing 2.5 fold greater uptake than 1 μm particles and 6-fold greater uptake than 10 μm particles in the Caco-2 cell line, with the increase in uptake becoming 15-250 fold greater using an in situ intestinal loop model in rats [*124*].The release of the therapeutic payload of nanoparticles can be controlled through various means including, but not limited to, pH degradation of particles [*6, 125*], cleavable peptides attached to the therapeutic [*126*], and diffusion through the carrier wall [*124*]. A multitude of nanoparticles have been explored in drug delivery to the brain including liposomes, polymersomes, and metal nanoparticles[*108*].

The most widely explored nanoparticle for delivering therapeutics through the BBB is the PEGylated immunoliposome, a lipid based vesicle conjugated with PEG (to increase stability and decrease protein adhesion) and monoclonal antibodies (to target endothelial cell receptors), with the transferrin receptor being the most common target [*127–129*]. Their use as protein and non-viral gene carriers to cross the BBB has been extensively reviewed elsewhere [*129–132*].

Although various options are available, the only nanoparticle system yet shown to cross the BBB without the attachment of specific targeting ligands is a polymeric based system. Poly(butyl cyanoacrylate) (PBCA) nanoparticles coated with polysorbate 80 are thought to function through adsorption of apolipoproteins and endocytosis [*123*]. Recently, nanoparticles have begun to be explored as vector and enzyme delivery vehicles for their ability to protect biological therapeutics from degradation and control their release, limiting associated toxicity [*124*]. Before first applying a nanomedicine to GM1 Gangliosidosis, it is important to understand the mechanism of cellular uptake of intravenously injected nanoparticles.

2.5.2. Overcoming Barriers

Although there is not yet an available treatment for LSDs with CNS involvement, ERT and gene therapy methods have shown successes both in clinical and pre-clinical settings, with potential towards reaching the brain. Remember, the BBB poses a difficult barrier to overcome by conventional treatments. The endothelial cells in the brain hinder delivery of small molecule drugs due to their tight intercellular junctions, low pinocytic potential, and expression of efflux transporters [*133*]. Before being able to transport

therapeutics through the BBB, it is important to understand the possible methods of transport and the biology behind them.

Conceptually, the BBB may be overcome by disrupting barrier integrity or by exploiting physiological properties already in place for transport of essential molecules into the brain. In general, small molecules enter the brain through carrier-mediated or active efflux transport, while large molecules access the brain by receptor-mediated transport [*134*]. Through receptor-mediated transcytosis (RMT), proteins on the surface of endothelial cells are used to internalize important molecules[*135*], which are then distributed into the brain parenchyma. Ideally, these proteins would be brain endothelium specific. To take advantage of RMT, a drug or carrier needs to be attached to a ligand specific for a receptor protein on the surface of the cell[*136*].

To execute the regulatory function of the BBB, transporters are already in place to deliver essential molecules to the brain. As such, transporter systems exist for amino acids, glucose, monocarboxylic acids, amines, hexoses, thyroid hormones, purine bases, nucleosides, peptides, insulin, growth hormone, and low density lipoprotein[*17*, *51*, *137*]. While many common blood constituents have natural mechanisms for brain uptake (Table) and may themselves function as targeting ligands, physiological properties should be considered carefully before choosing an effector molecule for RMT. For example, transferrin is the second most abundant protein in serum, with a concentration of 3 mg/mL[*138*] and a half-life of around 8 days[*138*]. Due to its high concentration, this transmembrane glycoprotein may saturate the transferrin receptor[*139*] to effectively block (or heavily dilute) attachment of a therapeutic or carrier. Insulin has a short serum

half-life and may induce hypoglycemia[*139*], dismissing its use as a targeting attachment. Similar to the molecules discussed above, insulin-like growth factors and immunoglobulin G may produce undesired side effects if they are introduced at supraphysiologic concentrations. Other receptors on endothelial cells of the BBB may not transcytose molecules, rendering them ineffective for direct delivery to the brain parenchyma. The neonatal Fc receptor (for antibody binding) only regulates transport from the brain into the blood and the scavenger receptor, class B only facilitates endocytosis, as nutrients transported by this receptor are used up within endothelial cells[*134*, *140*]. If the scavenger receptor were chosen for brain delivery, a method of exocytosis from endothelial cells would also be required.

While natural ligands of the BBB may be inappropriate for RMT for a variety of reasons, the receptors for these molecules are likely to be better targets and have shown success in transferring particles through the BBB[*141–143*] (Table 2.6). Currently under investigation as brain delivery targets are receptors for insulin[*51, 137–140, 144*], transferrin[*51*, *137*, *138*, *140*], insulin-like growth factor[*134*, *140*], leptin[*138*, *140*], lipoprotein[*114*, *137–140*, *145*], and diphtheria toxin[*137*]. For example, peptidomimetic monoclonal antibodies (MAbs)[*131*] or short peptides [*138*] were used to bind to transferrin and insulin receptors for BBB transport[*131*],also known as a “Trojan horse” strategy. However, because transferrin receptors are enriched throughout the brain vasculature[*44*, *128*], and in the liver and spleen[*129*], they do not specifically target the brain. In a study using the transferrin receptor in mice, therapeutic concentrations were increased within the brain, but increased in higher concentration within other organs, like

the spleen and liver, showing off-targeting[*128*]. This effect may cause harm with therapeutic delivered to undesirable tissues. Studies using transferrin receptor transport across the BBB have only been done in animals, as there are no humanized transferrin antibodies established to target the transferrin receptor[*139*]. In contrast, a humanized antibody to the insulin receptor has been engineered to cross the BBB in human brain capillaries in vitro[*139, 142*].

Most recently, BBB binding domains of ApoE and ApoB have been shown to bind to the low density lipoprotein receptor (LDLR) family and transcytose through the BBB when attached to enzymes in mucopolysaccharidosis (MPS) mice[*114, 145*]. The LDLR family includes LDLR- related protein 1, which has a higher brain permeability than transferrin[*114*] over a five minute time span in both cortical and subcortical regions of the brain[*146*]. In MPS I cell lines that overexpress LDLR-related protein 1, transport of the therapeutic enzyme through an in vitro BBB model was mediated using a derivate of the binding domain of ApoE. In the same study, an ApoE binding domain-enzyme complex was administered intravenously to MPS I mice. After harvesting the brain and depleting it of capillaries, 10-30 fold increases of enzyme activity were measured, demonstrating that large amounts of enzyme had penetrated into the parenchyma and were not solely confined to the brain vasculature[*114*] . Another study in MPSIII mice showed that the conjugation of a domain of ApoB leads to 10-15% higher enzyme activity than untagged control, with enzyme localized to neurons and astrocytes[*145*]. The LDLR family has been shown to facilitate transport to the abluminal side of the

BBB, activating neurons and glia cells[*145*]. Thus, apolipoproteins hold promise for wide distribution of therapeutics throughout brain tissue.

In addition to targeting constituents of the brain endothelium for transcytosis, the BBB may also be overcome if the integrity of the cell barrier is compromised, as occurs naturally in certain diseases such as cancer [*44*]. Perhaps the most common method of inducing BBB disruption synthetically is through the use of an osmotic diuretic drug, commonly called a hyperosmotic solution[*44*]. An osmotic diuretic causes endothelial cells to lose intracellular fluid and shrink[*55*]. As shown in Figure 2.2b, as endothelial cells shrink, the tight junctions between them widen[*9*], allowing therapeutic agents of greater than 400-600 Da to traverse the BBB. It is believed that tight junctions increase in radius from 7-12 Angstroms in an intact BBB to ~200 Angstroms in the disrupted barrier[*147*], a transient effect[*139*, *147*] that can last up to 2 hours[*55*]. In general, proteins or particles in the bloodstream smaller than 200 Angstroms should gain access to the CNS[*134*, *139*], allowing for the transport of therapeutic-loaded nanoparticles.

Drugs used as disrupting agents include mannitol and arabinose[*9*, *147–149*], injected at a concentration of 1.4 moles per liter and at 1.6 moles per kilogram, respectively[*55*, *147*]. Some procedures are fairly invasive, such as carotid injection or placement of an intra-arterial catheter, requiring general anesthesia before administration[*139*, *147*, *149*]. However, mannitol is given through less invasive intravenous methods. Mannitol, an osmotic diuretic drug, disrupts the BBB through the shrinking of endothelial cells and the stretching of tight junctions in a transient effect [*139*, *147*] that can last up to 2 hours[*55*, *108*]. BBB disruption methods have shown

long-term health effects including seizures, brain damage, loss of cognitive function, vascular damage, astrogliosis, and chronic neuropathic changes[*44*, *55*, *114*, *134*, *148*]. Like receptors expressed in multiple tissues, BBB disruption with an osmotic diuretic is not a brain-specific delivery method. Therefore, mannitol or other agents could affect the entire body, and potential side effects of multi-organ therapeutic delivery should be carefully considered and evaluated in preclinical experiments. Experimental procedures for analyzing BBB integrity, including Evans blue staining, albumin immunohistochemistry, and dynamic magnetic resonance imaging, can be found elsewhere[*149*].

2.5.3. Potential Carriers for Use in Intravenous Delivery

Though the methods of drug delivery to the brain discussed above have had some success in clinical trials and as approved treatments, safer, more uniform and more effective approaches are essential for optimal therapy of CNS disorders. With the use of targeted carriers and cell-specific ligands, intravenous delivery through the BBB may become a clinical reality. When choosing a novel carrier for brain delivery via the vascular system, it is important to consider size, stability, and therapeutic and targeting payloads.

Liposomes are made up of an amphiphilic phospholipid bilayer, similar to a cell membrane[*129*], that creates a spherical carrier (Figure 4) with a typical diameter between 100 and 300 nanometers[*150*]. Although liposomes are extremely biocompatible, they may not persist in the blood stream for a sufficient amount of time to reach the brain. Therefore, most liposomes incorporate a polymer stabilizer conjugated

on the surface of the liposome in order to increase circulation time[*12*, *127*, *129*, *151*, *152*]. Without the presence of polymers, liposomes tend to aggregate in the blood, decreasing their stability[*129*, *153*]. However, in the presence of a polymer, steric hindrance may occur due to the length of the ligands, negatively affecting targeting[*127*].

With respect to brain delivery through the vascular system, liposome studies take advantage of the increased half-life that comes with conjugating PEG on the surface, also known as PEGylation. Receptor specific moieties can be attached to either the distal end of the PEG strand or directly to the surface of the liposome[*129*]. PEGylated, targeted liposomes may attach a multitude of BBB receptors, of which transferrin is the most common[*127*, *128*]. The first in vivo study with PEGylated liposomes used a MAb, OX26, to the rat transferrin receptor[*127*]. This study proved that PEG reduces the clearance rate of unconjugated liposomes 66 fold and that the introduction of OX26 led to rat brain uptake of 0.03% of the injected dose per gram compared to free daunomycin and non-conjugated liposomes which displayed a maximum brain uptake less than 0.01% of the injected dose per gram[*127*]. A study published by Ko, *et al*., 2009, used PEGylated liposomes targeting the transferrin receptor to deliver a polyethylenimine polyplex of oligodeoxynucleotides, comparing distribution of targeted and nontargeted liposomes in mice [*128*]. Brain accumulation increased by only ~0.33%, compared to spleen accumulation that increased by close to 100%[*128*], showing that the transferrin receptor may not only be present in the brain microvasculature. The spleen has a leaky endothelium, which could also be contributing to the increased accumulation. However, brain accumulation was measurable, meaning facilitated transport occurred. Early studies

note the presence of the transferrin receptor in rapidly dividing cells [*154*], as well as erythroid cells and placental tissue [*155*]. However, the transferrin receptor appears to be found on all nucleated cells of the body, with different levels of expression based upon the cells' need for iron [*156*].The limiting factor with PEGylated liposomes is the low payload for targeting moieties of approximately 30 antibodies for an 85 nm diameter liposome[*127*]. A unique study by Lindqvist and coworkers used PEGylated liposomes to deliver a peptide derivative drug model with ligands to target glutathione, although this receptor is not present on the BBB, because of its high levels in leaky cancerous cells [*12*, *157*]. Although using a ligand specific to glutathione may not provide intravenous treatment for all brain maladies, it may provide a viable, noninvasive treatment for brain cancer using nanocarriers, where leaky vasculature is present. From the first in vivo study in 1996, the amount of injected dose per gram of brain tissue from liposome delivery has increased, showing progress in the field. Table 2.7 lists a more comprehensive, but not all inclusive, summary of liposome research with brain delivery in the past ten years.

Though metal nanoparticles may be immunogenic or toxic, leading to accidental cell death[*48*], they have many advantages and are clearly effective in proof-of-concept experiments, some of which are discussed below. Metal nanoparticles can take on many different shapes and sizes, between 1 and 100 nm in diameter, based upon which particle is used as a carrier. Some currently used nanoparticulate carriers are gold, silver, and iron oxide. The small size and high surface area to volume ratio of nanoparticles allows for a high therapeutic payload and the integration of contrast agents[*158*]. In one study, an average of 1335 Daunomycin molecules per 15 nm gold nanoparticle was reported- a

much larger payload than typically found in liposomes[*126*, *159*]. Like liposomes, metal nanoparticles have short half-lives in the blood stream, and, therefore, many are conjugated with a polymer for stabilization purposes[*160–162*]. Studies with chitosan-based and gold-based nanoparticles generally have utilized RMT for delivery. However, some gold-based nanoparticle studies and the majority of iron oxide-based studies take advantage of the magnetic properties of the metals for barrier disruption and targeting[*161–163*]. In a study published by Chertok, *et al*., 2011, magnetic iron oxide particles with polymeric stabilizer strands were injected into a carotid artery of a glioma-bearing rat[*163*]. After targeting with a magnetic field, the activity of a reporter enzyme (*lacZ*) increased by 400% in brain tissue compared to the same complex without magnetic targeting[*163*]. A later study used MRI-guided, focused ultrasound to disrupt the rat BBB and found a 336% increase in uptake of gold nanoparticles in the disrupted hemisphere versus the undisrupted hemisphere[*162*]. The gold nanoparticles were found to be present in both the brain parenchyma and perivascular spaces[*162*]. Table 2.8 highlights additional exciting work involving nanoparticle delivery to the brain.

Polymersomes, or polymeric vesicles, are made up of two or more block copolymers comprising at least one hydrophilic and one hydrophobic polymer. Because of their amphiphilic nature, polymersomes can encapsulate hydrophilic molecules within their interior and hydrophobic molecules in their membrane[*6*]. Block copolymers will self-assemble into a multitude of different structures based upon their hydrophilic mass fraction and the overall molecular weight[*4*]. Figure 2.4 shows the potential size of polymersomes compared to metal nanoparticles and liposomes, illustrating polymersome

properties that relate to its dimension. The size of the membrane and interior of the vesicle increases with increasing molecular weight[*164*]. A hydrophilic mass fraction greater than 45% leads to undesirable structures, including micelles, rods, and spheres, while a hydrophilic fraction between 25 to 40% by mass will form vesicles, extrapolated using PEG as a hydrophilic block[*4*]. A broad size range of polymeric vesicles is possible, with one study reporting polymersomes between 70 nm and 50 μm[*165*]. Polymersomes, by nature, are tunable on the molecular level[*5*] and may take advantage of many different release mechanisms. They can be responsive to pH, temperature, redox-potential, light, hydrogen bonding, electrostatic force, magnetic field, ionic strength, concentration of glucose, and other external stimuli[*6, 166*]. Hydrophilic and hydrophobic polymers already FDA-approved for use in humans[*3*] (Table 2.9) are being considered for polymersome synthesis[*4, 6*], including polylactide (PLA), which is biodegradable[*165*]. As with other carriers and drug delivery systems[*129*], PEG may be used to increase the stability of polymersomes and decrease uptake by the reticuloendothelial system due to its resistance to protein adsorption and cell adhesion[*6*].

Studies are being conducted with a multitude of polymeric components with different release mechanisms[*167–171*]. The majority of these studies provide proof of concept to establish polymersomes as viable drug delivery vehicles. With respect to brain delivery, many studies are using biodegradable polymersomes that have a pH sensitive release. When a model therapeutic peptide (NC-1900) was encapsulated in biodegradable polymersomes (PEG-polycaprolactone) conjugated with the targeting moiety, OX26, an optimized payload of 34 targeting antibodies produced a maximum distribution of around

0.14% injected dose per gram rat brain[*172*]. Another study by the same group found that targeting the transferrin receptor increased brain uptake of PEG-poly(ε-caprolactone) by 2.3 to 2.8 fold in rat brains after tail vein injection, proving the utility of OX26 for brain delivery using polymersomes [*173*]. A 2012 study highlighted the use of unique ligands for GM1 ganglioside and prion protein[*174*], finding the GM1-binding peptide G23 to be most effective, with a maximum distribution of 0.10% injected dose per gram rat brain in the cerebellum when conjugated to a polybutadiene-b-PEG polymersome. Also, hybrid technologies are under development, such as the delivery of gold nanoparticles loaded with a therapeutic via polymersomes, which provide increased stability and minimal surface adhesion of proteins [*175*]. A summary of polymersome-based strategies for brain delivery is presented in Table 2.10.

2.5.4. CNS-Directed Delivery of Enzymes via Nanoparticles

The ultimate goal of nanoparticle-mediated ERT is to improve the distribution of enzyme to the brain of LSD patients without invasive surgeries. An initial step on the path to human clinical application is demonstration of feasibility and efficacy. To that end, arylsulfatase B (ARSB) was coated onto the surface of PBCA nanoparticles in a proof-of-concept study towards the treatment of MPS VI. ARSB is already clinically available for MPS VI patients as Naglazyme, but after IV administration free enzymes are rapidly cleared from circulation and are unable to cross the BBB. PBCA nanoparticles were formed over 2.5 hours of stirring, filtered through 40-100 μm membranes to remove aggregates, and protected during lyophilization with 3% mannitol. Lyophilized PBCA nanoparticles were rehydrated using aqueous solution with varying concentration of

ARSB, 1 – 3 mg/mL. Rehydration led to monolayer adsorption of ARSB onto the surface of PBCA nanoparticles, found by fitting data to the Langmuir adsorption model. Various pH conditions were studied to obtain a negative surface charge for maximum enzyme binding (pI= 7.5). Although pH had an effect on adsorption of ARSB, the concentration of ARSB used in initial rehydration had the largest effect. Increased loading capacity was found with increasing concentration of ARSB, although the loading efficiency was decreased. The maximum loading capacity was 67 µg ARSB/mg nanoparticle surface at a pH of 6.3. The release of ARSB was studied in both serum and tris buffer, with 30 and 32% of ARSB desorbed after 60 minutes respectively [*176*]. ARSB activity appears to have been measured after rehydration and release, demonstrating enzyme function, but values were not reported. This study showed stable monolayer adsorption of enzyme on the surface of polymeric particles in 10% serum, which could lead to a viable therapeutic option, if ARSB activity is maintained, for brain delivery using the right targeting moieties.

ASM was functionalized to the surface of both polystyrene (PS) and PLGA polymer nanocarriers as a model treatment for Niemann-Pick Disease (NPD) type B. Garnacho, *et al.*, enhanced the uptake of ASM in the lung with an antibody specific to Intercellular Adhesion Molecule 1 (ICAM-1). ICAM-1 mediates adhesion of fibrinogen and leukocytes to inflammation sites, and therefore may be a viable target due to pronounced inflammatory responses in LSD patients[*23*]. Both anti-ICAM carriers and immunoglobulin G (IgG) (control) carriers were injected into C57BL/6 mice, a common laboratory mouse. Real-time fluorescence imaging showed attachment of anti-

ICAM/ASM carriers to lung endothelium within 5 minutes after injection and their location indicated that these nanoparticulate carriers withstood shear stresses up to 50 dynes/cm^2. Neither of the injected carriers showed elevated albumin uptake by the lung indicating no pathological signs of edema or injury to lung tissue, though elevated albumin was detected after injection of TNF-α as a control to mimic an inflammatory response. Staining showed the co-localization of anti-ICAM/ASM carriers with pulmonary endothelial cells, with no uptake of the IgG/ASM control. After 30 minutes, uptake of ASM in the lung was enhanced from 6.5 ± 0.6% ID per gram of lung with free enzyme injection to 50.7 ± 5.6% ID per gram of lung for the anti-ICAM/ASM polymeric nanocarrier. Although specific ASM activity in the lung was not directly measured, approximately 60% of the anti-ICAM/ASM polymeric nanocarrier injected was found in the lung[*177*]. Although there is not CNS involvement in this LSD, this study provides insight on the possibility of enzyme targeting to specific areas of the body through appropriate ligand attachments. Further work is needed to study the maintenance of enzyme activity upon attachment and the application of this treatment towards neurologic manifestations of disease.

Mayer, *et al.*, created multi-wall lipid-core nanocapsules (MLNC) with the goal of enhancing delivery of α-L-iduronidase to organs, thereby reducing the necessary dosage from conventional ERT in the treatment of MPSI. MLNCs were functionalized with laronidase, a commercially available ERT of α-L-iduronidase, with the location of attachment unclear. Multiple formulations were studied, but enzyme activity was maintained with one specific formulation, L_1-$MLNC_1$, with 0.05% chitosan and 11

μg/mL laronidase used during MLNC formation. In an MTT assay using L_1-$MLNC_1$, 90% of MPSI fibroblasts were viable with nanoparticle concentrations lower than 0.232 μg/mL and 100% of fibroblasts were viable with nanoparticle concentrations lower than 0.0232 μg/mL. The nanoparticle formulation was not taken in to the cell via standard receptor-mediated endocytosis (mannose-6-phosphate receptor), leaving the specific cellular uptake mechanism unknown. Studies in MPSI mice indicated that L_1-$MLNC_1$ injection led to higher enzyme activity in all organs compared to injection of free laronidase. However, no enzyme activity was found in the CNS with either method of treatment[*178*]. The possibility of ligand attachment was not discussed, although this may help the enzyme cross the BBB and treat the CNS with the added protection of the MLNCs.

Though these studies do not demonstrate direct delivery of lysosomal enzymes to the brain, they demonstrate maintenance of lysosomal enzymatic activity when attached to nanoparticles. Nanoparticles provide a platform that can both protect lysosomal enzyme and provide attachment of ligands targeted to the brain. More work with nanoparticles in appropriate LSD models needs to be done to determine the efficacy of enzyme delivery to treat neuropathic LSDs.

2.5.5. CNS-directed delivery of vectors via nanoparticles

The majority of gene therapy approaches to treat LSDs with CNS involvement have made use of viral vectors. However, approaches using nanoparticles may be able to deliver non-viral vectors, DNA plasmids, potentially eliminating the associated toxicity and immunogenicity of viral vectors. Non-viral gene therapy tends to have low

transfection efficiency, which may be overcome by the coupling of nanoparticles[*179*]. It is important to note that nanoparticles may have their own safety and immunogenicity concerns that need to be further explored. Fabry disease is a viable candidate for gene therapy approaches, as there is only a single gene defect. Although ERT is currently available for Fabry disease, it presents many of the burdens previously discussed. Fabry disease is a LSD without CNS involvement, but information from this study is applicable to future possible treatments. Solid lipid nanoparticle(SLN)-based nonviral vectors were encapsulated with either pCMS-EGFP, a plasmid encoding EGFP, or pR-m10α-Gal A, a plasmid encoding α-galactosidase A. Neither plasmid affected the particle size distribution of the SLNs. The SLNs bound DNA, shown by agarose gel electrophoresis, and protected it from deoxyribonuclease I (DNase I). *In vitro* studies showed that plasmid DNA was released in the presence of a 1% sodium lauryl sulfate (SDS) solution. Human hepatocellular carcinoma cells (Hep G2) were treated with SLNs carrying pR-m10-α-Gal A plasmid, as the liver has been used as an enzyme production factory, secreting enzyme into the blood stream to be taken up by other organs. After 72 hours, Hep G2 cells showed a 12 fold increase in enzyme activity with the most effective formulation studied (dextran-protamine-DNA-SLN) compared to untreated cells[*32*]. The use of SLNs to deliver plasmid DNA provides a promising platform towards the treatment of LSDs with CNS involvement.

Del Pozo-Rodriquez, *et al.*, also employed SLN-DNA technology to deliver pCMS-EGFP as an attempt to overcome barriers associated with viral vectors, including immunogenicity, oncogenicity, and small therapeutic payload, as well as improve

systemic delivery of plasmid DNA, which is rapidly eliminated from circulation after IV injection. SLN-DNA vectors with a mean size of 276 nm were shown to protect DNA from DNAse I and had no effect on viability of HEK293 kidney cells. Between 14% and 40% of treated cells expressed EGFP after 24 hours and 7 days respectively. Mice treated with SLN-DNA showed EGFP expression in 100% of representative hepatic and splenic sections on day 3 post-injection and 17% of these same sections on day 7 post-injection[*179*]. The goal of both the previous and current studies was to create an "enzyme factory" of the liver for enzyme secretion into the circulation. However, this strategy would not allow for sufficient treatment of the brain, as free enzyme in the blood has not been shown to cross the BBB at physiologically relevant concentrations. Thus, alternative methods, like enzyme modification, are needed to aid in transcytosis of enzyme produced by systemic organs. The use of brain-specific targeting ligands, discussed elsewhere[*108*], attached to SLNs may aid in delivery directly to the brain.

Organically modified silica nanoparticles (ORMOSIL) of 30 nm were surface functionalized with amino groups to bind pEGFP-n2, an EGFP peptide. The use of silica nanoparticles may be beneficial, as they can be degraded through the biochemical decomposition of the silicon-carbon bond and therefore will be cleared from the body. pEGFP-n2 was attached to ORMOSIL nanoparticles at a loading concentration of 135 µg of DNA per 10^{14} nanoparticles, while protecting the plasmid DNA from degradation. ORMOSIL nanoparticles with pEGFP-n2 were given to mice via intracerebral administration, with injection into ventral midbrain and lateral ventricle. EGFP expression was documented around the left ventricle, in the dorsal lateral and

intermediate / medial septal nuclei, in the dorsal striatum lateral to the injected ventricle, in the cingulate and motor cortices, and in pyramidal neurons of the CA3 hippocampal region. The expression from this non-viral vector either equaled or exceeded a similar treatment using a herpes simplex viral vector. No toxicity was found to be caused by ORMOSIL nanoparticles up to 4 weeks after transfection [*180*]. Thus, though nanoparticle-based gene therapy is in the early phases of development for clinical application to neuropathic LSDs, the platform for further refinement has been established.

2.5.6. Major Points Related to Nanoparticle-Mediated Delivery to treat LSDs

A major obstacle towards nanoparticle-mediated delivery to treat neuropathic LSDs is the lack of information available about the long term toxicity of these nanomaterials. Though studies presented here did address the toxicity of nanoparticles for neuropathic LSDs to some degree [*177*, *178*], formal toxicity studies have not been reported in most cases. Some nanoparticles do not degrade and may be present in the cell for an extended period of time, causing unknown harm. Secondly, an effective dose of nanoparticles must be determined. Though clinical doses for ERT are known for many non-neuropathic LSDs, doses of novel nanoparticles that target the brain may bear little relation to IV doses of unencapsulated enzymes for systemic disease. Further studies need to be conducted varying dosing regimens of nanoparticle-mediated delivery in both small and large animal models before this will be well understood.

Recent studies have pointed towards the possibility of advancing ERT to the CNS through the application of nanoparticulate carriers. The maintenance of enzyme activity

after attachment has been shown[*176*, *178*] and the option of targeting to enhance specific organ uptake has been investigated[*177*]. Although the components for a delivery vehicle that may be beneficial in treating the brain have been demonstrated, the discovery of a carrier that crosses the BBB in the treatment of LSDs with CNS involvement has yet to be shown.

2.6. Figures and Tables

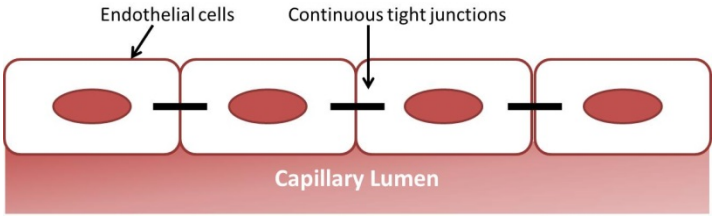

Figure 2.1. Continuous endothelial cells connected by tight junctions lining the capillary walls in the BBB. *This schematic can apply to epithelial tissues and endothelial cells throughout all capillaries. However the presence of continuous tight junctions is limited to the brain and intestine endothelium.*

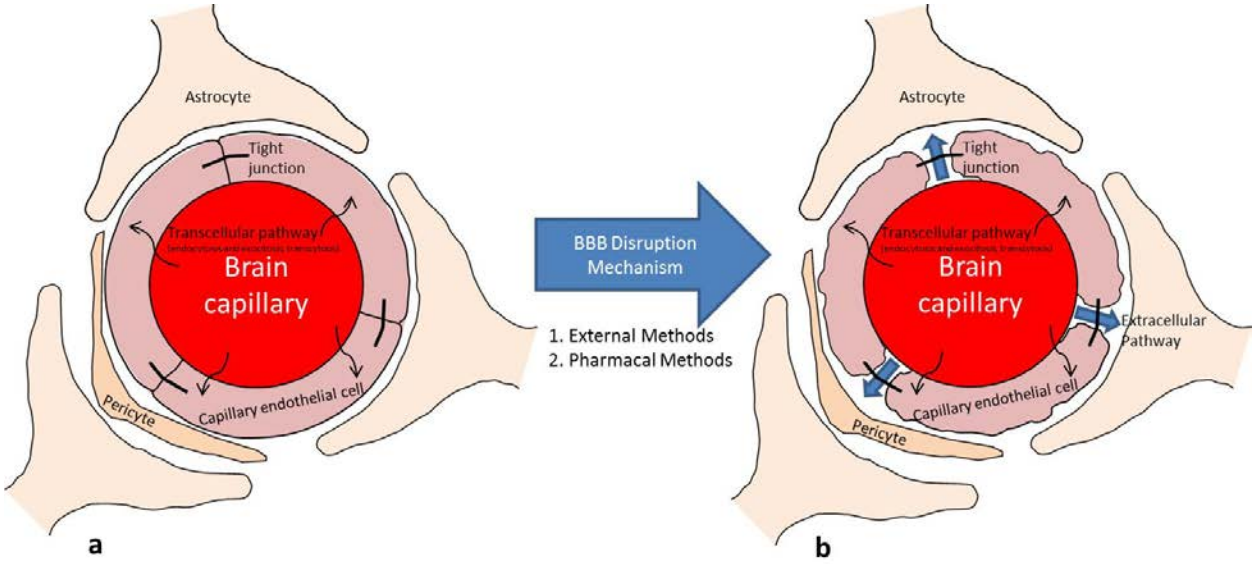

Figure 2.2. The effect of osmotic diuretics on BBB constituents and possible transport through the BBB. *(a) An intact BBB, with astrocytes, endothelial cells, and tight junctions. The black arrows show the only known method of transport for therapeutics greater than 400-600 kDa (transcytosis). (b) The BBB after disruption, with shrunken endothelial cells and widened tight junctions* [*9*]*. Arrows denote the possible path of both transcytosis and passive transport (bigger arrows). Figure adapted from* [*9*, *10*]

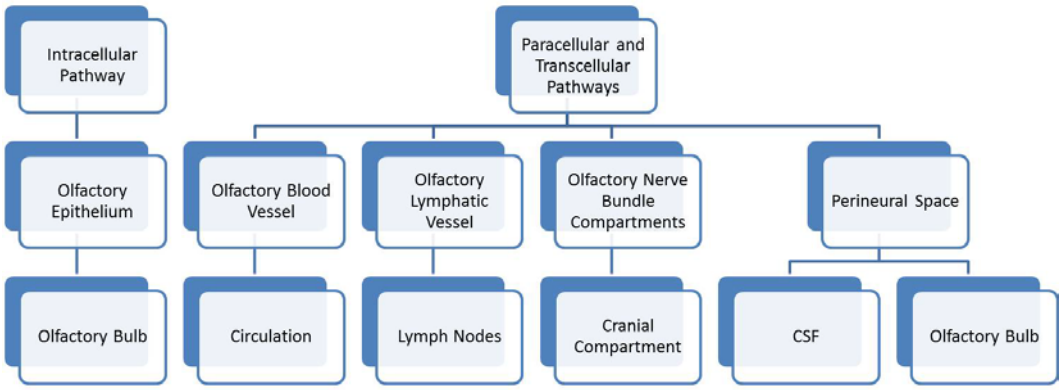

Figure 2.3. Possible Pathways of Therapeutics to the CNS Through Intranasal Administration. *If a molecule takes the intracellular pathway, it will end up in the olfactory bulb and ultimately the brain. However, the other two pathways, paracellular(intracellular space between cells) and transcellular(through cell membrane) do not guarantee transport into the brain. Adapted from* [*11*].

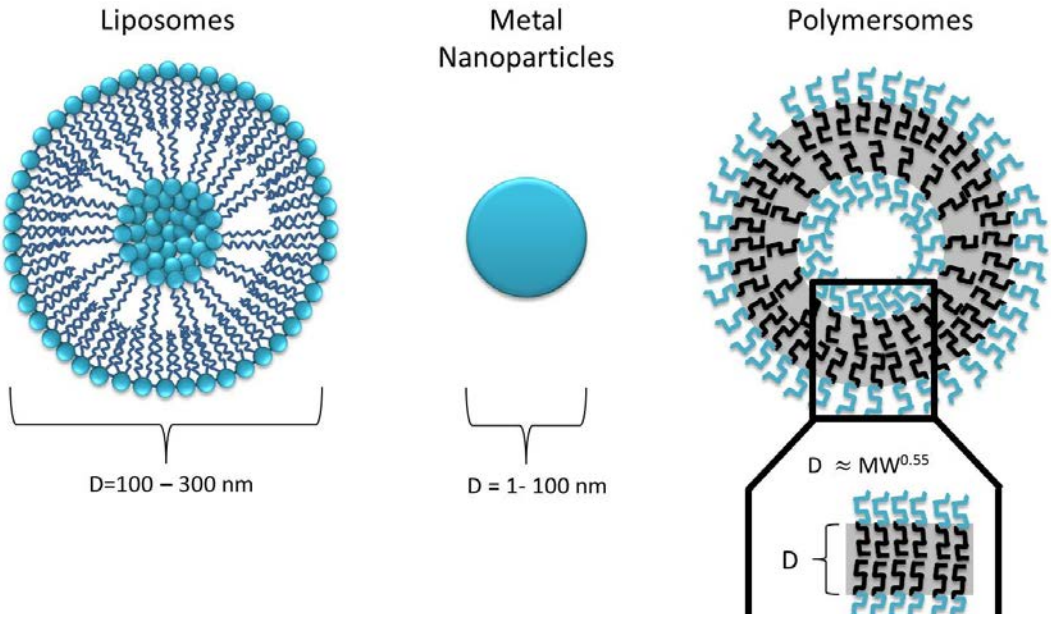

Figure 2.4. Schematic representing structure and size of liposomes, metal nanoparticles, and polymersomes. *Liposomes are made up of phospholipid bilayers and typically have a diameter (D) between 100 – 300 nm, although they can be slightly smaller. Metallic nanoparticles used in brain delivery fall between 1 and 100 nm in diameter. Polymersome membranes are made up of hydrophilic (blue) and hydrophobic (black) copolymers. The thickness of particle hydrophobic membrane is based on molecular weight (MW) of the components. Adapted from* [*4, 12*]

Table 2.1. Description of some major lysosomal storage disorders. Information regarding the deficient enzyme, primary symptoms, incidence, and age of onset are presented in a systematic fashion. Note that this is only a small portion of the total (>50) lysosomal storage diseases. *Bold and italicized font denotes clinically approved enzyme replacement therapy available

Lysosomal Storage Disease	Deficient Protein	Primary Symptoms	Incidence	Age of Onset	Sources
Tay-Sachs Disease	Hexosaminidase A	cherry red macular spots, delayed development, spasticity, CNS involvement	Race dependent	Infantile - adult	[*26*, *118*]
Sandhoff Disease (GM2 Gangliosidosis)	Hexosaminidase A and hexosaminidase B	cherry red macular spots, delayed development, spasticity, CNS involvement	1 in 422,000	Infantile - adult	[*26*, *118*, *181*]
GM1 Gangliosidosis	β-galactosidase	cherry red macular spots, hypotonia, delayed development, hepatosplenomegaly, CNS involvement	1 in 100,000 to 1 in 200,000	Infantile- adult	[*26*, *118*]
Fabry's Disease*	α-galactosidase	CNS involvement, pain in hands and feet, impaired sweating, dark red rashes, starburst pattern on cornea	1 in 117,000	5 years – adult	[*27*]
Pompe Disease (Glycogen Storage Disease Type II)*	α- glucosidase	Cardiac complications progression to heart failure, respiratory difficulties, spontaneous movements	1 in 40,000	Infantile-adult	[*27*, *118*, *182*]
Gaucher disease*	β- glucosidase	CNS involvement, organomegaly, bone anomalies, cytopenia	1 in 57,000	6 months - adolescence	[*22*, *27*]
Hurler Syndrome (MPS I)*	α-L-Iduronidase	Short stature, large head with bulging frontal bones, cardiomyopathy, speech delay	1 in 175,000	childhood	[*118*, *183*]
Hunter Syndrome (MPS II)*	α-L-Iduronidase	Respiratory tract infections, diarrhea, skin lesions, umbilical and inguinal hernia	1 in 166,000	Infancy - adolescence	[*118*, *184*]
Marteaux-Lamy (MPS VI)*	Arylsulfatase B (ARSB)	Elevated urinary GAGs, short stature, cardiac valve disease, reduced pulmonary functions, corneal clouding, degenerative joint disease	1 in 1,505,160	Infancy - adolescence	[*118*, *185*]
Niemann-Pick Disease (NPD)	Acid sphingomyelinase (ASM)	Type A: neurodegenerative, death by 3 years; Type B: disease of liver, spleen, and lung, little CNS involvement; Type C: enlarged liver and spleen, jaundice, neurological symptoms between ages 4-10, death by 20 years	1 in 100,000 to 200,000	Infantile - adulthood	[*186*]
Mucopolysaccharidosis VII (MPSVII)	β-glucuronidase (GUS)	Glycosaminoglycan (GAG) storage is kidney, cornea, brain, skeletal system	1 in 250,000	Childhood	[*187*, *188*]
Metachromatic leukodystrophy (MLD)	Arylsulfatase A (ARSA)	Widespread CNS and peripheral nervous system (PNS) involvement	1 in 40,000 to 160,000	Infantile - adulthood	[*189*, *190*]
Globoid-cell leukodystrophy (GCL)	Galactocerebrosidase (GALC)	progressive neurodegeneration and demyelination, extensive	1 in 100,000 to 250,000	Neonatal - adulthood	[*191*]

		neuroinflammation in the CNS and PNS			
Aspartylglucosaminuria (AGU)	Aspartylglucosaminidase (AGA)	neurodegenerative	1 in 18,500 in Finland	Childhood	[*192, 193*]

.

Table 2.2. Types of cell junctions found within endothelial cells layers throughout the vasculature and their defining properties with regards to potential carrier transport. *The width caused by connections determines that maximum size (in diameter) of a carrier that could transport through by diffusion. Information obtained from sources* [*1*, *2*].

Type of cell junction	Classification of cell junction	Type of endothelium	Associated Proteins	Width caused by connections
Tight junctions	Occluding junction	Continuous	Occludins, claudins [*194*]	12 Angstroms
Spot junctions	Anchoring junction	Continuous	Cadherins [*195*]	100 Angstroms
Fenestrae	Communicating junction	Fenestrated	PV1, caveolins [*196*, *197*]	200 – 1,000 Angstroms
Gap junctions	Communicating junction	Discontinuous	Connexins [*198*]	1,000 – 10,000 Angstroms

Table 2.3. **In Vivo *Gene Therapy Clinical Trials for LSDs.*** *Information regarding current clinical trials for* in vivo *gene therapy treatment of neuropathic LSDs is provided. In summary, most clinical trials employed intracerebral injections of adeno-associated viral vectors, with some success in alternative routes using AAV9.*

Clinical Trial	Injection Method	Viral Vector Used	Serotype	Disease Focus	Phase and Status
NCT01474343	Intracerebral	Adeno-associated	AAVrh10	Sanfilippo Syndrome A (MPS IIIa)	Phase 1 Completed in 2014
NCT01801709	Intracerebral	Adeno-associated	AAVrh10	Early onset metachromatic leukodystrophy	Phase 1/2 Recruiting
NCT0015126	Intracerebral	Adeno-associated	AAV2	Late Infantile Neuronal Ceroid Lipofuscinosis	Phase 1 Active
NCT01414985	Intracerebral	Adeno-associated	AAVrh10	Late Infantile Neuronal Ceroid Lipofuscinosis	Phase 1/2 Recruiting
NCT01161576	Intracerebral	Adeno-associated	AAVrh10	Late Infantile Neuronal Ceroid Lipofuscinosis	Phase 1 Recruiting
NCT02716246	Intravenous	Adeno-associated	AAV9	Sanfilippo Syndrome A (MPS IIIa)	Phase 1/2 Recruiting
NCT02725580	Intrathecal	Adeno-associated	AAV9	Juvenile Neuronal Ceroid Lipofuscinosis (Batten Disease)	Phase 1/2 Recruiting

Table 2.4. Enzyme Replacement Therapy Clinical Trials for LSD. *Information regarding currently ongoing clinical trials for enzyme replacement therapy is presented here. In general, clinical trials are focused on either improving the current standard of care with different proteins, doses, or different methods of administration (oral), or increasing the reach of enzyme replacement therapy to neuropathic LSDs. In this table, drugs such as migalastat, eliglustat, Zavesca and perhaps others are not traditional forms of ERT. They are chaperones (to increase the stability of endogenous enzyme) or glucosyl ceramide synthase inhibitors (to inhibit the production of storage material).*

Clinical Trial	Enzyme Used	Route of Administration	Disease Focus	Phase and Status
NCT00455104	agalsidase α and β	intravenous	Fabry disease	Phase 4 Recruiting
NCT01218659	Migalastat hydrochloride	Oral	Fabry disease	Phase 3 Completed
NCT02097251	UX003 recombinant human GUS	Intravenous	MPS VII	Single patient study Status unknown
NCT02230566	UX003	Intravenous	MPS VII	Phase 3 Ongoing, not recruiting
NCT01856218	UX003	Intravenous	MPS VII	Phase 1/2 Ongoing, not recruiting
NCT00943111	eliglustat tartrate	Oral	Gaucher's disease	Phase 3 Ongoing, not recruiting
NCT01885936	Albuterol	Oral	Late-onset Pompe disease	Phase 1/2 Recruiting
NCT02185651	Zavesca prior to ERT to mitigate infusion related reactions	Oral	Pompe disease	Phase 1 Recruiting
NCT01572636	Laronidase with hematopoietic stem cell transplant	Intravenously before transplant	MPS I	Recruiting
NCT01685216	velaglucerase alfa	Intravenous	Gaucher's disease	Phase 1/2 Completed in 2015

Table 2.5. Lysosomal Storage Diseases Treated With Enzyme Replacement Therapies.
The enzyme used for therapy is listed in the second column ('Treatments'), while the commercially available drug name is found in the third column ('Treatment Status'). All of these enzyme replacement therapies are clinically approved.

Lysosomal Storage Disease	Enzyme Replacement Therapy	Treatment	Source
Fabry's Disease	Algalsidase alfa Agalsidase beta	Replagal Fabrazyme	[*24*, *117*]
Pompe Disease (Glycogen Storage Disease Type II)	Alglucosidase alfa	Lumizyme Myozyme	[*24*, *117*, *119*]
Gaucher disease	Velaglucerase alfa Imiglucerase Taliglucerase alfa	Cerezyme Elelyso VPRIV	[*24*, *117*, *119*]
Hurler Syndrome (MPS I)	Laronidase	Aldurazyme	[*24*, *117*, *119*]
Hunter Syndrome (MPS II)	Idursulfase	Elaprase	[*24*, *117*, *119*]
Maroteaux-Lamy (MPS VI)	Galsulfase	Naglazyme	[*24*, *117*, *119*]

Table 2.6. Commonly discussed serum constituents with receptors present on the blood-brain barrier. *Concentration and half-life values are given for a healthy human, with both male and female values taken into consideration.*

Serum constituent	Binds to	Serum concentration	Molecular Weight	Serum Half life	Feasibility as targeting moiety	References
Transferrin	Transferrin receptor	2.3-3.9 mg/L	80 kDa	8 – 9 days	Receptors become saturated with transferrin	[*138*, *139*, *199*]
Insulin	Insulin receptor	Fasting, 43-186 pmol/L	5.8 kDa	~ 10 days	Could cause hypoglycemia; short half-life	[*11*, *139*, *199*, *200*]
Insulin-like growth factor I	Insulin-like growth factor receptor	Varies widely with age and gender; Over lifespan: Male range from 31-627 µg/L, Female range from 11-506 µg/L	7.65 kDa	On the scale of hours	Higher concentrations required to induce hypoglycemia compared to insulin	[*11*, *134*, *199*, *201*]
Insulin-like growth factor II	Insulin-like growth factor receptor	464 – 856 µg/L	7.5 kDa	On the scale of hours	Need to synthesize with a decreased affinity to proteins, as 99% bound to IGF-binding proteins	[*11*, *131*, *199*, *201–203*]
Leptin	Leptin receptor	<16.8 µg/L	16 kDa	25 minutes	Brain transport impaired during obesity	[*11*, *204–206*]
Immunoglobulin G	Neonatal Fc receptor	8.0-15.0 g/L	150 kDa	26.9 days	Transport only facilitated from brain to blood	[*11*, *134*, *199*, *207*]
Low-density lipoprotein	Scavenger receptor type B Low-density lipoprotein receptors	< 3.36 mmol/L	0.387 kDa		Used up after transport into endothelial cells; therefore, transport not facilitated into brain parenchyma	[*134*, *199*]

Table 2.7. Summary of recent studies of liposomal nanocarriers for treatment of neurological conditions in the past 10 years. *The majority of in vivo studies related to liposomes involve conjugated PEG. From the first in vivo study in 1996, the amount of injected dose per gram of brain tissue has increased, showing progress in the field. The use of the glutathione and folate receptors occur in cancer studies, while the transferrin receptor has been more widely applied.*

Nanocarrier System	Model	Delivery Method Employed	Drug Delivered	Source	Year
PEGylated Liposome	in vivo, rats	RMT with OX26 mAb to transferrin receptor	Daunomycin as antineoplastic	[*139*]	1996
	in vitro, rat brain tumor model	RMT with folate to folate receptor	Doxorubicin as antineoplastic	[*183*]	2007
	in vitro, mouse BBB culture in vivo, mice	RMT with 8D3 mAb to transferrin receptor	Polyethylenimine/DNA complex as proof of concept	[*140*]	2009
	in vivo, rats	RMT with folate to folate receptor	Doxorubicin as antineoplastic	[*184*]	2009
	in vivo, rats	RMT with glutathione	DAMGO, a peptide derivative drug model as antinociceptive	[*174*]	2012
Bi-ligand Liposome	in vivo, rats	RMT with transferrin-poly-B-arginine to transferrin receptor	*lacZ* plasmid DNA as gene therapy	[*185*]	2013

Table 2.8. Summary of recent metallic nanoparticles studied in vivo to treat neurological disease in the past 10 years. *Although the chitosan- and human serum albumin-based nanoparticles are not metallic, the studies contain interesting information on the use of the transferrin receptor in vivo. Metallic nanoparticles have increased in nanoparticle delivery studies more recently.*

Nanocarrier System	Model	Delivery Method Employed	Drug Delivered	Source	Year
PEGylated chitosan-based nanoparticle	in vivo, Swiss albino mice	RMT with OX26 mAb to transferrin receptor	Anticaspase peptide Z-DEVD-FMK to increase neuronal cell survival after cerebral ischemia	[*160*]	2005
Human serum albumin nanoparticles	in vivo, mice	RMT with either OX26 or R17217 mAb to transferrin receptor	Loperamide as a model drug	[*208*]	2009
PEGylated iron oxide nanoparticles with starch coating	in vivo, rats induced glioma tumors	Magnetic targeting	None delivered, distribution studied	[*161*]	2011
Iron oxide nanoparticles with heparin coating	in vivo, rats induced glioma tumors	Magnetic targeting with MRI-guided alignment	β- galactosidase modified with polycationic Polyethylenimine domains	[*163*]	2011
Gold nanoparticles with thiolated PEG	in vivo, rats	Magnetic resonance imaging guided focused ultrasound	None delivered, distribution studied	[*162*]	2012
Gold nanoparticles with peptide CLPFFD	In vitro, co-culture of bovine brain endothelial cells and new born rat astrocytes (BBB model) In vivo, rats	RMT with peptide sequence THRPPMWSPVWP to transferrin receptor	None delivered, distribution studied	[*209*]	2012

Table 2.9. FDA approved polymers used in polymersomes. *Information regarding approved polymers on the FDA website, using the Inactive Ingredient Database*[*3*]. *Information regarding polymer use in polymersomes from multiple review articles* [*4–6*]

Polymer	Acronym	Hydrophilic/Hydrophobic	Administration Route(s) Approved
Polyethylene glycol (or oxide if low MW)	PEG (or PEO)	Hydrophilic	Dental, Intra-articular, Intralesional, Intramuscular, Intrasynovial, Intravenous, Nasal, Ophthalmic, Oral, Rectal, Respiratory, Soft Tissue, Subcutaneous, Sublingual, Topical, Urethral, Vaginal
Polyacrylic acid	PAA	Hydrophilic	Topical, Transdermal
Polyethylene Terephthalate	PET	Hydrophobic	Transdermal
Polylactide	PLA	Hydrophobic	Intramuscular, Periodontal
Poly(dimethylsiloxane) (aka Dimethicone)	PDMS	Hydrophobic	Dental, Intravenous , Oral, Topical, Transdermal, Vaginal

Table 2.10. Summary of recent studies of polymersomes for treatment of neurological conditions in the past 10 years. *PEG is a common component of polymeric vesicle carriers. Polymersomes are desirable for brain delivery due to their high levels of stability when compared to other synthetic carriers. As the use of polymersomes for brain delivery is newer, distribution has not been measured in some of the studies listed.*

Nanocarrier System	Model	Delivery Method Employed	Drug Delivered	Source	Year
Poly(ethylene glycol)-poly(ε-caprolactone) polymersome	in vivo, rats	RMT with OX26-PO mAb to transferrin receptor	Peptide, NC-1900 as a model peptide	[*172*]	2008
Poly(ethylene glycol)-poly(lactide) polymersome	in vitro, mouse endothelia line in vivo, mice	RMT with lactoferrin	Peptide, NC-1900 as a model peptide	[*210*]	2009
Poly(ethylene glycol)-poly(ε-caprolactone) polymersome	in vitro, bEnd.3 cells in vivo, rats	RMT with transferrin receptor	Peptide, coumarin-6 as a fluorescent probe	[*173*]	2011
Polybutadiene-b-poly(ethylene glycol) polymersome	in vitro, human brain microvessel endothelial cells (hCMEC/D3) in vivo, mice	RME with GM1 ganglioside targeted peptide or prion targeted peptide	None delivered, distribution studied	[*174*]	2012
Poly(ε-caprolactone)-b-poly(ethylene oxide)-b-poly(2-vinylpyridine)-b-poly(ethylene oxide)-b-poly(ε-caprolactone) polymersome	Release studies	Not yet employed	Gold nanoparticles with Nile red as a hydrophobic drug model	[*175*]	2013

Chapter 3: Passive Formation of Polyethylene glycol-b-Poly(lactic acid)Polymersomes Results in Limited Control over Nanoparticle Properties

This work required the careful selection of appropriate materials for the formation of polymersomes. Based upon Discher, et al, block co-polymers with a hydrophilic fraction between 25 and 40% led to the self-assembly of polymersomes over other undesirable structures [*4*], creating the initial constraints for material selection. Second, polymersomes can be formed using many self-assembly techniques including, but not limited to passive dissolution, solvent injection[*211–213*], solvent evaporation [*167*, *171*, *214*], nanoprecipitation [*170*, *215*], microfluidics [*216–218*], and simple dialysis [*219*]. It was important to select a technique that would both work for the polymeric materials selected and be translatable to clinical treatments. Some of the solvent based techniques use harsh chemicals that are difficult to remove. Initial polymersome formation studies were performed carefully with the goals of probing the process polymersome formation and creating polymersomes capable of delivering a payload through the BBB.

3.1. Materials and Methods

3.1.1. Polymer Materials

An initial search of the literature provided a list of potential components for block co-polymers based upon what had been previously used to create polymersomes. From here, research was done to determine if the polymeric component was FDA approved or biodegradable, as well as what molecular weights were available for purchase (Table 3.1). Polyethylene glycol was the immediate choice for the hydrophilic component in our block co-polymer, as it is commonly used in drug delivery applications to increase the

circulating half-life of carriers. In the case of the treatment of GM1 gangliosidosis, it is desirable for a payload to be released into the lysosome of cells. Because of this, it was desirable to select a hydrophobic block co-polymer component that was biodegradable, which decreased our choices. Based upon the availability of purchasable block co-polymer and trying to keep the hydrophilic molecular weight close to 25 – 40% of the block, PEG(1000)-b-PLA(5000) was chosen for the formation of polymersomes (Polysciences, Inc).

3.1.2. Polymersome Formation

The co-polymer polyethylene glycol (1,000)-b-poly(lactic acid) (5,000) (Polysciences) self-assembled in water at concentrations between 0.6 and 1 weight percent. Polymersome formation was monitored using dynamic light scattering methods in a NICOMP 3800. Dynamic light scattering methods use a laser and a detector at 173° to measure the Brownian motion of particles in a cuvette sample. The intensity that is measured is dependent on particle specific properties, as well as the varying refractive indices of the solvent and the particles. The NICOMP 3800 uses a stationary laser for analysis. It also has a range of acceptable intensity values between 300-500 kHz and a diameter range of calculation between 5 nanometers to “several microns”. Dynamic Light Scattering (DLS) measurements were taken both prior to and anterior to lyophilization to monitor property maintenance of polymersomes.

3.1.3. Lyophilization and Characterization

Following formation, the solution with self-assembled polymersomes dissolved in water was cryogenically frozen, using liquid nitrogen, to stabilize and finish the self-

assembly process. Following cryogenic freezing, the effect of different temperature profiles prior to freeze drying on polymersome integrity was studied. Particles were stored in a -20 °C freezer before lyophilization, stored in a -20 °C freezer, then thawed and frozen again before lyophilization, or immediately lyophilized prior to cryogenic freezing. Lyophilization was performed using a Labconco freeze dryer at a pressure of 0.040 mbar and a temperature of -52 °C. This change in pressure and temperature allows sublimation to occur, removing the water from the frozen sample and leaving a lyophilized cake of particles.

Following lyophilization, transmission electron microscopy (TEM) was used to determine the shape and size distribution of the polymersomes formed by rehydrated the lyophilization polymersomes and drop casting them onto a copper grid. The post-lyophilization sizes were interpreted using either the scaled images or ImageJ software (when possible) and compared to the diameter ranges found using the NICOMP 3800.

3.2. Results and Discussion

It was determined using DLS that polymersomes formed in this study did not have any statistically differences in average polymersome diameter prior to lyophilization via unique temperature profiles. Where they did differ was in the shape and size of polymersomes found after lyophilization via the different freezing conditions (Figure 3.1). The first image is a representative TEM image from lyophilization following cryogenic freezing and long term storage in a -20°C freezer. Typical of this temperature profile, it was difficult to find particles with membrane integrity and a distinct spherical shape. The elliptical shape found in Figure -1 was typical to particles found in this grid.

The middle image is a representative TEM images from lyophilization following cryogenic freezing, storage in a -20 °C freezer, and a freeze thaw process. With grids from this procedure (Figure 3.1 - 2) smaller polymersomes were present; however there was the appearance of some aggregates and irregular shaped particles. The third image is from lyophilization immediately following cryogenic freezing (Figure 3.1 - 3). Small polymersomes were present at a high density throughout the grid and the shape distribution appears to be fairly uniform (20 – 40 nm in diameter).

Regardless of the freezing temperature profile used, polymersomes were able to form via passive mixing, which is clear from both DLS data and TEM imaging. Membrane integrity appears to be more intact when using a freeze-thaw process prior to lyophilization when compared to solely long term storage in a -20 °C freezer. It is hypothesized that the extra freeze-thaw step may have allowed for extra swelling and extended self-assembly to occur. Immediate lyophilization after cryogenic freezing led to polymersomes with visible membrane integrity with smaller diameters than expected based upon the dynamic light scattering data. The area around the smaller polymersomes is thick and dark, indicating the presence of negative staining by PTA and suggesting the presence of a membrane. The size and shape distributions throughout the grids appear to be fairly uniform. This may have occurred because the self-assembly process was abruptly vitrified, which allowed for the same interaction time of the polymeric material with water – unlike the freeze-thaw process, in which certain areas may defrost more quickly, allowing for more rapid molecular interactions with water.

The most striking result from these initial studies was the change in polymersome structure following lyophilization. Figure 3.2 shows the differences in polymersome size distribution measured pre-lyophilization, via DLS, and post lyophilization, via TEM. It is clear that the polymersomes maintain the same size distribution behavior, as both trends follow similar curves. However, by glancing at the upper and lower x-axes, it becomes apparent that the average polymersome diameters measured after lyophilization was around 100 times smaller than the distribution visualized via DLS. It is hypothesized that the polymersomes collapsed after lyophilization, as the removal of water removed the driving force of self-assembly. Because the block co-polymers used to create polymersomes are amphiphilic, the hydrophobic interactions between the co-polymer and water are the driving force for vesicle self-assembly. When sublimation of this water occurs, the block co-polymer is forced to find this hydrophobic interaction elsewhere, potentially through attraction with its own neighboring area of hydrophobic membrane.

3.3. Conclusions

These initial studies presented in this chapter involved careful selection of polymersome building blocks, with a focus on the treatment of GM1 gangliosidosis. After a thorough search of the literature and FDA approved polymers, PEG-b-PLA became the best choice based upon its ability to decrease complement protein tagging through the hydrophilic PEG component and its ability to undergo hydrolytic cleavage through the hydrophobic PLA component. Based upon these studies, it became clear that immediately lyophilizing polymersomes after cryogenic freezing led to a more uniform shape and size distribution of polymersomes obtained. Because of this, this protocol was

maintained as carefully as possible through the duration of the work presented in this dissertation. Although both of these research components were critical to successful polymersome preparation, the most important information that came out of initial work involved the measurements of size distributions before and after lyophilization. Polymersomes that do not maintain their shape and size after lyophilization cannot be used in clinical therapies, as lyophilization is needed for long term storage of therapeutics in which reconstitution occurs prior to injection [*220–222*]. Because of this finding, it became necessary to look into other materials that may be able to replace the hydrophobic interaction that the drive the block co-polymer to become polymersomes in water, which led to the first published experimental paper, published in the journal Polymer and presented in Chapter 4.

3.4. Figures and Tables

Table 3.1. Polymeric Materials used in the formation of Polymersomes. Information regarding polymeric blocks is listed in the tables, including purchasable MWs, standing with the FDA, hydrophilicity, and biodegradability.

Polymer	Class	Molecular Weights Available	FDA Approved?	Hydrophilic or Hydrophobic?	Acronym	Biodegradable?
Polyethylene Glycol (or oxide)		100,000 to 8,000,000	+	hydrophilic	PEG/PEO	
Polybutadiene	Diene	1,500 to 200,000		hydrophobic	PBD	
Poly(ethylethylene)	Vinyl	Can't find		hydrophobic	PEE	
Polystyrene	Vinyl	192,000 to 400,000		hydrophobic	PS	
Polyacrylic acid	Acrylic	1,800 to 4,000,000	+	hydrophilic	PAA	
Polylactide		60,000 (Polylactic acid)	+	hydrophobic	PLA	+
Poly(caprolactone)	Ester	70,000 to 90,000		hydrophobic	PCL	+
Polyethylene terephthalate	Ester		+	hydrophobic	PET	
Poly(dimethylsiloxane)		~25,000	+	hydrophobic	PDMS	
Poly(trimethylene carbonate)				hydrophobic	PTMC	+
Poly(glutamic acid)		1,500 to 100,000		hydrophilic	PGA	
Polylysine		70,000 to 300,000 in solution		hydrophilic	PL	
Polyethylenimine	Amine	25,000 branched		hydrophilic	PEI	

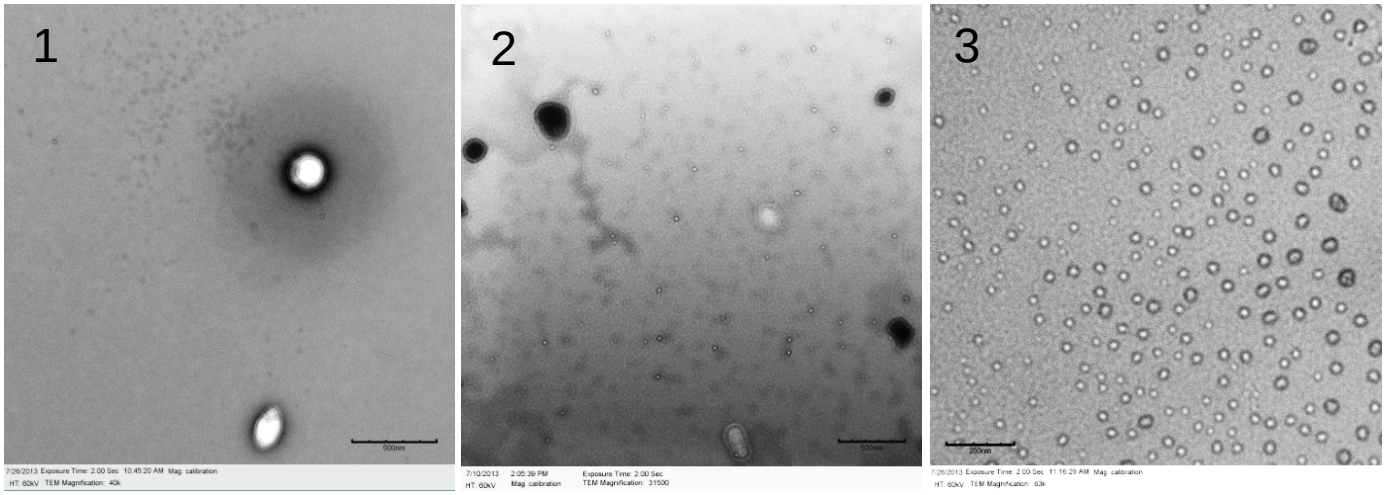

Figure 3.1. Representative TEM images of polymersomes formed using Procedure 1, 2, and 3, where Procedure 1 represents cryogenic freezing followed by long term storage in a -20 °C freezer prior to lyophilization, Procedure 2 represents cryogenic freezing, followed by a freeze thaw process prior to lyophilization, and Procedure 3 represents cryogenic freezing followed by immediate lyophilization.

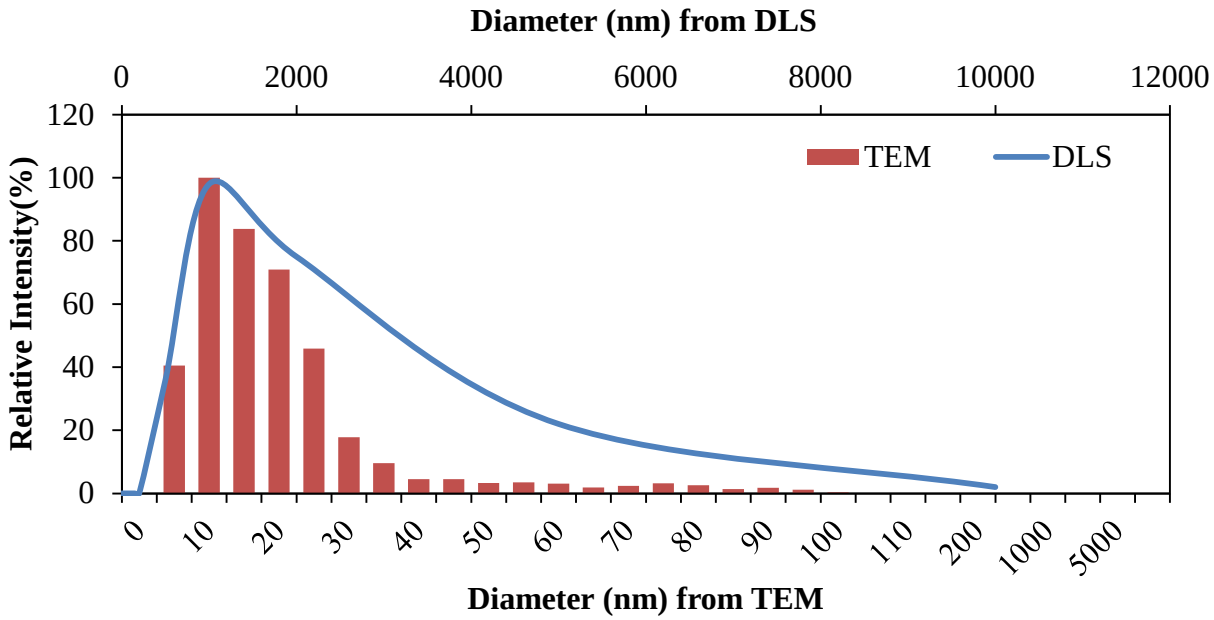

Figure 3.2. Comparative Polymersome Size Distributions from TEM and DLS analysis. Represented here are particle size distributions using both DLS and ImageJ analysis of TEM images collected on polymersomes that were lyophilized immediately following cryogenic freezing. The red bars and lower x-axis represent data gathered from TEM and the blue line and upper x-axis represent data gathered from DLS.

Chapter 4: Lyoprotectants Modify and Stabilize Self-Assembly of Polymersomes

Polymersomes, or polymeric vesicles, are made up of two or more amphiphilic block copolymers and can encapsulate both hydrophilic and hydrophobic molecules [*6*]. Block copolymers will self-assemble into a multitude of different structures based upon their hydrophilic/hydrophobic mass ratio and the overall molecular weight upon introduction to a solvent[*4*]. A hydrophilic fraction between approximately 25 and 40% by mass, determined using PEG as a hydrophilic block, have been shown to form vesicular structures in aqueous solvent [*4*]. The thickness of the membrane and diameter of the vesicle interior increase with increasing molecular weight of the hydrophilic component [*164*]. Polymersomes, by nature, are tunable on the molecular level [*5*] and may take advantage of many different release mechanisms including pH, temperature, redox-potential, light, hydrogen bonding, electrostatic forces, magnetic field, ionic strength, concentration of analytes, and other external stimuli [*6, 166*]. The ability to control the release mechanism and size of specific carrier regions through material selection makes polymersomes desirable platforms for drug delivery, as they show potential for delivery of a wide variety of therapeutics in various applications.

The work presented in this chapter involves the use of poly(ethylene glycol)-b-poly(lactic acid) (PEG-b-PLA) to create therapeutically deliverable polymersomes that could be produced and stabilized over a long period of time, allowing for more efficient intravenous delivery of both hydrophobic and hydrophilic therapeutics. Both components of this block copolymer are approved by the FDA for use in humans [*3*]. PEG is approved for 17 different routes of administration and PLA is approved for both

intramuscular and periodontal routes [*108*]. PLA is biodegradable and has been shown to cause release based upon pH-triggered hydrolysis [*6, 165, 167*]. As with other carriers and drug delivery systems [*129*], the incorporation of a PEG block may be used to increase the stability of polymersomes and decrease uptake by the reticuloendothelial system due to its resistance to protein adsorption and cell adhesion [*6*].

Although manipulation of block co-polymer composition and molecular weight can aid in control of polymersome size and shape, there is still a large variation in the final hydrodynamic size distribution. Formation methods exploited can lead to polydisperse samples. Particle size diameter of the nanoparticle system being used is an important consideration based upon the necessity of cellular uptake and required surface area to attach targeting or imaging moieties. In general, particle size diameters of drug delivery vehicles should be around 200 nm or less in order to allow for transcytosis through the cell membrane [*223*]. The nature of self-assembly leads to size variation and necessitates separation techniques.

Extrusion techniques are used, pushing polymersome solutions through membranes of various sizes under high pressure [*166*] to yield a defined size distribution of polymersomes. This can be time consuming and costly, while still not leading to a sharp enough size distribution for therapeutic delivery. By using lyoprotectant molecules during polymersome formation, further control over polymersome size can be achieved, reducing the need for costly and time consuming separation techniques and creating polymersomes that maintain their size and structure during long-term storage.

In this study, cryogenic freezing and lyophilization (or freeze-drying) was used to quench self-assembly. Lyophilization has been used to stabilize and preserve biological and pharmaceutical products for extended periods of time, allowing reconstitution into solution when necessary [*224*]. Reconstitution of polymersomes means the re-introduction of the lyophilized polymersomes into an appropriate solvent for injection. During reconstitution, polymersomes should maintain their average diameter. Both inulin, a polysaccharide, and mannitol, a sugar alcohol, have been previously explored for their hydrophilic nature as lyoprotectant molecules in polymersomes [*220*]. However, the focus of the previous study was on long-term storage of polymersomes, while our study was focused on controlling the dynamic nature of self-assembled systems needed to form polymersomes while maintaining size distribution. Because of this, the polymersome formulation method used was the most widely applicable method, taking advantage only of the hydrophobic interactions between the block co-polymer and water and allowing our results to be applicable to other polymer systems.

The objective of our study was to determine the effect of incorporating mannitol and inulin on polymersome properties including particle size diameter formed, moisture retention during lyophilization, and maintenance of particle size diameter after processing. We hypothesized that the incorporation of lyoprotectant molecules inulin and mannitol would increase the stability and maintain the size distribution of the formed polymersomes after lyophilization.

4.1. Materials and Methods

4.1.1. Materials

Co-polymer with 17% polyethylene glycol (molecular weight = 1000 Da) blocked with remainder poly(lactic acid) (molecular weight = 5000 Da) was used in all particle formation studies (Polysciences, Inc). Inulin (Alfa Aesar) and mannitol (Sigma Aldrich) were used as received. Deionized (DI) water was obtained for particle formation using a Millipore water filtration system. Millex syringe filter units of pore sizes 0.80 μm and 0.45 μm were used (Millipore). HYDRANAL Coulomat reagent (VWR) was used in Karl Fischer titration.

4.1.2. Polymersome Formation

Block co-polymer, PEG-b-PLA, was dissolved in deionized water at a concentration between 0.7 and 0.8 wt%/v. The solution was mixed for a period of 2.5 hours. Samples in which solely block co-polymer were dissolved are indicated as control studies. Inulin and mannitol were dissolved simultaneously in DI water with PEG-b-PLA at concentrations of 2, 5, and 8 weight percent per volume as lyoprotectant molecules in corresponding studies.

4.1.3. Particle Size Distribution Analysis

During polymersome formation, aliquots were drawn from the vial every half hour for 2.5 hours. Each aliquot was diluted to a polymersome concentration of 0.2 wt%/v, which showed consistent DLS measurements. Removal of a small sample size led to minimal changes in the driving force of polymer dissolution, which is proportional to

$e^{-\frac{\Delta G}{k_B T}}$ [225]. A total sample volume of 1 mL was pipetted into a plastic cuvette and placed in the Zetasizer to obtain the particle size distribution (PSD) of the sample. The PSD data was obtained prior to the use of both 0.80 µm and 0.45 µm membranes, as well as after the use of both membranes, which allowed for further study of smaller polymersomes. Data was collected and presented using intensity-weighted size distributions and percentage of polymersomes found in specific bins pre-determined by the software.

4.1.4. Cryogenic Freezing

After 2.5 hours, aliquots of polymersomes in water, with or without mannitol or inulin based upon the study, was vitrified using liquid nitrogen, causing the self-assembly to seize. After cryogenic freezing, the polymersomes suspended in water were placed in a freeze dryer under sublimation conditions (0.040 mbar and -52 °C), allowing the water to evaporate off and leaving behind polymersomes. This lyophilized polymersome sample, in the form of a powdery cake, was used in further analysis.

4.1.5. Fourier Transform- Infrared Spectroscopy

Identification of the lyophilized polymersome samples with and without lyoprotectant molecules was done using attenuated total reflection coupled with Fourier transform-infrared spectroscopy (ATR FT-IR). This method of analysis allows for solid samples to be examined and has a penetration depth of about 500 nm. Because of this, ATR FT-IR was capable of penetrating the hydrophobic membrane of the polymersomes and analyzing both the surface and interior core of the vesicle.

4.1.6. Particle Reconstitution

Polymersome size maintenance was measured by reconstituting the lyophilized samples into water at the same concentration used during initial formation. Therefore, an appropriate mass of powdery sample was added to 1 mL of DI water. Vortexing was applied for 5 – 10 minutes depending on the resistance to dissolution of the sample in order to reconstitute as many particles as possible. Then, the intensity-weighted PSD was obtained (Zetasizer Nano, Malvern) and compared to the intensity-weighted PSD found prior to lyophilization. A normalization value was measured by dividing the overall average diameter found post-lyophilization by the overall average diameter found pre-lyophilization. The closeness of this value to one indicates the closeness of the final diameter to the diameter initially studied.

4.1.7. Moisture Content Determination

Moisture content was determined using Karl Fischer titration methods in a C20X Coulometer (Mettler Toledo). The coulometer calculates moisture content based upon the amount of stoichiometric iodine formed due to the presence of water using the Bunsen reaction, which is as follows.

$$SO_2 + I_2 + 2H_2O \rightarrow H_2SO_4 + 2HI$$

The C20X electrochemically generates iodine and calculates the coulombs needed for generation. This measured charge, along with a known mass of sample, is used to derive the amount of water present in the sample down to the lower detection limit of 1 ppm.

Lyophilized samples were dissolved in the titration vessel, which held HYDRANAL coluomat reagent.

4.2. Results and Discussion

Particle size diameters of drug delivery vehicles should be around 200 nm or less in order to allow for increased transcytosis through the cell membrane and decreased clearance from circulation [*223*]. Therefore, the incorporation of additional molecules should have no negative impact on polymersome diameter in order to ensure proper cellular delivery. Polymersome formation was confirmed, and a 0.45 μm membrane produced polymersomes at an average diameter of 234.6 ± 131.4 nm within the first thirty minutes of dissolution (Figure 4.1). This particle size diameter stayed the same size over time, demonstrated by no statistical difference between values of 233.8 ± 99.4 nm at 60 minutes, 216.2 ± 53.5 nm at 90 minutes, 274.7 ± 23.8 nm at 120 minutes, and 226.9 ± 24.4 nm at 150 minutes. It is interesting to note that while the overall average hydrodynamic particle size diameter remained fairly similar, the standard deviation decreased over time. This means that the variation in polymersome diameter between trials decreased and the polymersome sample became less polydisperse over time. Without the incorporation of lyoprotectants, particles desirable for therapeutic delivery (≤ 200 nm in diameter) were formed at all time points. Although overall averages were above 200 nm in diameter, DLS data indicated that up to 74% of the polymersomes formed were in the desirable size range of less than 200 nm at all time points.

When inulin was incorporated into polymersomes during formation, diameters over all time points at all concentrations were not statistically different from the control

polymersome diameter. This behavior is expected as the thermodynamic stability of the polymersomes formed during self-assembly is dictated by the hydrophilic fraction of the co-polymer and the concentration of water [*226*]. The length of the hydrophilic component, polyethylene glycol, and the concentration of water was held constant for each study in this paper and therefore the overall size distribution should remain statistically the same. The incorporation of lyoprotectant molecules should not cause a change in the particle size diameters of the PEG-b-PLA polymersomes regardless of the concentration. The lowest polymersome diameters were found in the thirty minute aliquot at all concentrations of inulin – 188.6 ± 38.6 nm with 2 wt%/v, 213.1 ± 28.7 nm with 5 wt%/v, and 217.0 ± 9.2 nm with 8 wt%/v. In general, 8 wt%/v inulin incorporation led to the smallest deviation in polymersome diameter, and therefore the most control over the polydispersity of the sample. Incorporation of mannitol led to different results.

When mannitol was incorporated into polymersomes during formation, diameters were not statistically different when compared to control at all time points other than 120 minutes. At 120 minutes, the incorporation of both 2 wt%/v and 8 wt%/v mannitol led to statistically smaller polymersome diameters compared to control ($p < 0.025$). No statistical differences were found between polymersome diameters when comparing the different concentrations of mannitol incorporated at any time point. Although this data is not as expected, based upon thermodynamics of the system, it is not a negative effect on PSD. Hydrophilic molecules are not directly responsible for the hydrophobic assembly of polymersomes, but can affect the arrangement [*225*]. Therefore, the difference in hydrophilicity between inulin and mannitol, with different numbers of OH bonds, may

result in different attractive forces between these molecules and water. Because of this, differences in size of polymersomes formed may occur even though the hydrophilic fraction of the block co-polymer and the concentration of water remain constant. Although statistical differences were only observed at 120 minutes, trends were similar throughout all time points. With the incorporation of 2 and 8 wt%/v mannitol, decreased polymersome diameters compared to control were continually observed. The trend tended to occur with the incorporation of 5 wt%/v mannitol as well although greater deviations were generally observed. However, no statistical differences between polymersome diameters were observed when comparing constant concentration of mannitol at different time points.

In general, the deviations in polymersome diameter found when incorporating mannitol were larger than the deviations in polymersome diameter found when incorporating inulin. This holds true when comparing all concentrations incorporated for 30, 60, and 120 minutes during formation. Although the incorporation of mannitol led to statistically smaller polymersome diameters at 120 minutes, the incorporation of inulin may provide slightly more control over polymersome diameter, i.e., smaller standard deviations. Therefore, the incorporation of inulin is more promising towards our hypothesis that the incorporation of lyoprotectant molecules can decrease the necessity of expensive high pressure separation techniques.

Although we have demonstrated that these molecules do not statistically increase our polymersome diameter to a value above 200 nm, desirable for delivery, the most important measure of the effect of lyoprotectant molecules on polymersome maintenance

was size distribution after reconstitution. Reconstitution data is presented and summarized in Figure 4.2. In Figure 4.2, comparative PSDs are presented, which demonstrate the impact of lyoprotectant molecules on polymersome size maintenance. Particle size post-lyophilization was normalized to (i.e., divided by) the pre-lyophilization diameter. The normalization value for control polymersome PSDs was 4.63 ± 0.01, meaning that in general, hydrodynamic diameters of polymersomes were 4.63 times larger after lyophilization than before. The incorporation of any concentration of lyoprotectant showed a significant improvement in the normalization of particle size diameters compared to control, meaning that small amounts of lyoprotectant allow the size distribution overall to be more properly maintained after reconstituting. All concentrations of inulin preserved particle size after lyophilization, with normalization values ranging from 1.22 ± 0.01 (2 wt%/v) to 0.87 ± 0.01 (5 wt%/v).

Overall, particle size was most effectively preserved by 8 wt%/v inulin, with a normalized diameter of 0.99 ± 0.01 . All concentrations of inulin showed closer normalization values to control than their mannitol counterparts ($p<0.025$). Normalization values using mannitol varied more widely compared to inulin at the same concentration: 0.54 ± 0.01 with 2 wt%/v mannitol, 0.84 ± 0.01with 5 wt%/v mannitol, and 0.78 ± 0.00 with 8% wt%/v mannitol (Table 4.1). Mannitol (Molecular Weight (MW)= 182 g/mol) is smaller in size than inulin (MW = 5000 g/mol [*227*]) and therefore may be able to transport easier through the polymersome membrane during lyophilization. Because of this, mannitol may interrupt the van der waals forces of attraction occurring between PLA blocks in water that aid in self-assembly of PEG-b-

PLA amphiphiles. Although hydrophobic interactions dominate polymersome self-assembly, hydrophilic forces of attraction between lyoprotectants and water also influence polymersome formation, as hydrogen bonding may occur between water and lyoprotectant molecules [*225*]. Differences in mannitol and inulin size and structure, including the presence of different numbers of hydroxyl groups, may also cause differences in behavior upon reconstitution. The possible molecular configurations PEG-b-PLA can form in water are limited, as both hydrophobic (between PLA blocks) and hydrophilic (between PEG and water) interactions need to be accommodated.

ATR-FTIR spectra (Figure 4.3) show that both inulin and mannitol were found within the vesicle membrane at all concentrations studied. The penetration depth of ATR-FTIR (0.5 μm) allows for the visualization of spectra throughout the entire polymersome structure including the hydrophobic membrane and the hydrophilic brush and core. Lyophilized control polymersomes showed no broad peak at 3200 cm^{-1}, indicating the removal of water and no presence of OH bonds. As the concentration of lyoprotectant increased, the absorbance peak at 3200 cm^{-1} increased indicating the presence of OH bonds, which were not detectable in lyophilized polymersomes alone. Thus, as lyoprotectant increased in the formulation, either more lyoprotectant or more water was incorporated into the lyophilized polymersome. Mannitol showed the most incorporation at various concentrations compared to inulin potentially due to its smaller size. Based upon this ATR FT-IR data, both inulin and mannitol were incorporated during polymersome formation in water at 2 wt%/v, 5 wt%/v, and 8 wt%/v.

Following lyophilization and confirmation of lyoprotectant incorporation, Karl Fischer titration was done to measure the moisture content in lyophilized polymersomes. As the concentration of inulin increased during polymersome formation, moisture content after lyophilization decreased from 32534 ± 17472 ppm with 2 wt%/v inulin to 10117 ± 1532 ppm with 5 wt%/v inulin and finally 1828 ± 362 ppm with 8 wt%/v inulin. Each decrease in moisture content was statistically lower ($p < 0.01$) than the previous value. However, using our standard procedure for lyophilization, there was no statistical difference between moisture content at any concentration of mannitol. Moisture contents remained statistically the same from 5155 ± 1987 ppm with 2 wt%/v to 19873 ± 7400 ppm with 5 wt%/v to 8153 ± 4696 ppm with 8 wt%/v mannitol. It is important to note that moisture content using mannitol was lower than inulin at 2 wt%/v and was higher than inulin at 8 wt%/v ($p<0.05$ for both, Figure 4.4).

This data may indicate that, at higher concentrations, inulin is more adequately replacing water in the vesicular membrane of polymersomes during lyophilization when compared to mannitol. Karl Fischer titration data also suggests that mannitol is crystallizing during cryogenic freezing after polymersome formation, due to increased moisture contents after lyophilization. Mannitol at room temperature is known to crystallize, which would be detrimental to the encapsulation of biological therapeutics[*228*]. Crystallization of mannitol may help explain why moisture content does not correlate with mannitol concentration. Crystallization may also contribute to the lower normalization values when polymersomes with mannitol are reconstituted. In order to test this hypothesis, the effect of changing the freezing rate prior to lyophilization, a

process entitled “slow freeze” in this paper, was studied. Instead of immediately vitrifying self-assembly in liquid nitrogen after 2.5 hours, vials were placed into a -20 °C freezer and allowed to reach temperature over a period of 24 hours prior to lyophilization. As shown in Figure 4.48, slow freezing led to statistically lower residual moisture content in lyophilized samples compared to rapid freezing with liquid nitrogen. Thus, slower freezing minimizes water content in polymersomes formed with mannitol, which is known to form crystals during sublimation[*228, 229*] and at room temperature[*149*], suggesting that slower freezing is advantageous for the removal of water and limiting crystallization in the sample.

Karl Fischer titration data correlated with particle size after reconstitution. In the case of inulin incorporation, the lowest moisture content was associated with the most normalized particle size diameter when comparing distributions before and after lyophilization. However, the moisture content of lyophilized polymersomes with mannitol showed no statistical difference between concentrations. Decreased moisture content trends towards increased normalization with the incorporation of inulin, suggesting that lyoprotectants are better able to replace water at certain concentrations and this replacement of water within the vesicle leads to better polymersome size maintenance.

4.3. Conclusions

To analyze the effectiveness of lyoprotectant molecules and choose a concentration to appropriately control polymersome formation, it is important to keep in mind the desired application. Based upon the type of therapeutic being encapsulated and

delivery strategy, certain properties may be desirable over others. The time point to end formation and the concentration of lyoprotectant molecule to be incorporated is dependent on which property is most important for polymersome formation and maintenance: minimal particle size diameters of less than 200 nm to facilitate transcytosis through the cell membrane, minimal crystallization to ensure protection of therapeutics and maintenance of properties, or maximal polymersome size maintenance after lyophilization for long term storage.

Regarding polymersomes with diameters less than 200 nm, the only statistical difference was found with the incorporation of mannitol. If the primary goal is to obtain the smallest particle size diameter using these molecular weights of polyethylene glycol-b-poly(lactic acid), either 2 or 8 wt%/v mannitol should be incorporated and the polymersome formation should be stopped at 120 minutes ($d = 169.8 \pm 37.2$ nm or 153.1 ± 32.2 nm respectively). In both cases, the polymersome diameters were statistically lower than control. With inulin, particle size did not decrease using the current assembly procedure. Shorter time points may facilitate formation of polymersomes with diameters less than 200 nm, although this may lead to increased variability in polymersome size and decreased yield in the desirable size range.

Minimal crystallization is equally important, as crystallization can adversely affect biological therapeutics in the polymersome vesicle. If the primary goal of polymersome application is minimal crystallization and water content, 8 wt%/v inulin may be used with rapid freezing in liquid nitrogen. Though inulin was superior for minimizing moisture content during rapid freezing, mannitol yielded similarly low

moisture levels with slow freezing. The lowest moisture contents were 1721 ± 1130 ppm after slow freezing with 5 wt%/v mannitol or 1828 ± 362 ppm after rapid freezing with 8 wt%/v inulin. Thus, slow freezing may eliminate some of the concerns facing the incorporation of mannitol during polymersome formation.

Finally, and most importantly, the incorporation of lyoprotectants was hypothesized to maintain polymersome size after lyophilization. The primary goal of this study was to determine the lyoprotectant concentration that would lead to the highest level of control over polymersome diameter. In this regard, inulin proved to be the most promising, as polymersome size after lyophilization was almost perfectly maintained in the presence of 8 wt%/v inulin. Also important to note is that inulin had no bearing on particle size during self-assembly. Therefore, inulin is behaving in its hypothesized fashion. The incorporation of mannitol yielded polymersomes that were 16-46% smaller after lyophilization than before lyophilization. Although mannitol provided less control over the dynamic environment, reduced particle size may be beneficial for targeted delivery, depending on the constraints for both the therapeutic and the delivery site. Also, the use of mannitol may be beneficial for opening up tight junctions of the blood-brain barrier.

It is clear that the exact conditions under which polymersome formation should occur depend on the goal for treatment and the importance of certain variables explored in this study. The incorporation of mannitol and inulin during polymersome formation was hypothesized to increase control over maintenance of polymersome diameter through the high stress processing conditions of lyophilization. This study demonstrates that

polymersome formation can be controlled to generate consistent sizes both before and after freeze drying for long term storage, thus eliminating the need for high cost separation techniques. Particle diameters within the therapeutic target range of <200 nm provide substantial evidence that PEG-b-PLA polymersomes can be effective drug delivery carriers with the help of lyoprotectant molecules.

The use of mannitol at a concentration of 2 wt%/v as a lyoprotectant was used to aid in polymersome formation and maintenance of polymersome properties as proteins bovine serum albumin (BSA) and β-galactosidase (βgal) were encapsulated in Chapter 5.

4.4. Figures and Tables

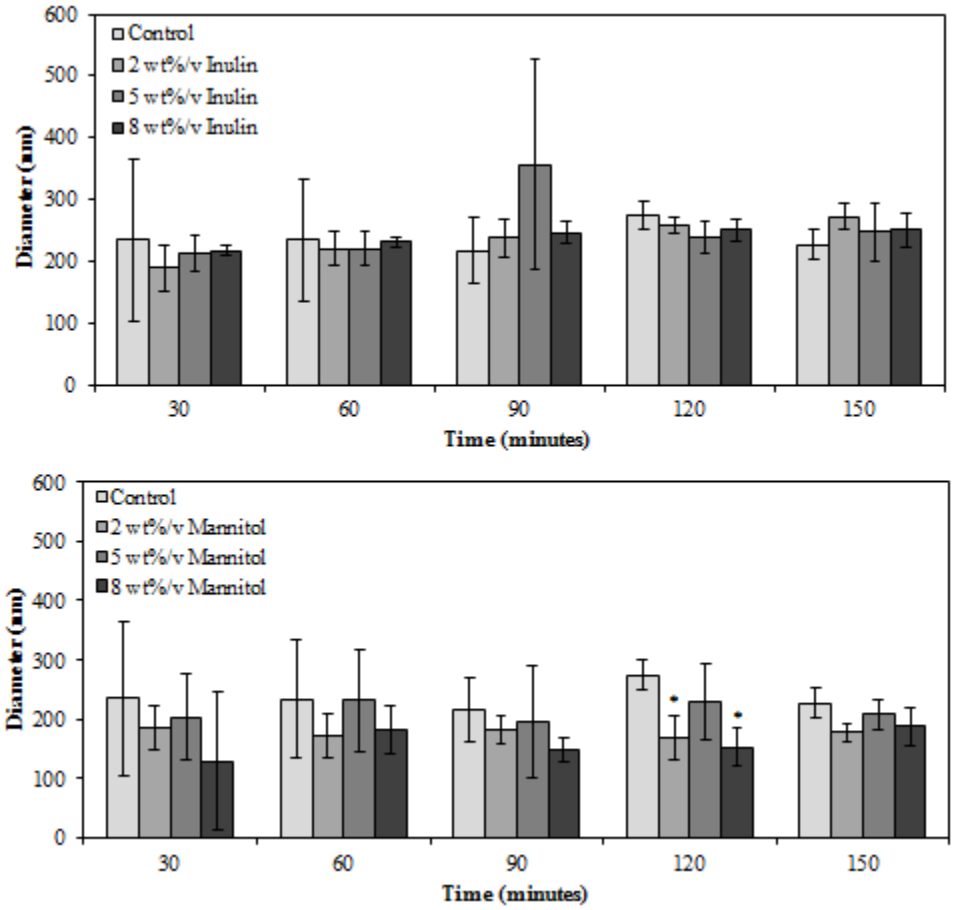

Figure 4.1. Particle Size Distributions Pre-Lyophilization with the incorporation of various concentrations of Inulin (top) and Mannitol (bottom). *Data presented here is after the use of a 450 nm membrane. (Top) Inulin has negligible effects on diameter of polymersomes when compared to control at most concentrations and time points. No statistical differences in diameters were found comparing all concentrations of inulin to control polymersomes. There were also no statistical differences between polymersome diameters using different inulin concentrations. (Bottom) Diameters are statistically the same with the incorporation of mannitol when compared to control at all time points other than 120 minutes. At 120 minutes, the incorporation of both 2 wt%/v and 8 wt%/v mannitol led to statistically smaller polymersome diameters compared to control ($p < 0.025$). No statistical differences were found between polymersome diameters when comparing the different concentrations of mannitol at any time point.*

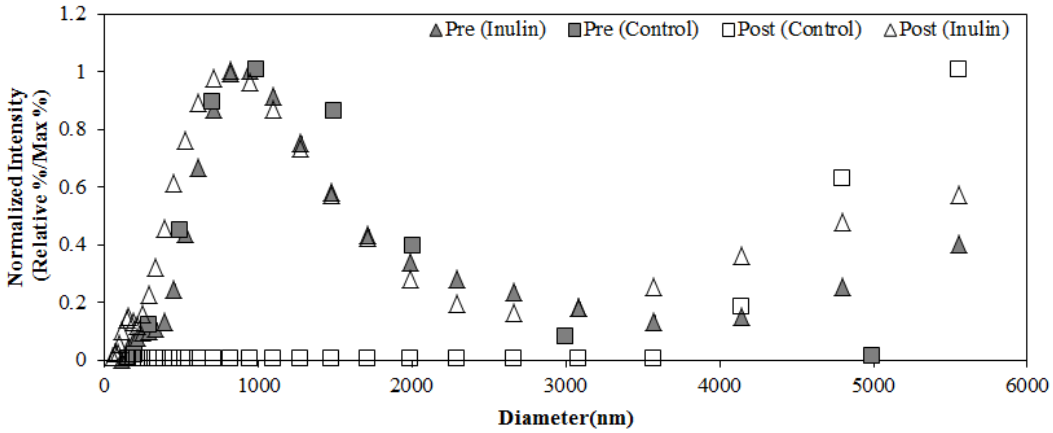

Figure 4.2. Representative Particle Size Distributions Before and After Lyophilization. *All distributions presented are prior to membrane separation to demonstrate particle size distribution. Intensity values at each diameter were normalized, with the maximum intensity in each distribution set to be equal to one to allow for appropriate comparison between distributions. "Pre" distributions are those prior to lyophilization and "Post" distributions are those after lyophilization. Without lyoprotectants, the peak in polymersome diameter before and after lyophilization was ~1000 nm and 5750 nm, respectively. With the addition of 8 wt%/v inulin, the peaks in polymersome diameter before and after lyophilization were both ~1000 nm. Also, the entire distribution was followed much more closely after the addition of 8 wt%/v inulin. In the therapeutic target range of < 200 nm, particle size post-lyophilization was only maintained in the presence of lyoprotectants.*

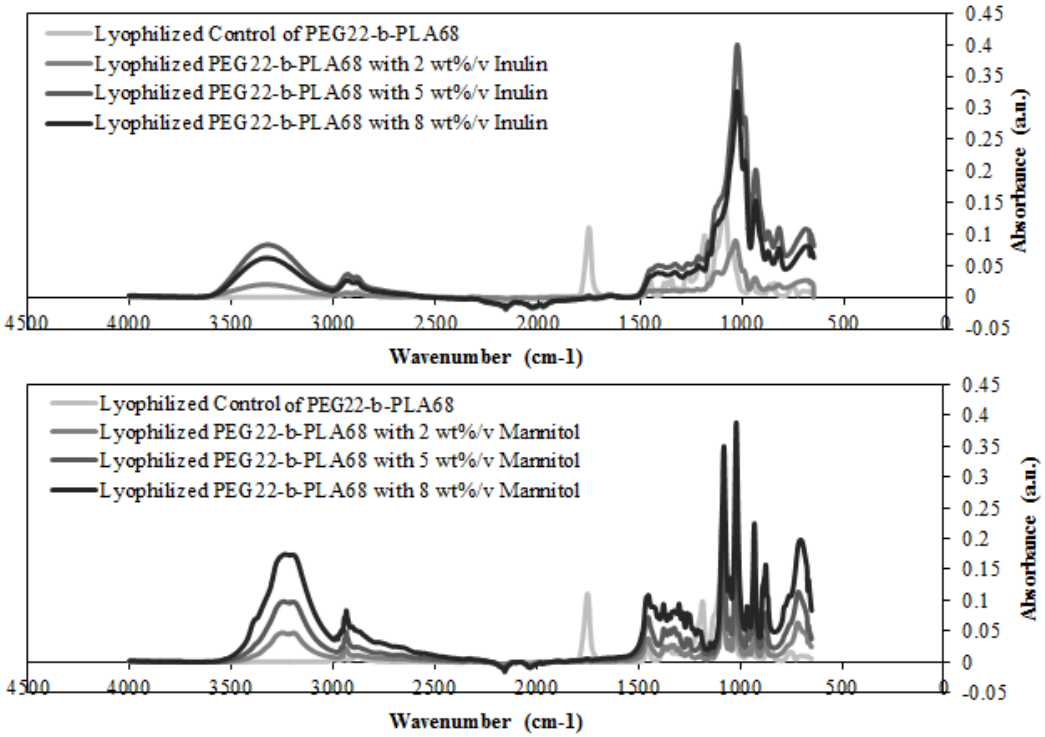

Figure 4.3. Baseline-Adjusted ATR-FTIR Spectra of Control Polymersomes and Lyoprotectant molecule incorporated Polymersomes. *Inulin spectra (top) indicate the presence of inulin at all concentrations due to the presence of a large band around 3200 cm^{-1}, indicating OH bonds. Mannitol spectra (bottom) indicate the presence of mannitol in the lyophilized polymersomes at all concentrations studied. The absorbance found at 3200 cm^{-1} increases with increasing concentration.*

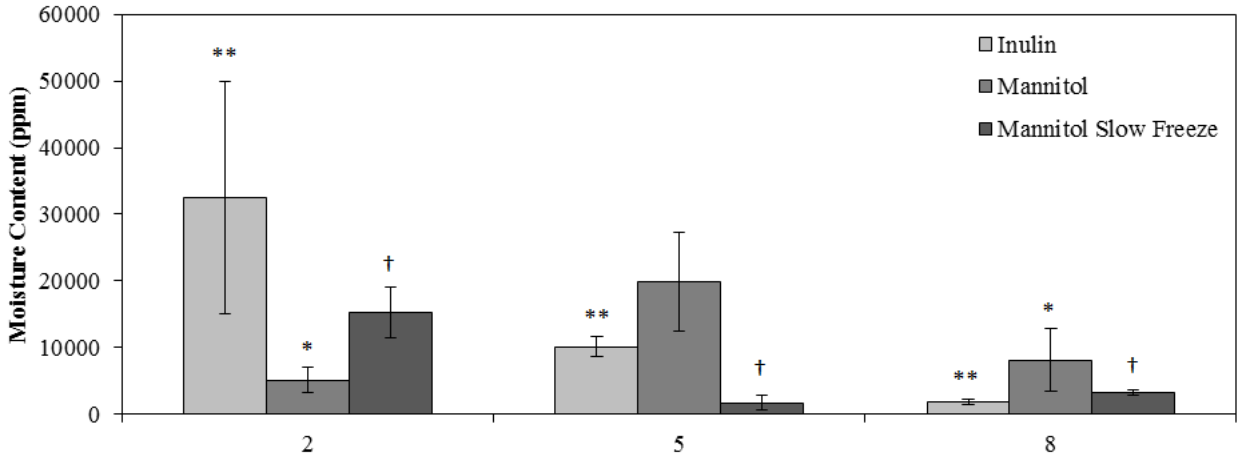

Figure 4.4. Moisture Content in Lyophilized Polymers with Lyoprotectant Molecules at Various Concentrations. *With respect to inulin, moisture content decreased with increasing concentrations incorporated during formation. Each concentration of inulin showed a statistically different moisture content compared to all other concentrations (** compares the concentration of inulin to both other concentrations, $p < 0.01$). Inulin and mannitol had statistically different moisture contents at both 2 and 8 wt%/v (* compares inulin to mannitol at the same concentration, $p < 0.05$). There was no statistical difference between moisture contents for all concentrations of mannitol. Mannitol slow freeze data was statistically different from its fast freeze counterparts († compares mannitol fast freeze data to mannitol slow freeze data at the same concentration, $p < 0.05$)*

Table 4.1. Particle Size Stability with Various Concentrations of Lyoprotectants after Lyophilization. *Normalized particle sizes were calculated by dividing post-lyophilization diameter by pre-lyophilization diameter. The incorporation of any lyoprotectant molecule at any concentration showed a significant improvement in normalization (*p<0.05).*

Lyoprotectant	Concentration (wt%/v)	Normalization
None	*0*	*4.63 ± 0.010*
Mannitol	2	0.54 ± 0.008*
Mannitol	5	0.84 ± 0.009*
Mannitol	8	0.78 ± 0.004*
Inulin	2	1.22 ± 0.008*
Inulin	5	0.87 ± 0.008*
Inulin	8	0.99 ± 0.009*

Chapter 5: Polyethylene glycol-b-Poly(lactic Acid) Polymersomes Encapsulate Bovine Serum Albumin and β-Galactosidase

Building on knowledge gained in Chapters 3 and 4, PEG-b-PLA polymersomes were encapsulated with proteins in an attempt to extend enzyme replacement therapy (ERT) to the brain. ERT has never been able to treat neuropathic manifestations of lysosomal storage disease (LSD) due to the presence of the blood-brain barrier (BBB). In order to effectively treat the brain, techniques need to be used to mitigate the transport of the missing enzyme through the blood-brain barrier. Polymersomes are nano-vesicles created from block co-polymers via self-assembly [*4*], with the potential to encapsulate and protect active enzymes in the blood-stream. PEG, as an hydrophilic block, increases the half-life of polymersomes over the circulation time of liposomes through limiting protein adsorption [*230, 231*]. PLA is a hydrolytically cleavable polymer with the ability to preferentially porate and degrade in neural lysosomes and release the encapsulated enzyme [*167, 232*].

PEG-b-PLA is used to form polymersomes for the purpose of encapsulating enzymes and proteins, using both bovine serum albumin (BSA) and bovine β-galactosidase (βgal) as model therapeutics. Prior to this dissertation, high molecular weight molecules, like proteins, have not been encapsulated in nanoparticles. Based upon the small size of nanoparticles, it is difficult to get a therapeutically-relevant dose of high molecular weight molecules incorporated. It is clear that the ability to deliver targeted proteins would make a large impact on the treatment of LSDs and all other enzyme-

oriented diseases, with the potential to change treatment methods to make them more disease specific and biologically relevant.

5.1. Materials and Methods

5.1.1. Polymersome Assembly

Polymersomes were created via solvent injection method. Polyethylene glycol(1000)-b-Poly(lactic acid) (5000) (PEG-b-PLA) was dissolved in dimethyl sulfoxide (DMSO) at 2 μmol/mL. The solution with dissolved PEG-b-PLA was injected into stirring water and 2 wt%/v mannitol at a constant rate of 1.062 μL/min using a 21 gauge needle and a syringe pump. After formation, polymersome diameters were measured via dynamic light scattering (DLS) in a ZetaSizer Nano (Malvern). Polymersomes were frozen slowly in a -20°C freezer overnight and lyophilized under sublimation conditions (0.040 mbar and -52 °C) for further use. Lyophilization allows for long term storage for future intravenous injections [*220*] and maintenance of polymersome properties over an extended period of time [*8*].

5.1.2. Protein Encapsulation during Formation

BSA was dissolved in 10 mL of stirring water at a concentration of 1 mg/mL prior to the injection of DMSO with PEG-b-PLA. This allowed for PEGPLA polymersomes to self-assembly around the existing BSA. After complete injection of the PEG-b-PLA in DMSO, approximately two hours, a 1 mL aliquot from the solution was placed into a 1000 kDa Float-a-Lyzer for four hours. Absorbance measurements at 280 nm were taken on dialysate samples to monitor loading of BSA.

5.1.3. Protein Encapsulation and Release after Lyophilization

BSA or βgal was dissolved in water at a concentration of 1 mg/mL. Concentrated solutions were added drop wise to lyophilized polymersomes to load the molecules into polymersomes. Following encapsulant loading, loaded polymersomes were placed into dialysis devices, Float-a-Lyzers (Spectrum Labs, 1000 kDa Molecular Weight Cut Off (MWCO)), which allowed unencapsulated material to dialyze through the membrane for a period of four hours. Dialysates were measured for absorbance at a wavelength of 280 nm for BSA and 230 nm for βgal in a Biotek microplate reader and compared to a standard curve to calculate encapsulant loading using the following equation:

$$Loading\ (\%) = \frac{mass\ added\ to\ polymersomes - mass\ released\ into\ dialysate}{mass\ added\ to\ polymersomes}$$

After removing any unencapsulated therapeutics via dialysis, loaded polymersomes were placed into either 0.1 M Tris buffer at pH 7.4 or 0.1 M acetate buffer at pH 4.8 for 24 hours. Dialysates were collected and analyzed in a microplate reader to determine mass released over the 24 hour period.

5.2. Results and Discussion

First, estimations on the number of molecules of BSA and βgal it was possible to encapsulate in a 200 nm polymersome, assuming that the proteins have closely packed atoms in their interior and were encapsulated in the most dense arrangement, using the following equations (Table 5.1) [*7*]:

$$V(nm^3) = \frac{\left(\frac{1}{\rho}\right)\left(\frac{cm^3}{g}\right) x\ 10^{21}\ \left(\frac{nm^3}{cm^3}\right)}{6.023\ x\ 10^{23}\ \frac{Da}{g}}\ x\ M\ (Da)$$

$$R_{min} = 0.066M^{1/2}$$

In lyoprotectant studies, mannitol was added as an encapsulant. Based upon mannitol's low molecular weight and size, it was able to be encapsulated at a high efficiency, with around 535 molecules per 200 nm polymersome. However, when introducing much larger molecular weight molecules, encapsulation becomes more difficult. It was estimated that only around 75 molecules of BSA and between 67 and 74 molecules of β-galactosidase were encapsulated, based on reports of varying molecular weight [*233–235*].

BSA was able to be encapsulated into polymersomes without affecting the polymersome diameter (Figure 5.1), which means polymersomes remain small enough to cross the BBB. BSA was successfully encapsulated both during and after formation (Figure 5.2). During formation, BSA was added to the stirring water prior to PEG-b-PLA injection, allowing for the formation of polymersomes around BSA. At first glance, it appears as if BSA was encapsulated at a high efficiency in this case, 90.0 ± 1.57%. However, in order to calculate the amount of BSA loaded, a number of assumptions needed to be made. From the 10 mL of stirring water, a 1 mL aliquot was taken for dialysis. The taking of this aliquot assumed uniform mixing of BSA and a uniform distribution of polymersomes. It was assumed that a mass of polymersomes taken is equal to one tenth of the mass of PEG-b-PLA added and that approximately one tenth of the

BSA added is in this aliquot prior to dialysis. When adding BSA in a concentrated 1 mL solution to lyophilized polymersomes, we have more control over both the mass of polymersomes and the mass of BSA in the dialyzed solution. Therefore, the loading efficiency of 31.6 ± 18.9% appears to be a more reliable figure. Compared to literature values, this loading percentage appears high [*236*]. However, we added a lesser mass of BSA, meaning that encapsulation could occur more efficiently.

Because of the greater reliability in the encapsulation efficiency determined using lyophilized polymersomes, βgal was also loaded in this manner, at an efficiency of 86.2 ± 12.2% (Figure 5.3). Again in this case, encapsulation efficiency is greatly dependent on the mass of encapsulant added. With only 1 mg βgal added, we obtain a high loading efficiency and a loading amount of 0.07 ± 0.01 mg βgal/mg PEGPLA polymersomes.

Polymersomes loaded after lyophilization with BSA were placed into both a pH 7.4 tris buffer and pH 4.2 acetate buffer to mimic physiologic and lysosomal conditions respectively (Figure 5.4A). In pH 7.4, there was a very limited amount of BSA released into the dialysate over 10 hours, indicated by only around a 10% by mass release. In contrast, when placed into pH 4.2, BSA release remained limited for a period of approximately 4 hours before demonstrating a burst effect, showing a large increase in release for the final 6 hours studied. Noticeable here is that the release behavior is as expected, based upon the poration of PLA at a low pH as it undergoes hydrolytic cleavage. PLA is a weak ester, which is protonated by hydrogen ions, allowing nucleophilic attack by water molecules and degradation of a higher molecular weight

polymer to a lower molecular weight polymer [*237*]. However, the calculated amounts of mass released were far too high based upon the calculated mass loaded.

Considering acetate buffer may be the problem, as acetate has the ability to cross-link any free amines that may be in solution, polymersomes loaded with βgal were placed into both a pH 7.4 tris buffer and a pH 4.8 citrate buffer to mimic physiologic and lysosomal conditions respectively (Figure 5.4B). Again, limited release of encapsulated βgal was found in the dialysates under pH 7.4 conditions, as expected. Very similar to the behavior of BSA released, under pH 4.8 conditions, a burst release of βgal from PEG-b-PLA polymersomes was observed over a period of 6 hours. Although the burst effect, again, is expected behavior, the mass of βgal found in the dialysate was around three times greater than the mass of βgal calculated to be encapsulated, which posed a major problem in proving the release mechanism from PEG-b-PLA polymersomes. This change in buffer did not necessarily change the release behavior of the protein.

When calculating protein concentration found in the dialysates, absorbance measurements were taken in a UV transparent plate at a wavelength of 280 nm. At this wavelength, the great majority of proteins will demonstrate some absorbance [*238*]. Although glassware is thoroughly cleaned and autoclaved, there may be other proteins adsorbing to the surfaces of the glass during dialysis, as proteins readily adsorb to solid-liquid interfaces [*239*]. This may limit our ability to calculate the concentration of one specific protein in the dialysate during both loading and formation, therefore skewing our data to a concentration of protein released greater than the concentration of protein added.

This increased protein adsorption to the surface of the beaker leaders to a lower calculated mass encapsulated than is actually occurring. In the case of release calculations, this increased protein concentration in the dialysate would lead to an increased amount of protein released under both conditions. These two conditions lead to a compounded error in the same direction, which is causing the very large amounts of protein released under pH 4.8 conditions. As glassware may be interfering with absorption measurements, fluorescence measurements are used to further refine loading and release calculations in Chapter 6.

5.3. Conclusions

It is clear from the results that both BSA and βgal are encapsulated into 200 nm polymersomes without negatively affecting the polymersome diameters, ensuring the brain delivery of loaded polymersomes is still a possibility. It is more difficult to determine is the exact amount of these two proteins successfully encapsulated and therefore, also difficult to determine the exact amount of these two proteins released under various pH conditions. The data demonstrates the difficulty in calculating protein content using absorbance. Because of this, loading and release studies of βgal are changed to include fluorescent measurements through the tagging of βgal with Alexa Fluor 488, a green fluorescent dye in Chapter 6.

5.4. Figures and Tables

Table 5.1. Relative Density, Molecular Weight, Volume, and Radius of Encapsulant Materials. Based upon [*7*], density and molecular weight were used to estimate the volume and radius of materials encapsulated into PEGPLA polymersomes. Using average polymersome sizes of around 200 nm, an estimated number of molecules per polymersome was established in the final column. The encapsulation of high molecular weight materials is much more difficult, as less molecules are capable of encapsulation on the nanoscale

Material	Density (g/cm^3)	Molecular weight (Da)	Volume (nm^3)	R_{min} (nm)	Molecules Encapsulated
Manntiol	0.43	182	0.703	0.37	535
β-galactosidase	1.37	68,000	82.4	2.69	74.2
		94,000	114	3.00	66.6
BSA	1.32	66,430	83.6	2.67	74.8

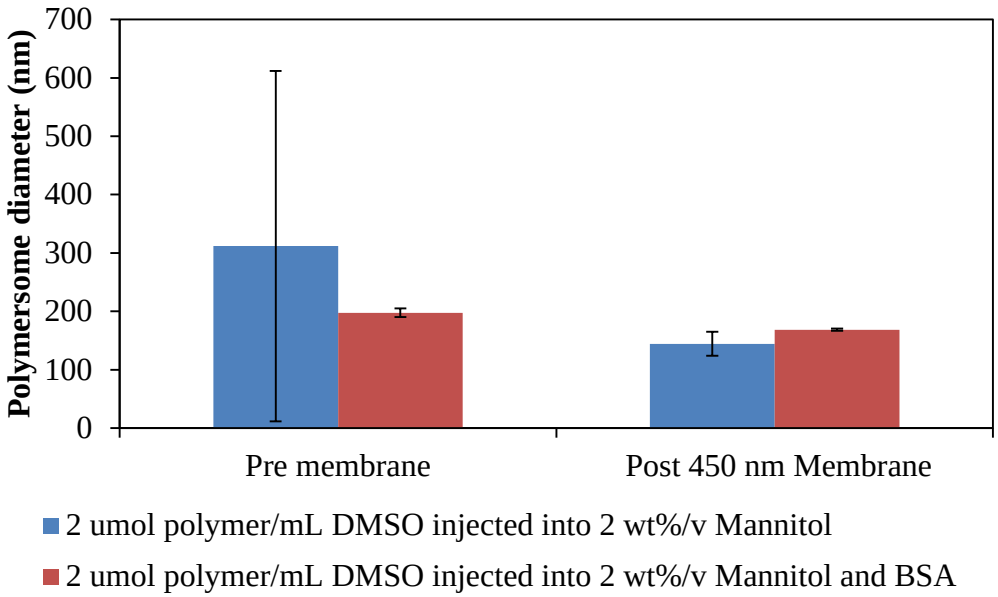

Figure 5.1. Average Polymersome Diameter after BSA Encapsulation. *Polymersomes loaded with BSA after lyophilization were measured via DLS. It was determined that there was no significant difference between empty polymersomes and BSA=loaded polymersomes ($p<0.05$).*

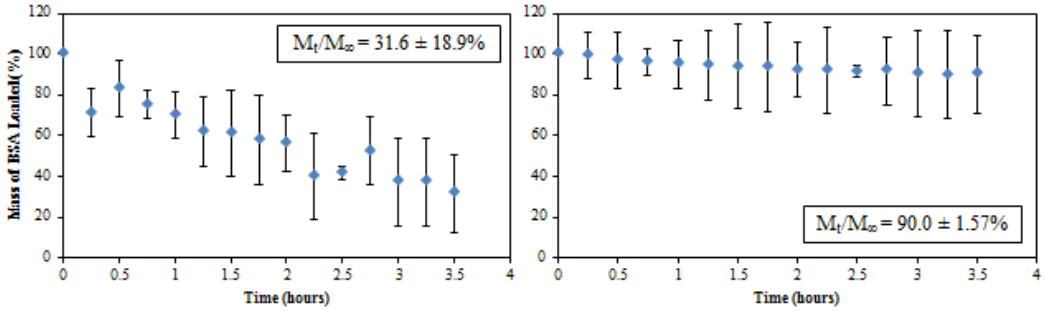

Figure 5.2. BSA Loading after Lyophilization (left) and during Formation (right). *Polymersomes loaded during formation (n=3) showed a higher loading efficiency than polymersomes loaded after lyophilization (n=3). However, difficulty in consistent mass balances may account for this difference.*

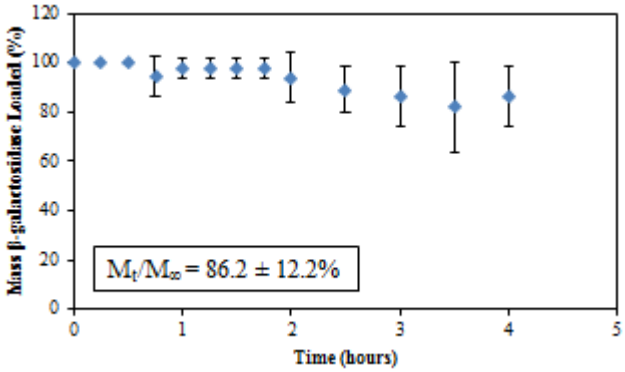

Figure 5.3. Loading Efficiency of βgal in Lyophilized Polymersomes. *Bgal was loaded at a high efficiency of 86.2 ± 12.2% into lyophilized polymersomes through a dropwise addition of 1 mg/mL βgal in water.*

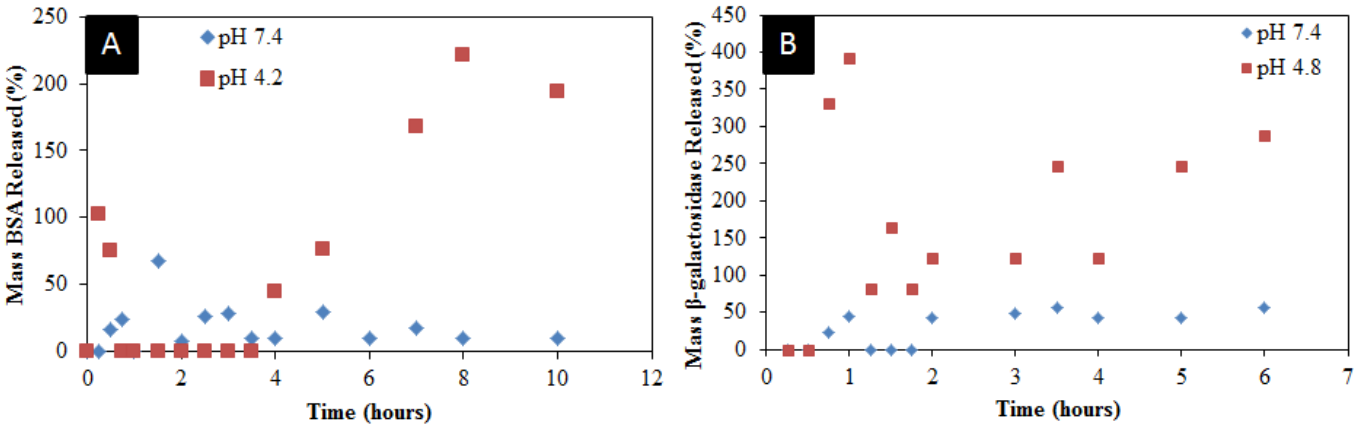

Figure 5.4. Release of BSA (A) and βgal (B) in pH buffers. *(A) It is clear that a larger amount of BSA is released over a period of 10 hours in a pH 4.2 versus a pH 7.4 buffer. However, the calculated amounts released exceeded the calculated amounts loaded. (B) It is clear that a larger amount of βgal is released in a pH 4.8 versus a pH 7.4 buffer. However, like BSA release, the calculated amounts released far exceeded the calculated amounts loaded. BSA release occurred in an acetate buffer and βgal release occurred in a citrate buffer.*

Chapter 6: Polyethylene glycol-b-Poly(lactic acid) Polymersomes as Vehicles for Enzyme Replacement Therapy

In this chapter, PEG-b-PLA polymersomes are presented as vehicles for ERT through loading and *in vitro* delivery of fluorescently-tagged βgal. This work was submitted for publication in Nanomedicine: Nanotechnology, Biology, and Medicine [*240*]. There are around 100 inherited metabolic disorders, resulting from a genetic mutation that leads to defective production of one necessary enzyme [*241*], with only around 20% of these diseases currently treatable and the majority bringing premature death. Falling into this category are neuropathic LSDs [*22*, *30*], which result from enzyme deficiencies that cause accumulation of undegraded substrate and swollen lysosomes [*242*]. Symptoms of neuropathic LSDs are extensively explained elsewhere [*243*]. If the brain is not involved, patients with LSDs may receive weekly to bimonthly infusions of purified enzymes that can enter cells and ameliorate systemic symptoms in a method of treatment called ERT. ERT has shown enormous clinical success in LSD patients, with 11 injectable and 3 oral ERT agents [*119*]. However, these treatments cannot cross the BBB and are rendered ineffective in neuropathic patients. Targeted treatment of the brain parenchyma through the vasculature would be ideal, as the average distance between a capillary and a neuron is only 8-20 μm [*10*], which would allow for more uniform treatment of the brain than traditional surgical injections.

Building on current ERT technology, with the goal of using noninvasive treatment pathways, nanoparticle drug delivery systems [*244–247*] and fusion proteins [*111*, *114*, *116*, *248*, *249*] are being explored to transport lysosomal enzymes across the BBB. However, complications with treatment arise related to protection of enzymatic function.

Small changes in the enzyme structure and folding can completely change activity, with some diseases resulting directly from misfolding [*250*]. Secondly, functional enzymes, although targeted to mannose-6-phosphate receptors for cellular uptake [*117*], are not targeted to specific tissues where the enzyme is needed most. Therefore, an optimal ERT vehicle crossing the BBB requires both a method of protection in the blood stream and a targeting ligand that permits transcytosis to neural cells.

Polymersomes fit both of these requirements and therefore have potential in brain delivery applications. They have a demonstrated ability to protect enzymes from degradation in the blood stream and encapsulate multiple therapeutics. Polymersomes also have versatility in release mechanisms and ligand attachment through a multitude of applicable bioconjugation techniques based upon polymer choice [*4–6*, *108*, *251*]. Polymersomes are made up of amphiphilic co-polymers that will self-assemble into vesicles when PEG is the hydrophilic component, or "block," and is present in a fraction between approximately 25 and 40% [*4*]. PEG is used in nanoparticle delivery to increase the half-life of particles in the blood stream, through limiting the adhesion of undesirable proteins that target nanoparticles for phagocytosis or non-specific cellular uptake [*252*]. PLA comprises the hydrophobic membrane of the polymersome due to its biodegradable nature, which allows for tuned release of therapeutic. The molecular weight of the amphiphile contributes to polymersome diameter [*4*, *253*] so that polymersomes can encompass a wide range of diameters, making them applicable as drug delivery vehicles for a variety of biological targets. PEG and PLA have already been approved by the FDA for different routes of administration [*3*, *108*]. Polymersomes also have increased

stability and increased *in vivo* circulation time [*167*, *253*] compared to PEGylated liposomes, which are currently used in four FDA approved medical treatments [*254*], which make them desirable vehicles for targeted drug delivery.

Although polymersomes have demonstrated potential to transport small molecules and drugs across *in vitro* models of the BBB, this is the first time they have been used in enzymatic treatments. Here PEGPLA polymersomes demonstrate the capacity to both encapsulate and release lysosomal β-galactosidase (βgal; EC 3.2.1.23) while maintaining its activity. Also, conjugation with an appropriate targeting ligand demonstrates that PEG-b-PLA polymersomes have promise as an effective nanoparticle-mediated ERT for CNS disease. Inherited metabolic disorders, including lysosomal storage disorders, would benefit greatly from an enzyme delivery vehicle that could cross the BBB, making therapy possible for currently untreatable and fatal childhood diseases.

6.1. Materials and Methods

6.1.1 Materials

Co-polymer with 16.67% polyethylene glycol (PEG, molecular weight = 1000 Da) blocked with the remainder poly(lactic acid) (PLA, molecular weight = 5000 Da) was used in all polymersome formation studies (Polyscience, Inc). Mannitol (Sigma Aldrich) at a concentration of 2 wt%/v was used as a lyoprotectant in all polymersome formation studies [*255*]. Millex syringe filter units of pore sizes 0.45 μm (Millipore) were used when stated. Homobifunctional PEG (molecular weight = 2000 Da) with NHS groups (JenKem Technology USA) was used to facilitate ligand attachment to the polymersome surface. Both a blue reactive fluorophore, CF350 Amine, and a red reactive

fluorphore, CF647 Amine, were used in ligand attachment (Biotium, Inc). Alexa Fluor 488 (AF488) (Thermo Fisher) was used as a market dye, and βgal isolated from bovine liver (Sigma Aldrich) was the tested therapeutic. Dialysis was performed using Float-a-Lyzer dialysis devices with a MWCO of 1000 kDa (Spectrum Labs). AF488 Protein Labeling Kit (Life Technologies) was used to fluorescently tag βgal.

6.1.2. Polymersome Synthesis

Polymersomes were created via solvent injection method. Polyethylene glycol(1000)-b-Poly(lactic acid) (5000) (PEG-b-PLA) was dissolved in dimethyl sulfoxide (DMSO) at either 2, 20, or 50 μmol/mL. The solution with dissolved PEG-b-PLA was injected into stirring water and 2 wt%/v mannitol at a constant rate using a 21 gauge needle and a syringe pump. After formation, polymersome diameters were measured via dynamic light scattering (DLS) in a ZetaSizer Nano (Malvern). Polymersomes were frozen slowly in a -20°C freezer overnight and lyophilized under sublimation conditions (0.040 mbar and -52 °C) for further use. Lyophilized polymersomes were reconstituted in solution for characterization via TEM. Normalization values were determined using previously published techniques [*8*].

6.1.3. Ligand Attachment on Polymersome Surface

Ligand attachment was facilitated during solvent injection. Both PEG-b-PLA at a concentration of 2, 20, or 50 μmol/mL and 1, 5 or 10 mg homobifunctional PEG (NHS-PEG2000-NHS) were dissolved in DMSO. The DMSO solution was injected into stirring water with 2 wt%/v mannitol and a 1:27 molar concentration of either CF647 Amine or CF350 Amine to NHS-PEG2000-NHS, with NHS-PEG2000-NHS in excess (Figure 6.1).

Attachment was confirmed via increase in polymersome diameter measured via DLS. Fluorescence microscopy allowed for the visualization of CF350 attachment using CytoViva Hyperspectral Fluorescence Microscopy. Polymersomes were fixed on slides using vectamount to maintain fluorescence prior to microscopy. Finally, slow-speed flow cytometry using a BD Accuri C6 Flow Cytometer, with appropriate color compensation controls, determined the number of particles labeled with CF647, using filter set 675/25 and AF488, using filter set 533/30. For flow cytometry, polymersomes were prepared with a red fluorescent ligand, CF647 Amine, and NHS-PEG(2000)-NHS to avoid bleed over between the blue and green channel when polymersomes were prepared with a fluorescent ligand and a fluorescent encapsulant simultaneously.

6.1.4. Encapsulant Loading and Release

AF488 or AF488 tagged βgal was dissolved in water at a concentration of 2 mg/mL. Concentrated solutions were added drop wise to lyophilized polymersomes to load the molecules into polymersomes. Following encapsulant loading, loaded polymersomes were dialyzed to remove unencapsulated material for a period of four hours (Figure 6.2, Steps 1-3). Dialysate samples were taken every fifteen minutes for the first two hours then and every half hour until the completion of the experiment. Dialysates were measured for fluorescence in a microplate reader and compared to a standard curve to calculate encapsulate loading using the equation in Chapter 5.

After removing any unencapsulated therapeutics via dialysis, loaded polymersomes were placed into either 0.1 M HEPES buffer at pH 7.4 or 0.1 M citrate buffer at pH 4.8 for 24 hours. Dialysates were collected and analyzed in a microplate

reader to determine mass released over the 24 hour period (Figure 6.2, Steps 4 and 5). βgal activity was calculated with the synthetic fluorogenic substrate, 4-methylumbelliferyl (4MU)-β-D-galactoside, as described [*256*].

6.2. Results and Discussion

PEG-b-PLA copolymer has been proven to self-assemble, forming vesicle structures within both DMSO and water. The solvent injection method was employed using a constant syringe pump rate of 1.062 µL/min. PEG-b-PLA polymersome diameters are highly tunable using the injection method through changing the initial block copolymer concentration, demonstrating PEG-b-PLA polymersomes are capable of being used in a wide variety of drug delivery applications. With PEG-b-PLA concentrations of 2, 20, and 50 µmol/mL, polymersomes formed at overall average diameters of 388.6 ± 108.4 nm, 574.9 ± 36.2 nm, and 2018 ± 311.7 nm respectively (Figure 6.3). Statistically, major variations in polymersome diameter occurred in the hydrodynamic diameter bin of 200 nm. Most notably, 2 µmol/mL PEG-b-PLA led to the formation of 74% of polymersomes with a diameter less than or equal to 200 nm (when summing the number of particles in both the 100 nm and 200 nm bins), the target size for potential delivery through the BBB using receptor mediated transcytosis [*215*], without the use of any extrusion or separation techniques. When using either 20 µmol/mL or 50 µmol/mL, a maximum of only 11 and 3% of polymersomes respectively fall into the desirable size range of 200 nm or less, to delay liver uptake and avoid kidney filtration [*215*].

Using 450 nm membrane filters during assembly produced smaller PEG-b-PLA polymersomes, with more narrow distributions, with a statistical decrease in polymersome diameter in both intensity-weighted and z-average size distributions when comparing initial PEG-b-PLA concentrations of 2 μmol/mL to 20 and 50 μmol/mL. Also important, PEG-b-PLA polymersomes formed using and initial copolymer concentration of 2 μmol/mL maintain their size following lyophilization, which is important for encapsulant loading and release (Table 6.1). Based on published polymersome equations [*125*], PEG-b-PLA polymersomes have a hydrophobic membrane core thickness around 3 nm, which is similar to the size of liposomal membranes [*172*, *257*]. Size distributions were highly similar to polymersome diameters formed using the same technique and a similar hydrophilic fraction of PEG-b-PLA [*215*]. Because of this, all loading, release, and attachment studies were performed using polymersomes formed with 2 μmol/mL PEG-b-PLA.

Ligand attachment was facilitated during polymersome formation via the injection method. The introduction of a functionalized PEG strand through the membrane using NHS-PEG(2000)- NHS allowed for the attachment of ligands with free amine groups. This bioconjugation chemistry allowed for the attachment of proteins, which have amine groups available for binding and can target receptors upregulated on the surface of the BBB. Control polymersomes, formed with 2 μmol/mL PEG-b-PLA and 2 wt%/v mannitol, formed at a diameter of 145 ± 21 nm after membrane extrusion (Table 6.1). Using either 1 mg or 5 mg of NHS-PEG(2000)-NHS and corresponding molar amounts of CF350 Amine, there was no statistical increase in polymersome diameter, indicating

that consistent ligand attachment was not achieved. Large variability of polymersome diameters was observed when using 5 mg of NHS-PEG(2000)-NHS to facilitate ligand attachment, with an average polymersome diameter of 203.8 ± 67.8 nm (Figure 6.4A), suggesting inconsistent attachment of CF350 between samples.

With the introduction of 10 mg NHS-PEG(2000)-NHS and appropriate amounts of CF350 amine, a statistical increase in polymersome diameter over control to 210 ± 8.6 nm was observed, demonstrating effective ligand attachment (Figure 6.4A). This large increase in size is expected due to the addition of an increased length PEG strand, PEG2000, as well as the CF350 molecule onto PEG-b-PLA polymersome surfaces, which are comprised of PEG1000. Ligand attachment was confirmed with hyperspectral fluorescence microscopy (Figure 6.4B), which showed the majority of polymersomes being labeled with a fluorescent blue color around the exterior of the vesicle. Flow cytometry confirmed ligand attachment, using CF647 instead of CF350 to avoid bleed-over between fluorescent channels, observed with both dynamic light scattering and microscopy, showing that 79.4 ± 21% of polymersomes were labeled with red fluorescence with the use of 10 mg NHS-PEG(2000)-NHS (Table 6.2). It is clear from the data that the use of 10 mg NHS-PEG(2000)-NHS with corresponding molar amounts of either CF350 Amine or CF647 Amine has the ability to facilitate ligand attachment, showing the promise of PEG-b-PLA polymersomes to attach an appropriate targeting protein to cross the BBB.

Having demonstrated attachment of a ligand to the polymersomes, the next step was to test their encapsulation ability. Encapsulation was confirmed through the use of

AF488 only using both hyperspectral fluorescence microscopy (Figure C) as well as flow cytometry (Table 6.2). Microscopy demonstrated that polymersomes had a centrally located green fluorescence after introducing AF488. Flow cytometry demonstrated that after dialysis had removed any unencapsulated AF488, 90.1 ± 12.7% of polymersomes presented with green fluorescence (Table 6.2). Furthermore, flow cytometry measurements were done on polymersomes that were both encapsulated with AF488 and attached to CF647, showing that 86.7 ± 11.6% of polymersomes presented both colors. Thus, around 90% of polymersomes were capable of simultaneously attaching a mock targeting ligand and encapsulating a mock therapeutic. PEG-b-PLA polymersomes are potentially a valuable platform for the targeted delivery of therapeutics, with both high encapsulation and attachment efficiencies.

The ultimate goal of this research is to deliver lysosomal βgal to patients with GM1 gangliosidosis. Thus we explored βgal encapsulation in polymersomes. After being tagged with AF488 to permit visualization of encapsulation, βgal retained 24 ± 13% of its native activity. While the AF488 tag decreased the activity of βgal substantially, AF488 was used only to facilitate measurement of encapsulation and ultimately will not be included in the therapeutic construct. The enzyme of interest, βgal, was tagged with AF488 and encapsulated into PEG-b-PLA polymersomes at an efficiency of 72.0 ± 12.2% or 0.011 ± 0.008 mg AF488 βgal/mg polymersomes (Figure 6.5). Loading percentage was high in comparison to other loading studies [*219*, *258*, *259*] due to the low mass of 1 mg of βgal per 10 mg of polymersomes used as the driving force for encapsulation. However, when looking at loading by mass, PEG-poly(caprolactone)

particles were capable of loading NC-1900 as a therapeutic at a much higher quantitiy of ~0.19 mg NC-1900/mg polymersomes [*172*]. The same behavior was observed with a system entitled Polydoxsome, which saw a 24 times greater loading by mass of doxorubicin than what is observed when βgal is loaded into PEGPLA polymersomes [*215*]. This may be due to the dramatically decreased size of NC-1900 and doxorubicin in comparison to βgal, which may also have an impact on drug release behavior.

Dialysis data demonstrates that during the first hour of washing, the majority of unencapsulated AF488 βgal is removed through the membrane. Although the buffer is exchanged every hour to ensure that the system doesn't reach equilibrium and maintain a driving force for diffusion, there is no further removal of AF488 βgal during the final three hours. This four-hour washing period ensures that all AF488 βgal that was not encapsulated is removed from the polymersome solution before changing to release conditions.

PEG-b-PLA polymersomes are degradable by hydrolytic cleavage. PLA is an ester, making it a poor electrophile, which is attacked by H+ ions in solution to make this bond more electrophilic. As the electrophilicity of the ester increases, water can attack and degrade the bond in a simple hydrolysis reaction, leading to the degradation of the PLA membrane in PEG-b-PLA polymersomes. Because the driving force for this reaction is the protonation of the ester bond in PLA, PEG-b-PLA polymersomes should degrade more rapidly in an acidic environment, such as that of the lysosome. This behavior has been demonstrated previously in PEG-b-PLA polymersomes with release of small molecule therapeutics NC-1900[*172*], paclitaxel[*125*] and doxorubicin[*125*, *215*]. The

addition of block co-polymer blends of 75% PEG-b-Polybutadiene with 25% PEG-b-PLA in the formation of polymersomes has also been used to alter release profiles by changing the availability of degradable sites [*125*]. Such release behavior suggests that PEG-b-PLA polymersomes should release their payload more rapidly in the low-pH environment of the lysosome than in the neutral pH of the blood stream, making them the ideal nanocarriers for the treatment of LSDs.

When PEG-b-PLA polymersomes were placed in a 0.1 M HEPES buffer of pH 7.4, slow release of AF488 βgal from the membrane was observed, at an average rate of ~ 1 mass % per hour over the period of 24 hours. The rate of release was much more rapid when PEG-b-PLA polymersomes were place in a 0.1 M citrate buffer of pH 4.8, observed by ~ 3.5 mass % per hour release of AF488 βgal over the first 8 hours. The release curve in pH 7.4 maintained the same rate of release throughout the entire study period, indicating that in this case, PEG-b-PLA polymersomes display zero order kinetics of release, meaning the release from the polymersomes is independent of concentration. However, the rate of release demonstrated in pH 4.8 plateaued after 8 hours, with no further release observed over the next 16 hours, indicating that in the acidic case PEG-b-PLA polymersomes display Fickian release behavior, in which the release rate is affected by the concentration of encapsulant already released [*260*]. Mean release percentages of AF488 βgal were higher in the acidic buffer at all time points and achieved statistical significance at 6 and 8 hours, when they were 4.5 and 3-fold higher respectively than values from the neutral buffer ($p<0.05$; Figure 6.6). Thus, the release behavior of PEG-b-

PLA polymersomes in the current study is consistent with degradation through hydrolytic cleavage.

Previous reports with PEG-b-PLA polymersomes demonstrated release behavior similar to that of the current study over the initial 8 hours under acidic conditions. Unlike previous studies that encapsulated molecules < 1 kDa in size, including both NC1900 [*172*] and doxorubicin [*215*], we observed a plateau, demonstrating a highly decreased release rate of βgal, which ranges between 68 and 94 kDa depending on the species from which it is isolated [*233–235*]. In our case, βgal isolated from bovine liver is between 68 [*261*] and 68.7 [*262*] kDa in size. This ~125 fold difference in molecular size may be responsible for the plateau in release that is observed in our study, with release occurring rapidly close to the surface. We hypothesize that is more difficult for the large protein βgal to continue to transport through the pores that form in the polymersomes over an extended period of time, as some βgal may be blocking these pores through adsorption to the PLA membrane over time. It has been shown that hydrolysis of PLA, a degradable polymer, increases the adsorption of proteins [*263*]. Therefore, as PLA is becoming hydrolyzed under acidic conditions, βgal is both able to escape the polymersome and more likely to adsorb to the membrane, leading to potential pore blocking and the observed decreased release rate. Limited release could also be contributed to a concentration effect. We hypothesize that pores produced by cleavage of PLA require a concentration gradient to drive release of the relatively large βgal protein. If so, decreasing concentrations of βgal as it is released from inside the polymersome will eventually lead to decrease in the release forces. Nevertheless, the βgal release profile

reported herein suggests that PEG-b-PLA polymersomes may be a valuable platform for targeting the lysosomal compartment, where treatment is needed.

It has been demonstrated that PEG based amphiphiles can exist for an extended period of time in the circulation [*253*], necessitating minimal leakiness in the blood stream prior to delivery across the BBB and into neural cells. Initial studies indicate minimal leakiness of AF488 βgal from PEG-b-PLA polymersomes at physiologic pH (pH 7.4), such as the bloodstream, for at least 6 hours. When PEG-b-PLA polymersomes loaded with AF488 βgal were then moved into an acidic environment similar to that of the lysosome (pH 4.8), a burst release was observed and maintained over 2 days' time (Figure 6.7). This protection and maintenance of release behavior of AF488 βgal contributes to the burden of proof that PEG-b-PLA polymersomes demonstrate potential for delivery of enzymes through the BBB.

6.3. Conclusions

Polymersomes are easily formed with 2 μmol/mL PEG-b-PLA in a consistent, deliverable size range of 147.2 ± 24 nm after membrane separation. Polymersomes in this size range have the ability to encapsulate therapeutics and bind to targeting ligands, making them a promising vehicle for targeted drug delivery. Effective binding of CF350 and CF647 using NHS-PEG(2000)-NHS has been proven through DLS, fluorescence microscopy, and flow cytometry. PEG-b-PLA polymersomes were also able to encapsulate AF488-tagged βgal, the missing enzyme in GM1 gangliosidosis, at a relatively high efficiency. Enzymatic activity was maintained upon loading, ensuring that PEG-b-PLA polymersomes have the potential to protect active enzyme in the blood

stream. PEG-b-PLA polymersomes are also able to deliver enzyme preferentially under acidic conditions, like those that are present in the lysosome, demonstrated through release kinetics found in pH 7.4 and pH 4.8 buffers.

PEG-b-PLA polymersomes are drug delivery vehicles that have demonstrated potential to encapsulate and release therapeutics under specific conditions, with the ability to bind model targeting ligands with amine groups using techniques that are translatable to the attachment of BBB-penetrating proteins. Polymersome formation is tunable using the injection method, allowing for the creation of a multitude of size ranges necessary for different applications. The universal chemistry used in bioconjugation allows for the attachment of any targeting ligands with amine groups present, meaning that PEG-b-PLA polymersomes can be used to target many disease states. Finally, PEG-b-PLA polymersomes can encapsulate relatively high molecular weight enzymes while maintaining their activity, which has not yet been demonstrated in the literature. We have also demonstrated a high level of control over the creation of PEG-b-PLA polymersomes and will continue to pursue them as a platform for targeted enzyme delivery. With further development, PEG-b-PLA polymersomes may help change the way we treat LSDs with CNS involvement, making effective treatments available to patients. The ability of PEG-b-PLA polymersomes to effectively treat GM1 gangliosidosis felines was tested using a proof-of-concept cellular model in Chapter 7.

6.4. Figures and Tables

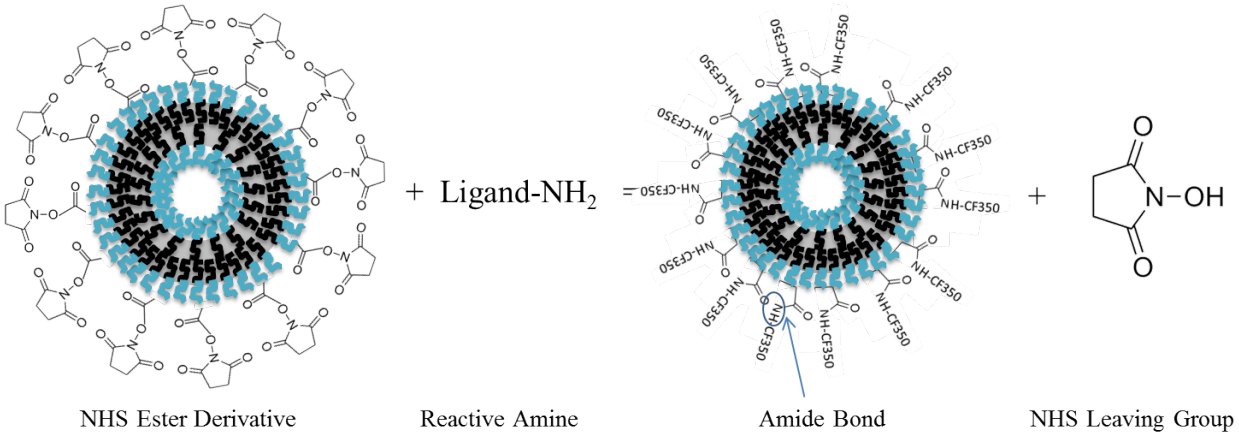

Figure 6.1. Schematic Illustrating the Attachment of Model Ligands to PEGPLA Polymersome Surfaces. *Polymersomes are made up of hydrophilic PEG (blue) and hydrophobic PLA (black). Through the introduction of an additional homobifunctional strand of PEG, some NHS ester groups become present on the surface of PEG-b-PLA polymersomes. NHS ester derivatives interact with available amine groups on a model ligand (in this case CF350 or CF647), forming an amide bond on the surface of PEG-b-PLA*

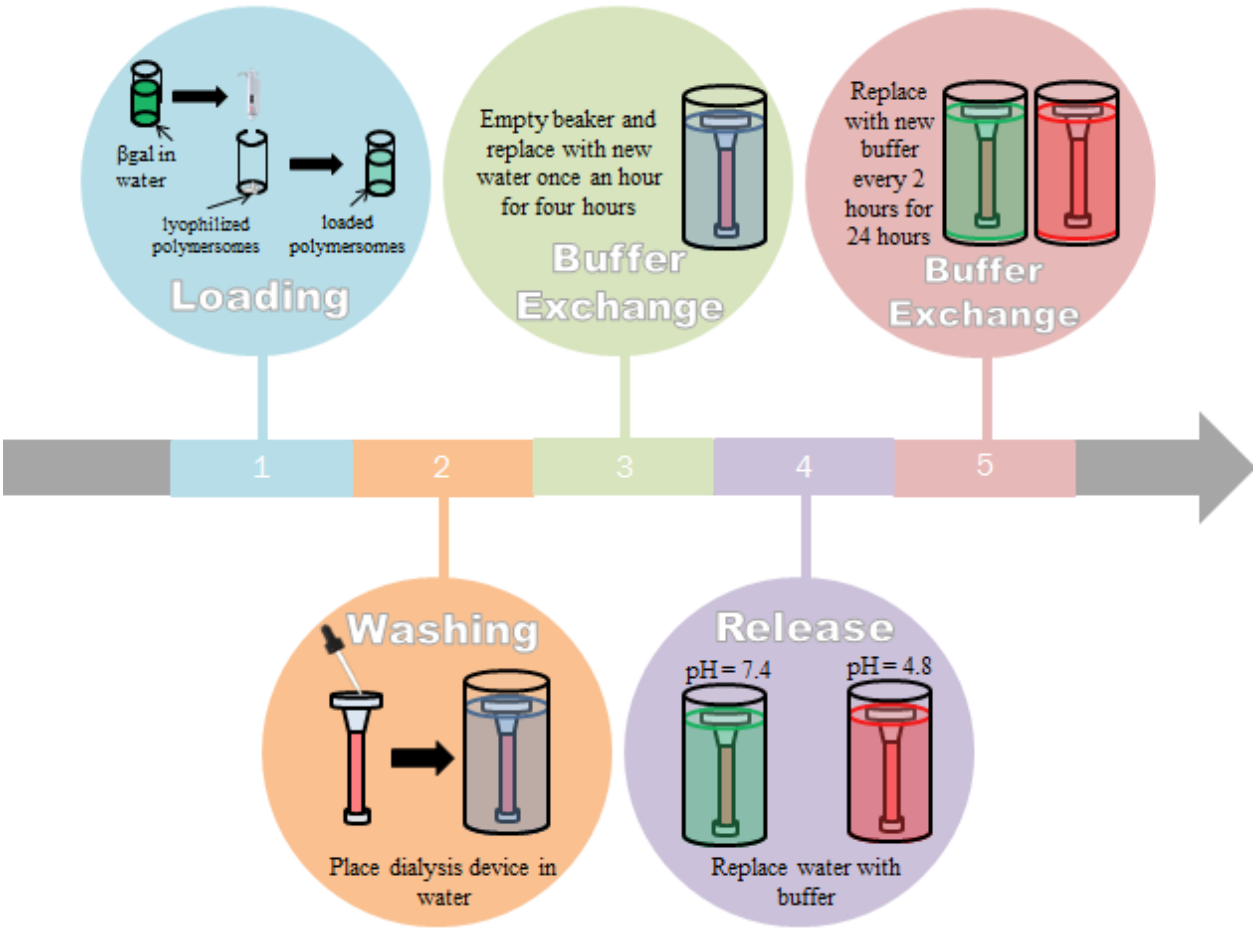

Figure 6.2. Timeline of Loading and Release Studies. *(1) Lyophilized polymersomes are loaded with AF488 βgal. (2) Loaded polymersomes were added into the inner membrane of a Float-a-Lyzer device, which were then placed in water for removal of any unencapsulated AF488 βgal. (3) The water was exchanged every hour for a period of four hours to ensure that an equilibrium in AF488 βgal concentration between the inside of the membrane and the dialysate was not reached prematurely. (4) Water was replaced with one of two buffers, either lysosomal (pH 4.8) or physiologic (pH 7.4). (5) The buffer was exchanged every two hours for a period of 24 hours to study the release over time.*

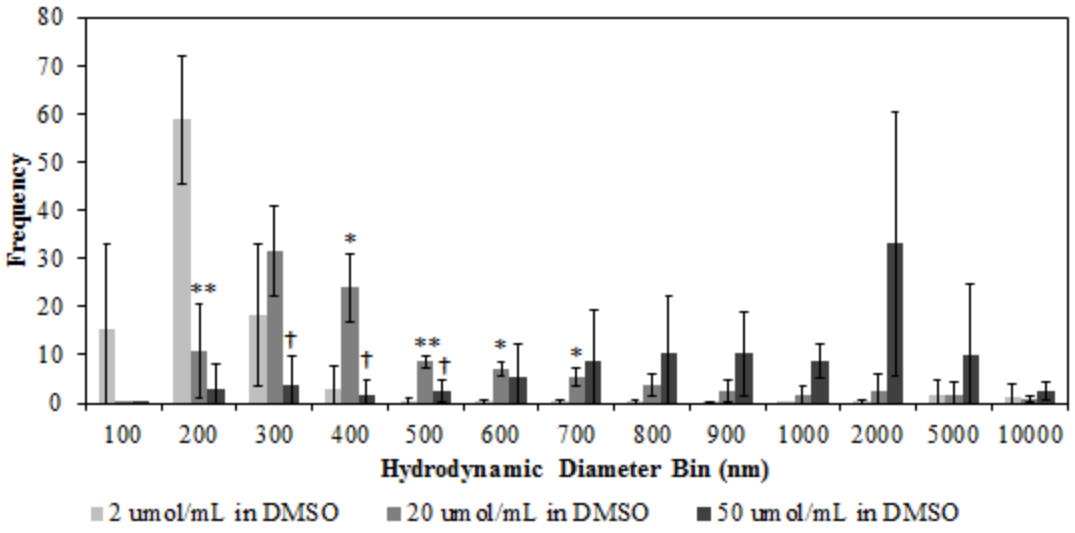

Figure 6.3. Histogram of Polymersome Diameters formed via the Injection Method. *Varying concentrations of PEG-b-PLA in DMSO prior to injection in water led to varying diameter distributions. Initial PEG-b-PLA concentrations of 2 µmol/mL led to an overall average polymersome diameter of 388.6 ± 108.4 nm, 20 µmol/mL led to an overall average polymersome diameter of 574.9 ± 36.2 nm, and 50 µmol/mL led to an overall average polymersome diameter of 2018 ± 311.7 nm. Shifting from low to high concentration leads to 74.2, 10.9, and 3.0% of polymersomes formed less than 200 nm in diameter. Some hydrodynamic diameter bins display significantly different polymersome frequencies from 2 µmol/mL (* $p<0.05$, ** $p<0.01$, n=3). In some hydrodynamic diameter bins, an initial concentration of 50 µmol/mL PEGPLA leads to polymersome frequencies that are statistically different than using an initial concentration of 20 µmol/mL († $p<0.05$).*

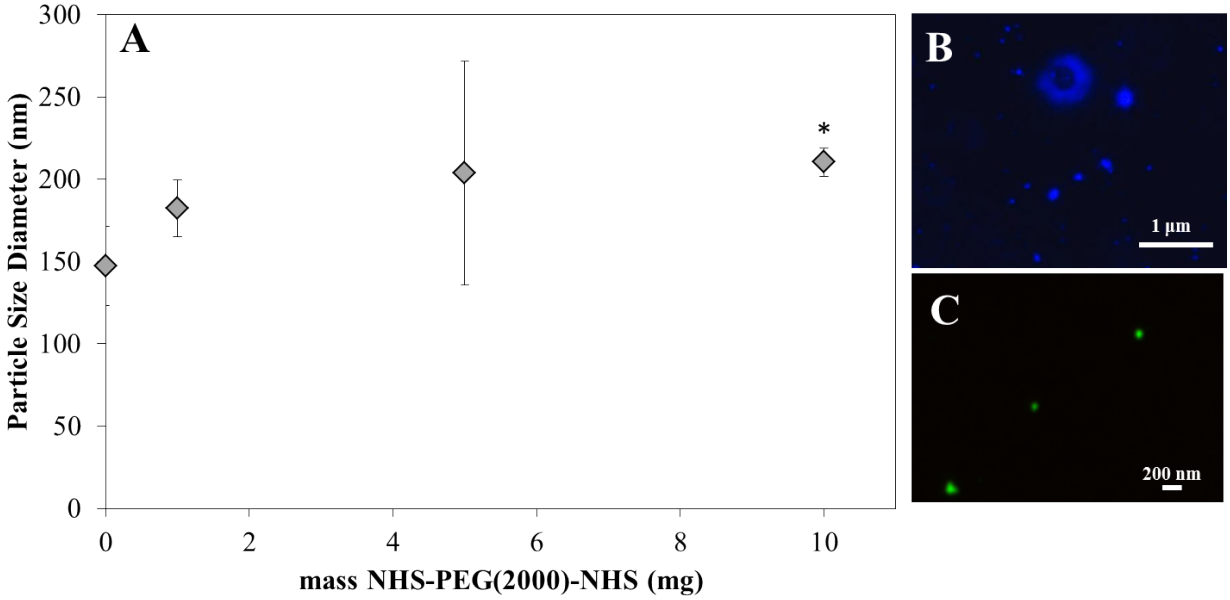

Figure 6.4. (A)Dynamic Light Scattering Data of Polymersome Diameter vs. mass NHS-PEG(2000)-NHS. *The only increase in polymersome diameter was observed through the introduction of 10 mg NHS-PEG(2000)-NHS with appropriate molar ratio of CF350 Amine (* $p < 0.05$, $n=3$).* ***(B) Fluorescence Microscopy of Ligand Attachment using a CytoViva Microscope.*** *Presented here is a representative image of attachment of CF350, a blue fluorescent ligand, to the surface of polymersomes through the introduction of NHS-PEG(2000)-NHS. In large polymersomes, it is clear that the blue color is localized around the exterior of the polymersomes.* ***(C) Fluorescence Microscopy of Encapsulation using a CytoViva Microscope.*** *Presented is a representative image demonstrating encapsulation of AF488, a green fluorescent molecule, into the polymersome vesicle.*

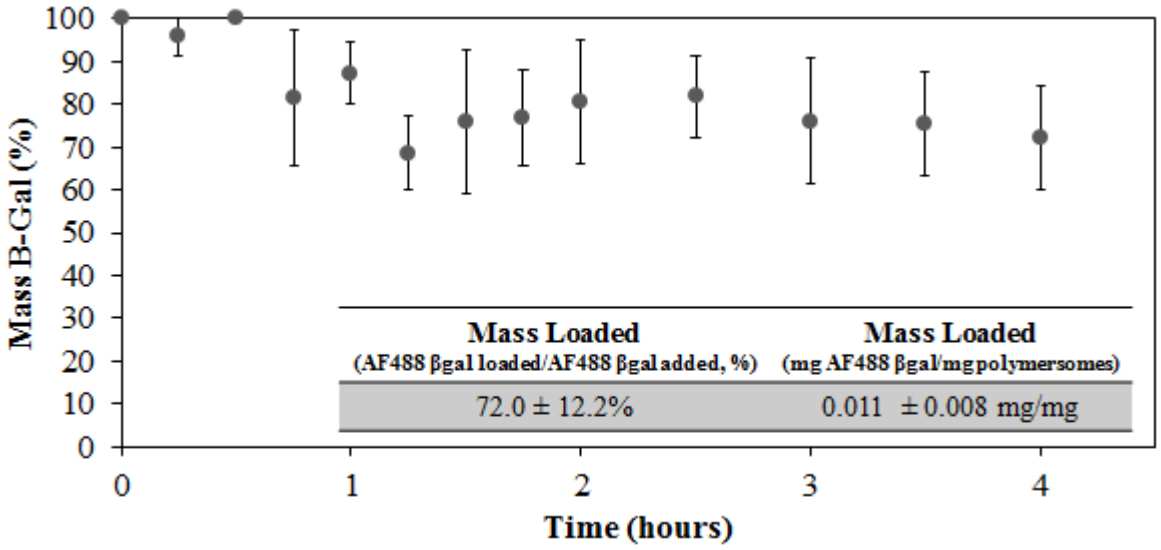

Figure 6.5. Mass of AF488 βgal in Dialysate Samples taken over four hours during Polymersome Loading. *Data indicates an immediate washing away of any unencapsulated AF488 βgal through the dialysis membrane (1000 kDa). Loading calculations were based off calibration curves plotting known concentrations of AF488 βgal to their corresponding fluorescence measurements. Concentrations were multiplied by the known volume of dialysate to determine mass released in the dialysate. This measurement was subtracted from mass added to polymersomes (mass added to polymersomes – mass released in to dialysate) and divided by the mass added to polymersomes to determine AF488 βgal mass percent loaded.*

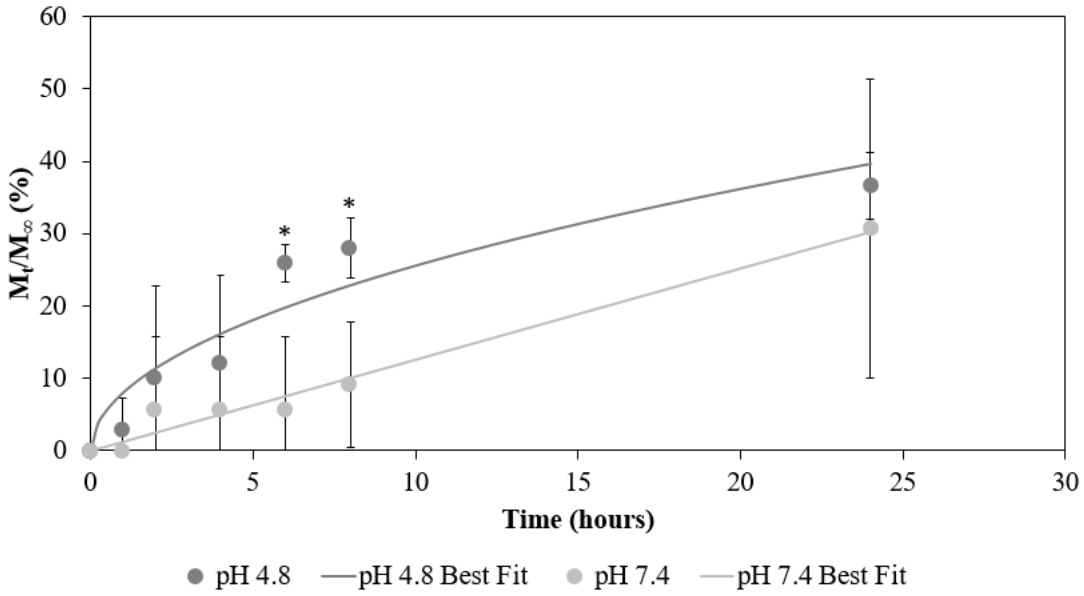

Figure 6.6. Release Curves demonstrating In Vitro Release of AF488 βgal from PEGPLA Polymersomes under pH 4.8 and pH 7.4 conditions (n=3). *Release curves are show the mass (%) of AF488 βgal from polymersomes over a period of 24 hours. Statistical increase in release was observed in pH 4.8 over pH 7.4 at hours 6 and 8 ($p<0.05$). It is also clear from the release curves that different kinetics are followed under the different conditions, with polymersomes exhibiting half order release in pH 4.8 and first order release in pH 7.4.*

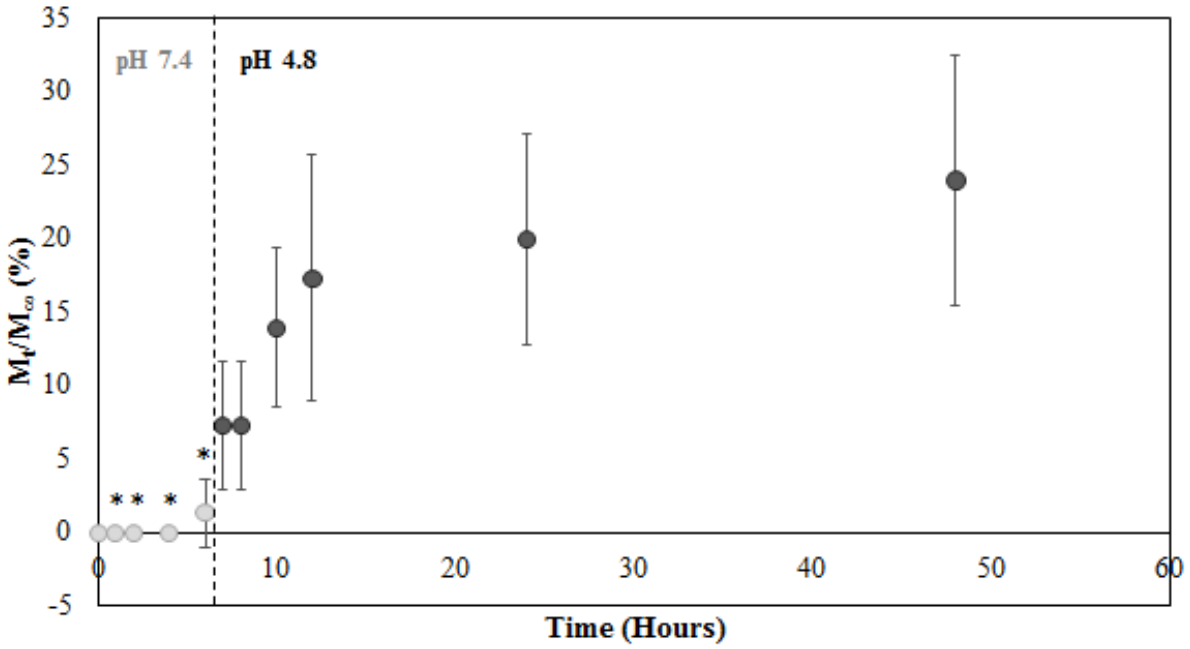

Figure 6.47. Release Curves demonstrating In Vitro Release of AF488 βgal from PEGPLA Polymersomes under pH 7.4 conditions for 6 hours and pH 4.8 conditions for 48 hours. *Release curves are show the mass (%) of AF488 βgal from polymersomes over a period of 48 hours. The light gray time points indicate pH 7.4. The color of time points switches to dark gray to demonstrate movement of PEGPLA polymersomes into pH 4.8 conditions. Asterisks denote statistical differences from the amount released at 48 hours in pH 4.8 ($p<0.05$).*

Table 6.1.PEGPLA Polymersome Size Data after Formation via the Injection Method. *Both intensity and z-average diameters, as well as polydispersity index (PDI) were determined using DLS after separation using 450 nm filters. Normalization values were determined by measuring polymersome diameters after lyophilization. The closeness of the value to 1 indicates the closeness of the original polymersome diameter to that found after lyophilization [8].* $p<0.05$ when compared to same variable at initial PEG-b-PLA concentration of 2 µmol/mL.*

Initial Concentration PEGPLA (µmol/mL)	Intensity Weighted Diameter (nm)	Z-Average Diameter (nm)	PDI	Normalization Value
2	145 ± 21	134 ± 20	0.07 ± 0.02	1.2 ± 0.2
20	192 ± 13*	182 ± 13*	0.09 ± 0.04	4.7 ± 3.2
50	180 ± 17*	189 ± 30*	0.16 ± 0.10	0.5 ± 0.1

Table 6.2. Encapsulation and ligand attachment during polymersome production. *Polymersomes (2 umol/mL PEG-b-PLA and 2 wt%/v mannitol) encapsulated AF488 (green fluorescence) and bound CF647 (red fluorescence). Flow cytometry gates were set using both deionized water and control polymersomes with no red or green fluorescence. "AF488 only" indicates polymersomes that were encapsulated with AF488 and not attached to CF647. "CF647 only" indicates polymersomes that were attached to CF647 without encapsulation of AF488. "AF488 and CF647" refers to polymersomes that both encapsulated AF488 and were attached to CF647. (n=3)*

Molecule Used in Polymersome Formation	Green Particles found in Green Channel Only (%)	Red Particles found in Red Channel Only (%)	Double Labeled Particles found in both the Red and Green Channels (%)
AF488 Only	90.1 ± 12.7%	0.05 ± 0.07%	6.8 ± 10.2%
CF 647 Only	0.03 ± 0.06%	79.4 ± 21%	3.4 ± 4.8%
AF488 and CF647	4.6 ± 1.4%	7.9 ± 12.3%	86.7 ± 11.6%

Chapter 7: β-galactosidase Loaded Polymersomes Facilitate Enzyme Replacement Therapy In GM1 Gangliosidosis Fibroblasts

In this work, PEG-b-PLA polymersomes are tested for their ability to provide effect ERT in a proof-of-concept 2D cellular model of GM1 Gangliosidosis. As presented in Chapter 2, approximately 1 in 100,000 to 200,000 children annually and diagnosed with GM1 Gangliosidosis [*243*]. GM1 gangliosidosis results from a mutation in the GLB1 gene that encodes for the enzyme βgal [*34–37*]. Because β-galactosidase is not present within the lysosome, GM1 ganglioside is not properly catabolized. GM1 ganglioside, along with keratan sulfate and some specific oligosaccharides which are also substrates of β-galactosidase, are stored in the lysosomes of cells [*37*], causing ultimate apoptosis of neural cells. This alteration in ganglioside catabolism and neural cell death causes severe CNS symptoms including severe CNS degeneration, ataxia, and premature death, with no treatment available on the market and no hope for parents of young diagnosed patients. Ultimately, regardless of the age of onset of disease, the symptoms are the same and GM1 gangliosidosis remains untreatable by any form of therapy.

The current standard of care for non-neuropathic LSDs is enzyme replacement therapy (ERT), in which the exogenous enzyme is infused into the patient in IV infusions that can occur as frequently as weekly or as infrequently as bimonthly depending on the enzyme being infused [*24*]. The goal of this project is to extend the use of enzyme replacement therapy to the brain through synthesized polymeric vesicles called polymersomes. Polymersomes are made from an amphiphilic block co-polymer polyethylene glycol(1000)-b-poly(lactic acid)(5000) (PEGPLA). PEG provides a

hydrophilic brush for the polymersomes, limiting protein adsorption and PLA provides hydrolytic cleavage, which allows for release of the therapeutic in the lysosome of cells, which have an acidic environment. Lysosomes are where enzymes are needed for degradation of storage products.

The missing enzyme in GM1 gangliosidosis, β-galactosidase (βgal) is incorporated into the polymersome vesicle core [*240*]. In the case of GM1 gangliosidosis, storage products result in high areas of inflammation, which causes an increased production of tumor necrosis factor-α (TNFα). This results in the upregulation of the low-density lipoprotein family of receptors (LDLRs) [*264*, *265*]. The use of ApoE provides a targeted pathway [*112*, *116*, *266*] for receptor mediated transcytosis of PEGPLA polymersomes loaded with βgal creating an ideal platform for enzyme delivery targeted to the brain.

7.1. Materials and Methods

7.1.1. Materials

Block co-polymer polyethylene glycol (PEG, molecular weight = 1000 Da)-b-poly(lactic acid) (PLA, molecular weight = 5000 Da) (PEGPLA) was used to form polymersomes (Polysciences, Inc). Dimethyl sulfoxide (DMSO) was used in polymersome formation (Sigma Aldrich). Mannitol (Sigma Aldrich) at a concentration of 2 wt%/v was used as a lyoprotectant in all polymersome formation studies [*8*]. Homobifunctional PEG (molecular weight = 2000 Da) with NHS groups (JenKem Technology USA) was used to facilitate ligand attachment to the polymersome surface. Recombinant human apolipoprotein E (ApoE) 3 (Sigma Aldrich) was used in ligand

attachment (Biotium, Inc). The missing enzyme in GM1 gangliosidosis, β-galactosidase (βgal) isolated from bovine liver (Sigma Aldrich) was used as a therapeutic. Dialysis was practiced using Float-a-Lyzer dialysis devices with a molecular weight cut off (MWCO) of 1000 kDa (Spectrum Labs). Anti-LDLR antibody produced in rabbit (Sigma Aldrich) was used with Donkey anti-Rabbit IgG secondary antibody tagged with Alexa Fluor 594 in immunofluorescence.

7.1.2. Polymersome Synthesis

Polymersomes were formed via the injection method, in which PEGPLA block co-polymer is dissolved in DMSO, as presented in Chapter 5. As in Chapter 5, polymersomes were frozen in a -80 °C prior to lyophilization under sublimation conditions. Following freezing, polymersomes were lyophilized under sublimation conditions (0.040 mbar and -52 °C) for further use.

7.1.3. B-galactosidase Loading

After lyophilization, 1 mg/mL solution of β-galactosidase (βgal) in water was added to a 10-fold mass of polymersomes, allowing for polymersome loading. Polymersomes both with and without ApoE ligand attachment were loaded with βgal, using the loading procedure presented in Chapter 5.

7.1.4. Apolipoprotein E Attachment to Polymersome Surface

When stated, polymersomes were attached to ApoE during formation. For this to occur, 10 mg of NHS-PEG(2000)-NHS was incorporated into the 101 μL of DMSO and 0.1 mg of ApoE was added to the 10 mL of stirring water prior to injection of PEGPLA.

The presence of NHS facilitates an amide bond between the polymersome surface and free amide groups on ApoE. This protocol has been submitted for publication in Nanomedicine [*240*]. ApoE attachment was monitored through DLS and a Lowry Assay for protein content [*267*].

7.1.5. Serum Stability

Empty polymersomes were added to 10, 20, and 40% fetal bovine serum in PBS and feline plasma at concentrations of 2, 4, and 8 mg/mL. Absorbance measurements were taken at a wavelength of 200 nm every five minutes for a period of one hour. If the polymersomes are breaking down, absorbance should be increasing and transmittance (%) should be decreasing as the light becomes absorbed.

7.1.6. Immunofluorescence

To confirm the presence of low density lipoprotein receptors (LDLR) and prove the potential for ApoE-mediated uptake in cell models, Anti-LDLR was used as a primary antibody with donkey anti-rabbit IgG, conjugated to Alexa Fluor 594 as a secondary antibody in immunofluorescence studies. The presence of LDLR was tested in both GM1SV3, immortalized GM1 gangliosidosis feline fibroblasts, and NSV3, immortalized normal feline fibroblasts. Untreated, primary-only, and secondary-only stains were used as controls.

7.1.7. Cell Culture, Internalization, and Treatment

NSV3 and GM1SV3 cells were seeded into 24 well plates at a constant concentration of 0.05×10^4 cells per well and incubated overnight at 37 °C and 5% CO_2

in Dulbecco's Modified Eagle Medium supplemented with 1 x antibiotic and antimycotic. After overnight incubation, cells were treated at various doses with free βgal, empty polymersomes, untagged polymersomes loaded with βgal, and ApoE-tagged polymersomes loaded with βgal. All doses were allowed to incubate with treatment for a period of 24 hours. After 24 hours incubation, media is changed and cells are manually scraped from the bottom of each well. The cells were collected in media and spun down at 400 x g for 5 minutes. After centrifugation, media was removed and cells were re-suspended in enzyme isolation buffer (0.1% Triton X-100 in 50 mM Citrate Phosphate buffer, pH 4.4 and 0.05% BSA) and disrupted by aspiration through an 18 ½ gauge needle. From here, enzyme isolates were frozen in liquid nitrogen for 10 minutes and thawed on ice two times prior to isolation of the supernatant for analysis. Enzyme activity of βgal was measured via 4-methylumbelliferone (4MU) enzyme assays on enzyme isolates from cells [*268*]. X-gal staining in an acidic buffer is also performed to visualize lysosomal βgal activity**.**

7.2. Results and Discussion

Control PEGPLA polymersomes, without any ligand attached, are formed at a diameter of 147 ± 24 nm via the injection method. Upon the addition of ApoE, DLS data indicates an increase in hydrodynamic diameter to 411 ± 302 nm, suggesting ligand attachment (Table 7.1). Although DLS reads this increase in diameter, the PEGPLA polymersomes are not increasing in size. Their apparent diameter increases due to the attachment of the full length human protein. Based upon the average size of human ApoE 3 of approximately 34 kDa, the apparent diameter of the associated sphere is estimated to

be approximately 2.2 nm, while the overall volume taken up by the protein is around 42 nm [*7*]. Because of this, the addition of ApoE fulling around the polymersomes is anticipated to increase polymersome diameter by approximately 4.4 nm and up to 84 nm. Because of this, it is believed that this dramatic increase in size may be due to polymersome agglomeration caused by protein binding to the surface, which allows the ApoE on neighboring polymersomes to interact. Upon ligand attachment, an increase in polydispersity index (PDI) is expected, meaning that the sample of PEGPLA polymersomes is becoming increasingly polydisperse, as it is unlikely that attachment would be highly uniform. This is observed by an increase in PDI from 0.07 ± 0.02 to 0.17 ± 0.05 (Table 7.1). Similar behavior was observed with the addition of a blue fluorescent molecule CF350, which was previously presented in Chapter 6 and published [*240*]. Finally, ligand attachment was confirmed by an increased measure of protein content from 0.18 ± 0.31 to 0.8 ± 0.61 mg protein per mL of sample via a Lowry assay (Table 7.1). Through the attachment of apolipoprotein E (ApoE), which has been shown to transport payloads through the BBB [*112*, *114*], PEGPLA polymersomes target the LDLR on the surface of the cells of the BBB, including neural and endothelial cells. Through encapsulation in PEGPLA polymersomes, βgal remains active and is able to be delivered into fibroblasts from cats with GM1 gangliosidosis diseased felines.

Before incubating PEGPLA polymersomes with cells, it is important to ensure their stability in serum, as this would demonstrate if any uncontrolled degradation of particles is contributing to the release of βgal from the vesicle core. It is also important to ensure that the polymersomes do not degrade immediately upon bloodstream injection, as

this would not allow βgal to be delivered in PEGPLA polymersomes across the BBB to its target site. At 0, 10, 20, and 40% serum, transparencies do not drop below 90% over the first hour at all concentrations explored, indicated that polymersomes are not degrading (Figure 7.1A). However, when using feline plasma, plotted under 100% in Figure A, incubation with 8 mg/mL polymersomes leads to a lower transparency, around 80%. The full spectrum of time data of polymersomes in feline plasma, over a period of 2 days (2880 minutes) shows this decrease in transparency occurs at 30 and 60 minutes. Transparency values increase to over 90% after 2 hours and continue to maintain full transparency over the next 46 hours (Figure 7.1B). At both 30 and 60 minutes, where the transparency drops below 90% with addition of polymersomes at all concentrations, the drop in transparency increases with increase concentration of PEGPLA polymersomes. This drop could be caused by two different factors. First, at higher concentrations, PEGPLA polymersomes take a longer period of time to dissolve and become incorporated in the feline plasma. Second, protein adsorption to the polymersome surface is occuring initially, and at a greater amount with higher concentrations of PEGPLA polymersomes. This could be causing aggregation, and therefore loss of transmittance. Regaining of transmittance could be due either to desorption of these proteins, or steric hindrance of polymersomes in solution caused by the adsorption of the protein, leading to increased dispersion in solution and therefore increased transmittance. Mulstein *et. al* observes this phenomena of serum-induced adsorption and desorption with adsorption of an enzyme arylsulfatase B onto poly(butyl cyanoacrylate) particles [*176*].

After ensuring that particles were stable in serum, *in vitro* studies were performed in GM1SV3 cells. GM1SV3 cells do not produce any βgal on their own, meaning that enzymatic activity is insignificant and x-gal staining leads to no blue color. However, NSV3 cells produce βgal normally. Therefore, the enzymatic activity measured on these cells and the blue color found using x-gal staining was determined to be normal and used as a control. Initial studies involved the addition of free βgal to GM1SV3 and NSV3 cells to determine a treatment threshold, defined as the dose at which βgal activity in GM1SV3 cells reached the βgal activity of untreated NSV3 cells. Treatment threshold was found occur at 1.45 mg/cm^2 βgal (Figure 7.2) At doses greater than this dose, enzyme activity of βgal was maintained at normal levels. Xgal staining confirmed this treatment threshold, with blue color indicative of increased βgal activity becoming present at a treatment level of 1.32 mg/cm^2 and maintaining activity throughout the rest of treatment levels.

Because of the defined treatment threshold, five different concentrations of encapsulated βgal, 0.175, 0.35, 0.7, 1.4, and 2.8 mg/cm^2 were added to both NSV3 and GM1SV3 cells. As a negative control, equivalent masses of empty polymersomes to each dose were incubated with cells. Free, or unencapsulated, βgal was also incubated with the cells at all five concentrations as a positive control. The final step prior to dosing the cells with untargeted and ApoE-tagged polymersomes was to prove the presence of LDL receptors on the surface of the cells. The presence of these receptors would ensure that GM1SV3 cells were an appropriate model for ApoE-mediated endocytosis. Anti-LDLR (red) was present around the full boundary of the cells and staining appeared to be punctate, which is indicative of receptor-related endocytosis [*102, 230, 269*]. Anti-LDLR

staining does not appear to be nuclear based upon limited to no co-localization with DAPI (blue) staining (Figure 7.3). We confirmed that LDL receptors were present on the surface of the cells, meaning receptor mediated transcytosis with ApoE-tagged particles could occur.

In vitro studies were done using the dosing presented in Table 7.2. Initial dosing involved 0.7, 1.4, and 2.8 mg/cm^2, with doses that are half of and double the treatment threshold. Although differences in enzyme activity of treated cells were observed, lower doses 0.35 and 0.175 were explored to see if larger differences in enzyme activity could be observed. The larger doses may have led to a particle saturation effect, where the maximum number of polymersomes that could be endocytosed has been endocytosed, with no increase in treatment efficacy apparent between the doses. These lower doses may decrease this particle saturation effect, making it less likely that a maximum number of polymersomes can be endocytosed by treatment. Enzyme assay results from all treatments and doses are summarized in Figure 7.4. The lowest doses of treatment, 0.175 and 0.35 mg/cm^2, show very little significant differences from βgal activity levels found in untreated GM1SV3 cells, although enzyme activity increases up to levels of approximately 1 fold normal. However, notably at the lowest dose, 0.175 mg/cm^2, βgal loaded polymersomes tagged with ApoE lead to statistically greater fold normal activity (1.08 ± 0.55) than free βgal at the same dose (0.05 ±0.08), meaning that the LDLR targeted particles were likely endocytosed easier than free βgal.

At the three higher doses, free βgal treatment remains statistically greater than control, at doses of 0.7, 1.4, and 2.8 mg/cm^2. At 0.7 and 1.4 mg/cm^2, both untagged and

tagged polymersomes reach activity levels comparable to that of free βgal treatment. However, at the highest dose of 2.8 mg/cm^2, both tagged and untagged polymersomes have statistically lower fold normal enzyme activity values than free βgal. This could be for a number of reasons including the mechanism of uptake and interactions between the enzyme and the hydrophobic polymersome membrane. Most lysosomal enzymes are naturally taken into cells through the mannose-6-phosphate (M6P) receptor. Native enzymes, as in free βgal treatment, are mannose-6-phosphorylated and easily taken up by the M6P receptor on cells. However, in the case of untagged polymersomes, either clatharin-mediated or caveolae-mediated endocytosis is required [*125*, *270*]. This non-specific process can be slower than M6P uptake. However, PEGPLA polymersomes without a tag and native βgal are unlikely to be taken up through the BBB by non-specific endocytosis, which has been demonstrated by very limited injected dose per gram in brain tissue. Although ApoE-tagged PEGPLA polymersomes show less enzyme activity than free βgal, ApoE has previously transported a payload through the BBB [*112*, *114*, *116*, *271*].

It is also possible that the entire dose of βgal is not reaching the lysosomes of GM1SV3 cells. Previous work indicates that as the PLA membrane is becoming hydrolytically cleaved, adsorption of protein (including βgal) to the hydrophobic membrane is increasing. This adsorption limits the release of βgal from the vesicle core, thereby inhibiting treatment [*240*]. The lack of high fold normal activity compared to free βgal in all polymersome treatments suggests that free βgal is not adsorbing to the surface

of the polymersomes upon formation, which is a positive result as it further proves that PEGPLA polymersomes are encapsulating and protecting βgal.

Enzyme assay results are presented in a box plot in Figure 7.5 so that results of PEGPLA polymersome treatments can be analyzed more effectively. Note that at the lowest dose explored, only ApoE tagged polymersomes can increase enzyme activity to statistically normal levels. However, at the highest three doses, both tagged and untagged polymersomes can effectively treat GM1SV3 cells with βgal. The working hypothesis is that PEGPLA polymersomes are already saturating the cells at a dose of 0.7 mg/cm^2. Because of this, enzyme activity is unable to continue to increase with increasing dose. This may be leading to the "step-wise" dose response visible in both untagged and tagged PEGPLA polymersomes with βgal treatment (Figure 7.5 C and D). At a certain dose, the treatment becomes effective, leading to βgal activity greater than untreated and greater than normal. Note that statistically improved enzyme activities are found at an extremely low dose of 0.175 mg/cm^2 when using ApoE-tagged polymersomes, while untagged polymersomes do not show a statistical increase in activity until doses of 1.4 mg/cm^2. This behavior is drastically different from the dose dependent response visualized after free βgal treatment (Figure 7.5A).

Panyam *et. al* noticed a similar effect in Human arterial smooth muscle cells, with saturating of poly(DL-lactide-co-glycolide) particles occurring at a dose of greater than 100 μg within the first 4 to 6 hours. In contrast, lower doses, 10-100 μg showed linear cellular uptake behavior [*272*]. At lower doses, the ApoE tagged PEGPLA polymersomes appear to have a greater therapeutic effect on the cells when compared to

untagged PEGPLA polymersomes at the same dose. This also supports the hypothesis that larger doses of empty polymersomes lead to a saturation of these nanoparticles within the cell via a nonspecific pathway. Studies in human breast cancer epithelial cells demonstrate that when endocytosis is blocked with chlorpromazine, inhibiting clathrin-mediated endocytosis, untagged poly(ethylene glycol)-polyester polymersomes uptake decreases by around 38%, while inhibition of caveolae-mediated endocytosis decreases uptake by around 20% [*125*].

Also, ApoE tagged polymersomes reach a statistically greater βgal activity at a lower dose of 0.175 mg/cm^2 compared to untagged polymersomes, which do not show therapeutic efficacy until a dose of 1.4 mg/cm^2. This demonstrates effective transport of βgal in PEGPLA polymersomes using receptor mediated transcytosis with LDLR. In the case of the GM1SV3 cell line, Figure proves that LDL receptors are present on cells but does not prove that these receptors are over-expressed, or present on the cells at a higher frequency than normal. This may be why, at higher doses, ApoE tagged polymersomes do not appear to have an increased therapeutic effect over untagged polymersomes, which would be demonstrated through increased βgal activity.

7.3. Conclusions

In summary, ApoE, a targeting ligand recently demonstrated to facilitate transport to the abluminal side of the BBB [*112*, *116*, *266*] is effectively incorporated through the introduction of NHS-PEG(2000)-NHS to the PEGPLA polymersome membrane. Addition of ApoE is confirmed by an increase in polymersome diameter from 147 ± 24 nm to 411 ± 302 nm and an increase in protein content from 0.07 ± 0.11 mg/mL to 0.8 ±

0.61 mg/mL (Table 7.1). PEGPLA polymersomes demonstrated high stability in 10%, 20%, and 40% serum, as well as feline plasma (Figure 7.1). After ensuring serum stability, GM1SV3 cells were treated with free βgal, empty polymersomes, untagged polymersomes loaded with βgal and ApoE tagged polymersomes loaded with βgal at five different doses, which were determined based upon free βgal studies (Figure 7.2). Lower doses of PEGPLA polymersomes seem to demonstrate an increased difference in fold normal βgal activity between ApoE tagged and untagged polymersomes, as these doses may not lead to saturation of polymersomes in GM1SV3 cells. Most notably, ApoE tagged PEGPLA polymersomes reached therapeutic efficacy, with βgal activity becoming statistically greater than untreated GM1SV3 cells at lower doses than untagged PEGPLA polymersomes, indicating that targeting was having an effect on cell treatment (Figures 7.4 and 7.5). In this study, polymeric carriers are created that can deliver active βgal into GM1SV3 cells through both receptor-mediated and non-specific endocytosis. With the use of targeting ligand ApoE and highly stable PEGPLA polymersomes developed here, delivery of active βgal through the BBB is possible. This method of treatment has the potential to cause a paradigm shift in the treatment of neuropathic lysosomal storage disorders, extending the current use of enzyme replacement therapies to treat the brain.

7.4. Figures and Tables

Table 7.1. Properties of Polymersomes with Targeting Ligands. *Size, PDI, and protein content of samples are presented in table form to demonstrate an increase in all of these properties, indicative of ligand attachment.*

Ligand	Size (nm)	PDI	Protein Content (mg/mL)
Control (no ligand)	147 ± 24	0.07 ± 0.02	0.18 ± 0.31
CF350	210 ± 9	0.13 ± 0.03	NA
ApoE	411 ± 302*	0.17 ± 0.05	0.80 ± 0.61*

Table 7.2. Summary of Treatment levels and βgal Doses incubated with GM1SV3 cells for 24 hours. *Different treatments included free βgal (βgal only), empty polymersomes, βgal loaded polymersomes, and βgal loaded polymersomes tagged with ApoE. The doses are measured in mg/cm2 βgal. Therefore, encapsulation efficiency is taken into account when determining the mass of polymersomes needed to equal a treatment level in mg/cm2 of βgal. For empty polymersomes, the mass of polymersomes that would equal a given dose of βgal, if encapsulated, is incubated with the cells (i.e. a mass equal to the dose of βgal loaded polymersomes).*

Treatment	Polymersomes	B-gal	ApoE	Dose (mg/cm^2)
Control	-	-	-	No
B-Gal Only	-	+	-	0.175
	-	+	-	0.35
	-	+	-	0.7
	-	+	-	1.4
	-	+	-	2.8
Empty Polymersomes	+	-	-	0.175
	+	-	-	0.35
	+	-	-	0.7
	+	-	-	1.4
	+	-	-	2.8
B-Gal Polymersomes	+	+	-	0.175
	+	+	-	0.35
	+	+	-	0.7
	+	+	-	1.4
	+	+	-	2.8
B-Gal + ApoE Polymersomes	+	+	+	0.175
	+	+	+	0.35
	+	+	+	0.7
	+	+	+	1.4
	+	+	+	2.8

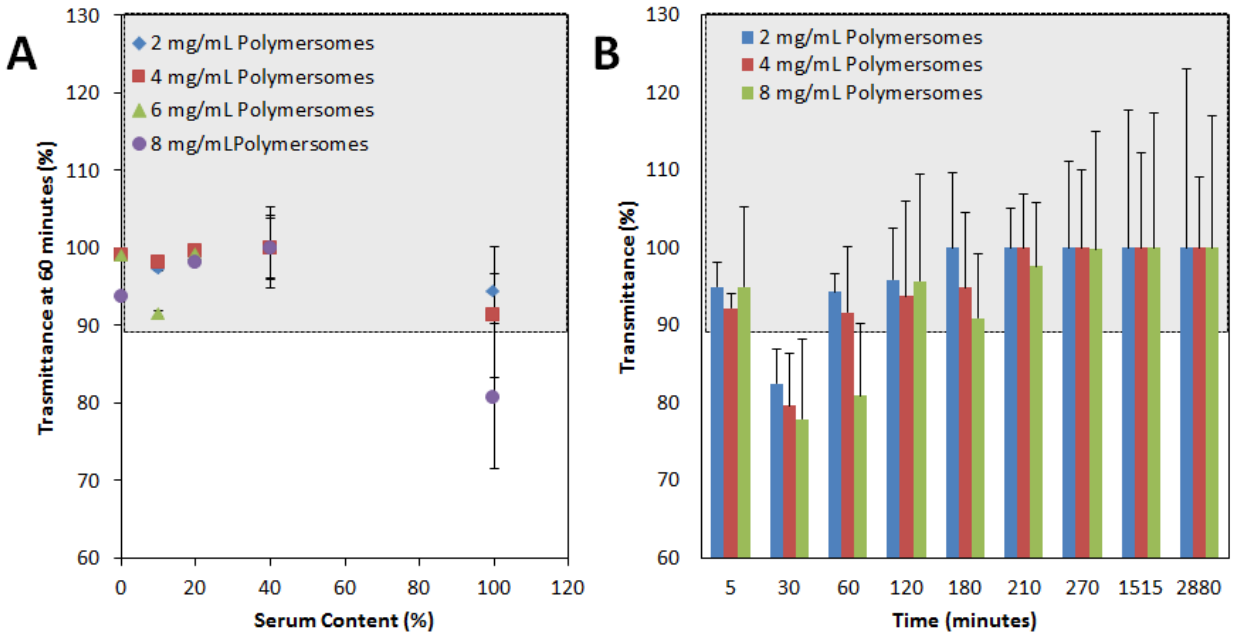

Figure 7.1. (A) Transmittance versus Serum Content after 1 Hour Incubation*. Empty polymersomes at 2, 4, 6, and 8 mg/mL were incubated at 0, 10, 20, 40, and 100% serum for one hour, with representative transmittance values are plotted. For all concentrations explored, only the maximum polymersome concentration in the maximum serum content showed a decrease in transmittance below 90%.* ***(B) Transmittance over time of PEGPLA polymersomes incubated in feline plasma.*** *All concentrations of polymersomes show high transmittance values, other than at a time point of 30 minutes to an hour. Transmittance values increase after an hour and continue to stay around 100%.*

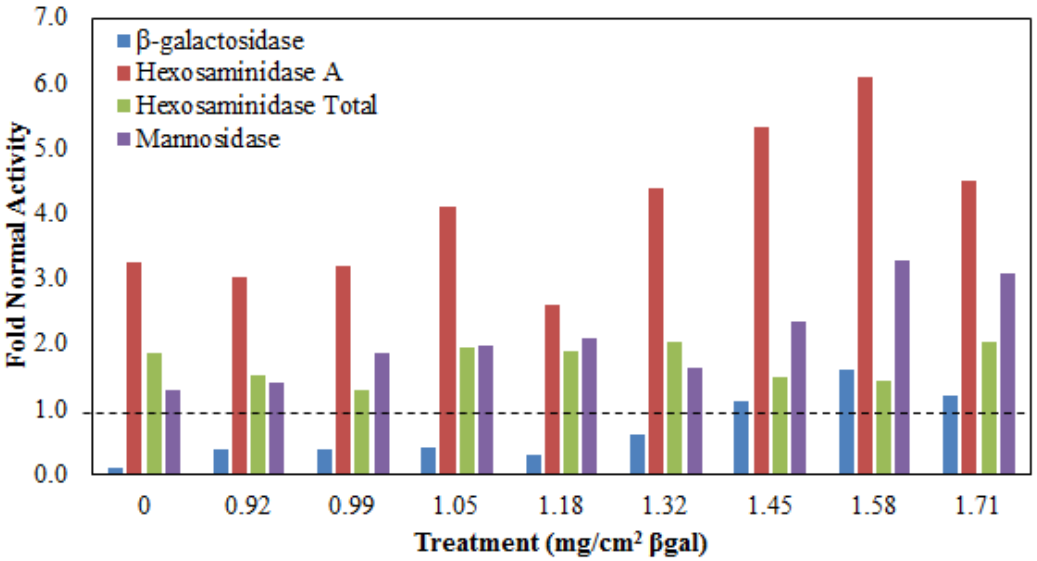

Figure 7.2. Dosing GM1SV3 cells with free βgal to determine treatment threshold. *GM1SV3 cells were treated with various concentrations of free βgal for 24 hours. Following incubation, enzyme activity of four enzymes was measured and compared to normal enzyme activity in NSV3 cells. Fold normal values at each concentration are plotted here. A fold normal of one indicates enzyme activity has increased to a normal level of enzyme activity.*

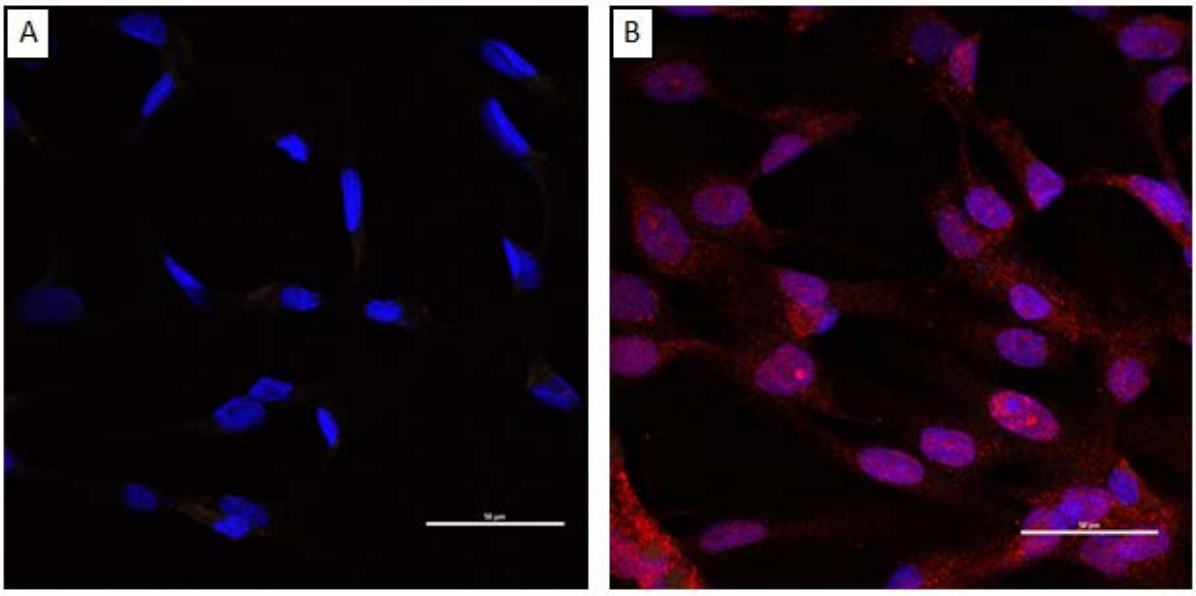

Figure 7.3. Anti-LDLR and DAPI stain on GM1SV3 cells. *Anti-LDLR (red) antibody was incubated with GM1SV3 and NSV3 cells, with Donkey Anti-Rabbit IgG conjugated to Alexa Fluor 594 as secondary antibody. (A) GM1SV3 cells without primary or secondary antibody. (B) representative confocal image of GM1SV3 cells with both primary and secondary antibodies. Both images have a scale bar of 50 µm.*

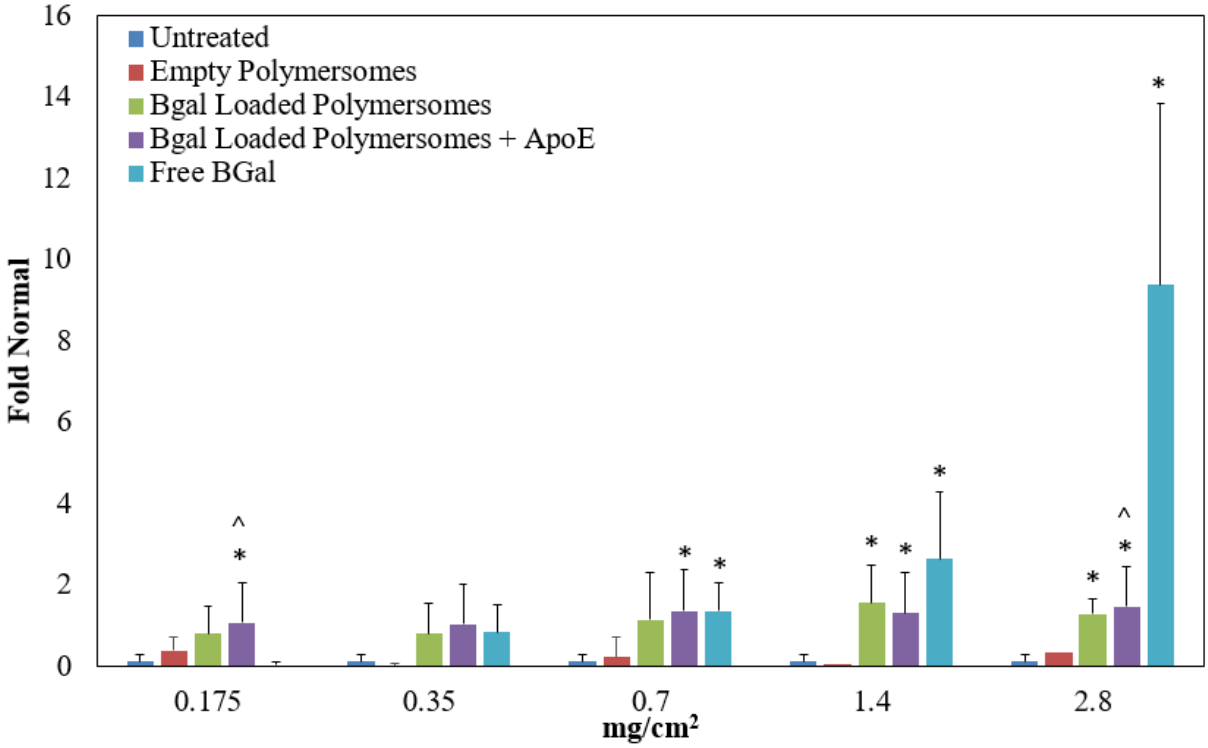

Figure 7.4. Fold Normal Enzyme Activity Values versus βgal Dose*. A fold normal value of one indicates βgal activity values have reached those found in normal control cells, NSV3. * indicates that fold normal values are statistically greater than untreated GM1SV3 cells ($p < 0.05$). ∧ indicates that fold normal values are statistically different than free βgal given at the same dose ($p < 0.05$).*

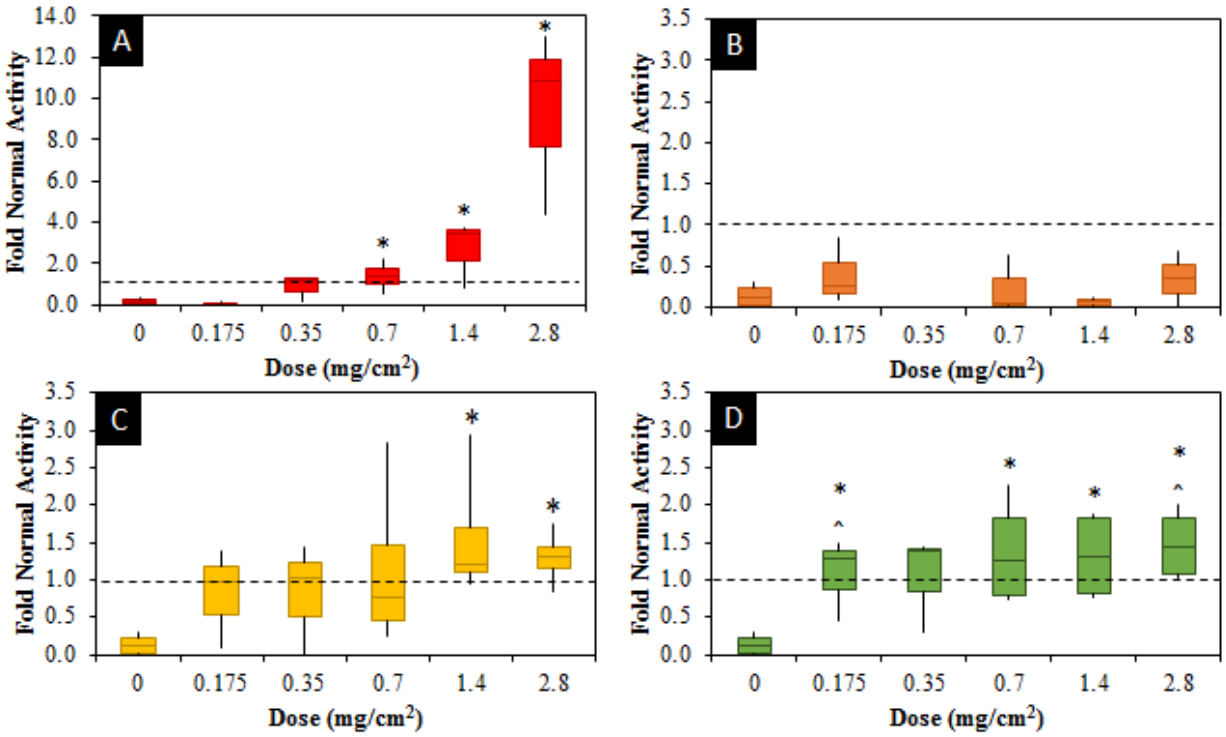

Figure 7.5. Fold Normal βgal Activity after Polymersome Treatment Versus βgal Dose. *(A) Free βgal treatment. (B) Empty polymersome treatment. (C) Untagged βgal-loaded polymersome treatment. (D) ApoE-tagged βgal-loaded polymersome treatment. Fold Normal values above or equal to one indicate effective treatment of GM1SV3 cells. * indicates statistically greater activity than untreated GM1SV3 cells ($p < 0.05$). ∧ indicates statistically different activity than GM1SV3 cells treated with free βgal.*

Chapter 8: Conclusions and Significance

Intravenous delivery of therapeutics to the CNS is desirable for treatment of many neurologic disorders. Two main barriers currently prevent targeted delivery to the brain. First, the BBB, made up of pericytes, astrocytes, and continuous endothelial cells connected by tight junctions, acts as a pseudo-size-exclusion barrier. The tight junctions only allow for molecules less than 7-12 Angstroms in diameter to pass through. However, lipid soluble materials and ions have different pathways. Although lipophilic molecules of a size less than approximately 400- 600 Da can travel freely through the BBB, the vast majority of developed therapeutic molecules do not fit this category. The second barrier, the sink action of the CSF, acts as a diluting mechanism, potentially removing a targeted carrier and associated therapeutic from the brain parenchyma.

One category of neuropathic diseases that would benefit greatly from non-invasive treatment through the BBB are LSDs. LSDs are difficult to diagnose and treat, leading to high morbidity and mortality. More than half of these autosomal recessive metabolic disorders affect the CNS leading to poor quality of life with significantly decreased lifespan. Thus, there is a substantial unmet need for better treatment strategies.

Currently explored treatment strategies for neuropathic lysosomal storage diseases include *ex vivo* and *in vivo* gene therapy, enzyme replacement infusions, as well as injectable nanocarriers delivering enzymes or genes. Recent advances in the development of AAV serotypes that are capable of crossing the BBB have provided improvements over more invasive intracranial delivery of viral vectors. However, novel data in a mouse

model of a LSD revealed a high incidence of oncogenesis associated with intravenous delivery of high AAV concentrations to neonates. The safety and efficacy of systemic AAV gene therapy must be further investigated in animal models. Ex vivo gene therapy has also been evaluated in recent clinical studies for MLD and preclinical studies for numerous other LSDs. Many obstacles remain with this approach, but impressive results have been achieved in clinical trials using a tailor-made transduction strategy and a carefully chosen patient population [*273*]. Gene therapy currently holds great promise for treatment of LSDs; however, modifications of enzyme or the use of non-viral vectors to target the CNS may ultimately have less intrinsic risk.

Enzyme replacement therapies are FDA approved and they have demonstrated efficacy in treating peripheral organs, but systemically injected enzymes cannot bypass the BBB to treat the CNS and also may not efficiently treat skeletal involvement. More recently, therapeutic enzymes have been directly targeted to the CNS through ICV catheters; however, this is associated with a high risk of infection. Both systemic and ICV delivery of enzyme necessitate weekly to monthly infusions for the duration of life placing a great physical burden on the patient and resulting in exorbitant financial costs. However, enzyme transport to the brain from an infusion would lead to a much more effective treatment strategy.

The BBB remains a difficult barrier to overcome by conventional treatments. Effective therapy for neuropathic LSDs through ERT has been conceptualized for decades, yet delivery to the CNS remains a major obstacle. Direct injection into the brain of enzyme or gene therapy vectors is promising, but homogeneous distribution

throughout the CNS is problematic and high levels of enzyme at the injection sites may not be safe. Multiple brain injections have shown considerable promise in terms of enhanced distribution, but it is expected that this would limit clinical translation due to safety concerns. Thus, effective delivery through the BBB remains a pressing issue for LSD therapy.

Three types of nanocarriers have the potential for use as intravenous carriers of therapeutic agents with transport through the BBB, including liposomes, metal nanoparticles and polymersomes. For a carrier to traverse an intact BBB, it should possess high blood stream stability at physiological pH (7.4) and have the ability to conjugate ligands that target the brain endothelium for transcytosis. Alternatively, the carrier may disrupt the BBB for therapeutic delivery through temporarily compromised tight junctions.

The efficacy of enzyme or gene loading as well as stability in nanocarriers for LSDs has also been studied. It is clear that nanoparticle strategies have high potential to lead to an injectable carrier that also transports efficiently to the brain. For most LSDs, the ideal treatment strategy is to deliver enzyme with sufficient activity both systemically and to the brain. While substantial progress has been made toward intravenous delivery of synthetic nanoparticles to the brain, further understanding of CNS physiology, drug distribution and transport kinetics as well as ways to clinically assess uptake and distribution is required. The efficiency of brain delivery must be improved, and off-target delivery outside the CNS must be minimized. In the past ten years, various strategies of creating the optimal brain-targeted nanocarrier have been explored which has led to

substantial growth in the field and demonstrated the future promise of this methodology for treating neurologic disease. However, this part of the field is still in its infancy with considerable challenges ahead, but it has very high potential to lead to major treatments in CNS disease.

This dissertation has laid out the development of a nanocarrier capable of encapsulating, protecting, and delivering an active enzyme, β-galactosidase, into the lysosome of neural cells in the treatment of a LSD, GM1 gangliosidosis. While at Auburn University, GM1 gangliosidosis took the lives of many children I knew. GM1 gangliosidosis causes developmental regress, frequent seizures, loss of control of muscle movement, blindness, and deafness in young children. It is a disease that is currently fatal in infancy because of the disease presentation in the central nervous system, with no method of treatment available, providing a large amount of motivation towards the development of a cure.

PEG-b-PLA was chosen as the amphiphile building block for polymersomes because of the limited complement protein adsorption demonstrated with PEG and the potential hydrolytic cleavage of the hydrophobic PLA component under low pH conditions, as in the lysosome. Although the material selection was appropriate, PEGPLA polymersomes did not maintain their shape and size after lyophilization and therefore could not be used in clinical therapies without the aid of lyoprotectants.

Mannitol and inulin were explored as lyoprotectants at 2,5, and 8 wt%/v. To create the smallest PEGPLA polymersomes using passive formation through mixing,

either 2 or 8 wt%/v mannitol should be incorporated and the polymersome formation should be stopped at 120 minutes (d = 169.8 ± 37.2 nm or 153.1 ± 32.2 nm respectively). In both cases, the polymersome diameters were statistically lower than control although these shorter time points may facilitate formation of polymersomes with increased variability in polymersome size and decreased yield in the desirable size range. In order to minimize crystallization and water content, 8 wt%/v inulin with rapid freezing in liquid nitrogen led to the lowest parts per million of water after lyophilization at 1828 ± 362 ppm. Slow freezing of polymersomes with 5 wt%/v mannitol prior to lyophilization had a similar effect to 8 wt%/v inulin with a residual water content of 1828 ± 362 ppm. Finally, 8 wt%/v inulin maintained polymersome size after lyophilization the best, with a normalization value of 0.99. The incorporation of mannitol yielded polymersomes that were 16-46% smaller after lyophilization than before lyophilization. Although mannitol provided less control over the dynamic environment, reduced particle size may be beneficial for targeted delivery, depending on the constraints for both the therapeutic and the delivery site. Also, the use of mannitol may be beneficial for opening up tight junctions of the blood-brain barrier. The lyoprotectant study demonstrated that polymersome formation can be controlled to generate consistent sizes both before and after freeze drying for long term storage, thus eliminating the need for high cost separation techniques.

Studies with lyoprotectants involved PEGPLA polymersome formation using passive mixing techniques. Although this was able to create small polymersomes, formation via diffusion led to a high dependence on timing to dictate polymersome size

and could lead to high polydispersities. Through the injection method, polymersomes were easily formed with 2 μmol/mL PEGPLA in a consistent, deliverable size range of 147.2 ± 24 nm after membrane separation. Polymersomes formed via the injection method followed similar behavior with lyoprotectants as those formed via passive mixing. Once it was clear that PEGPLA polymersomes could maintain their size distribution and behavior, protein encapsulation was studied. BSA, AF488, and βgal were easily encapsulated into 200 nm polymersomes without negatively effective the polymersome diameters, ensuring the brain delivery of loaded polymersomes is still a possibility. The use of absorbance measurements to determine loading and release behavior had high variation and did not lead to repeatable results. the difficulty in calculating protein content using absorbance. Because of this, loading and release studies of βgal were changed to include fluorescent measurements through the tagging of βgal with Alexa Fluor 488, a green fluorescent dye.

PEGPLA polymersomes encapsulated AF488-tagged βgal, the missing enzyme in GM1 gangliosidosis, at a relatively high efficiency of 72.0 ± 12.2% or 0.011 ± 0.008 mg βgal/mg PEGPLA polymersomes. Enzymatic activity was maintained upon loading, ensuring that PEGPLA polymersomes have the potential to protect active enzyme in the blood stream. PEGPLA polymersomes are also able to deliver enzyme preferentially under acidic conditions, like those that are present in the lysosome, demonstrated through release kinetics found in pH 7.4 and pH 4.8 buffers. Release of AF488 βgal was significantly greater under pH 4.8 conditions at hours 6 and 8 when compared to release under pH 7.4 conditions at the same time points. Noteably, it has been shown that

hydrolysis of PLA, a degradable polymer, increases the adsorption of proteins [*263*]. Therefore, as PLA is becoming hydrolyzed under acidic conditions, βgal is both able to escape the polymersome and more likely to adsorb to the membrane, leading to potential pore blocking and the observed decreased release rate after a period of 8-10 hours.

Effective binding of CF350 and CF647 using NHS-PEG(2000)-NHS has been proven through DLS, fluorescence microscopy, and flow cytometry. Most exciting, CF647 was attached to 79.4 ± 21% of polymersomes and 86.7 ± 11.6% of polymersomes were capable of simultaneously attaching CF647 and encapsulating AF488. PEGPLA polymersomes were also able to bind to ApoE, a targeting ligand recently demonstrated to facilitate transport to the abluminal side of the BBB [*112, 114, 116*]. Addition of ApoE was confirmed by an increase in polymersome diameter from 147 ± 24 nm to 194 ± 3 nm and an increase in protein content from 0.07 ± 0.11 mg/mL to 1 ± 0.7 mg/mL.

PEGPLA polymersomes demonstrated high stability in 10%, 20%, and 40% serum, as well as feline plasma. After ensuring serum stability, GM1SV3 cells were treated with free βgal, empty polymersomes, untagged polymersomes loaded with βgal and ApoE tagged polymersomes loaded with βgal at five different doses, which were determined based upon free βgal studies. Lower doses of PEGPLA polymersomes (0.175 and 0.35 mg/cm^2) seem to demonstrate an increased difference in fold normal βgal activity between ApoE tagged and untagged polymersomes, as these doses most likely do not lead to saturation of polymersomes in GM1SV3 cells. Most notably, ApoE tagged PEGPLA polymersomes reached therapeutic efficacy, with fold normal βgal activity becoming statistically greater than untreated GM1SV3 cells, at lower doses than

untagged PEGPLA polymersomes, indicating that targeting was having an effect on cell treatment.

PEGPLA polymersomes are drug delivery vehicles that have demonstrated potential to encapsulate and release therapeutics under specific conditions, with the ability to bind appropriate targeting ligands, including ApoE, with amine groups using techniques that are translatable to the attachment of BBB-penetrating proteins. Polymersome formation is tunable using the injection method and polymersome sizes are maintained using 2 wt%/v mannitol as a lyoprotectant, allowing for the creation of a multitude of size ranges necessary for different applications. The universal chemistry used in bioconjugation allows for the attachment of any targeting ligands with amine groups present, meaning that PEGPLA polymersomes can be used to target many disease states. Finally, PEGPLA polymersomes can encapsulate relatively high molecular weight enzymes while maintaining their activity, which has not yet been demonstrated in the literature. We have also demonstrated a high level of control over the creation of PEGPLA polymersomes. PEGPLA polymersomes demonstrated delivery of an active enzyme βgal into GM1SV3 cells through both receptor-mediated (ApoE tagged polylmersomes) and non-specific endocytosis (untagged polymersomes).

With the use of targeting ligand ApoE and highly stable PEGPLA polymersomes developed throughout this dissertation, delivery of active βgal through the BBB is possible. **With further animal and clinical studies, this method of treatment has the potential to cause a paradigm shift in the treatment of neuropathic GM1**

Gangliosidosis, extending the current use of enzyme replacement therapies to treat the brain.

References

[1] Rapoport, S. I. *Blood - brain barrier in physiology and medicine*; Raven Press: New York, 1976.

[2] Alberts, B.; Johnson, A.; Lewis, J.; Raff, M.; Roberts, K.; Walker, P. *Molecular Biology of the Cell*; 4th ed.; Garland Science: New York, 2002.

[3] U.S. Department of Health and Human Services Inactive Ingredient Search for Approved Drug Products. http://www.accessdata.fda.gov/scripts/cder/iig/index.cfm.

[4] Discher, D. E.; Ahmed, F. Polymersomes. *Annu. Rev. Biomed. Eng.* **2006**, *8*, 323–41.

[5] Onaca, O.; Enea, R.; Hughes, D. W.; Meier, W. Stimuli-responsive polymersomes as nanocarriers for drug and gene delivery. *Macromol. Biosci.* **2009**, *9*, 129–39.

[6] Meng, F.; Zhong, Z.; Feijen, J. Stimuli-responsive polymersomes for programmed drug delivery. *Biomacromolecules* **2009**, *10*, 197–209.

[7] Erickson, H. P. Size and shape of protein molecules at the nanometer level determined by sedimentation, gel filtration, and electron microscopy. *Biol. Proced. Online* **2009**, *11*, 32–51.

[8] Kelly, J. M.; Pearce, E. E.; Martin, D. R.; Byrne, M. E. Lyoprotectants modify and stabilize self-assembly of polymersomes. *Polymer (Guildf).* **2016**, *87*, 316–322.

[9] Bellavance, M.-A.; Blanchette, M.; Fortin, D. Recent advances in blood-brain barrier disruption as a CNS delivery strategy. *AAPS J.* **2008**, *10*, 166–77.

[10] Abbott, N. J.; Rönnbäck, L.; Hansson, E. Astrocyte-endothelial interactions at the blood-brain barrier. *Nat. Rev. Neurosci.* **2006**, *7*, 41–53.

[11] Lochhead, J. J.; Thorne, R. G. Intranasal delivery of biologics to the central nervous system. *Adv. Drug Deliv. Rev.* **2012**, *64*, 614–28.

[12] Lindqvist, A.; Rip, J.; Gaillard, P. J.; Björkman, S.; Hammarlund-Udenaes, M. Enhanced Brain Delivery of the Opioid Peptide DAMGO in Glutathione PEGylated Liposomes: A Microdialysis Study. *Mol. Pharm.* **2013**, *10*, 1533–41.

[13] Organization, W. H. *Neurological disorders: public health challenges*; 2006.

[14] Barbu, E.; Molnàr, E.; Tsibouklis, J.; Górecki, D. C. The potential for nanoparticle-based drug delivery to the brain: overcoming the blood-brain barrier. *Expert Opin. Drug Deliv.* **2009**, *6*, 553–65.

[15] Kelly, J. M.; Bradbury, A.; Martin, D. R.; Byrne, M. E. Emerging therapies for neuropathic lysosomal storage disorders. *Prog. Neurobiol.* **2016**.

[16] Björklund, a; Lindvall, O. Cell replacement therapies for central nervous system disorders. *Nat. Neurosci.* **2000**, *3*, 537–44.

[17] Zhang, Y.; Miler, D. W. Pathways for Drug Delivery to the Central Nervous System. In *Drug Delivery: Principles and Applications*; Wang, B.; Siahaan, T.; Soltero, R., Eds.; John Wiley & Sons, Inc., 2005; pp. 29–53.

[18] Dhuria, S. V; Hanson, L. R.; Frey II, W. H. Intranasal Delivery to the Central Nervous System : Mechanisms and Experimental Considerations. *J. Pharm. Sci.* **2010**, *99*, 1654–1673.

[19] Abbott, N. J. Blood-brain barrier structure and function and the challenges for CNS drug delivery. *J. Inherit. Metab. Dis.* **2013**, *36*, 437–49.

[20] Meikle, P. J.; Hopwood, J. J.; Clague, a E.; Carey, W. F. Prevalence of lysosomal storage disorders. *JAMA* **1999**, *281*, 249–54.

[21] Ellinwood, N. M.; Vite, C. H.; Haskins, M. E. Gene therapy for lysosomal storage diseases: the lessons and promise of animal models. *J. Gene Med.* **2004**, *6*, 481–506.

[22] Gritti, A. Gene therapy for lysosomal storage disorders. *Expert Opin. Biol. Ther.* **2011**, *11*, 1153–67.

[23] Muro, S. Strategies for Delivery of Therapeutics into the Central Nervous System for Treatment of Lysosomal Storage Disorders. *Drug Deliv. Transl. Res.* **2012**, *2*, 169–186.

[24] Aetna *Clinical Policy Bulletin: Enzyme-replacement Therapy for Lysosomal Storage Disorders*; 2014.

[25] Dell'Angelica, E. C.; Mullins, C.; Caplan, S.; Bonifacino, J. S. Lysosome-related organelles. *FASEB J.* **2000**, 1265–1278.

[26] Heese, B. A. Current strategies in the management of lysosomal storage diseases. *Semin. Pediatr. Neurol.* **2008**, *15*, 119–26.

[27] Sands, M. S.; Davidson, B. L. Gene therapy for lysosomal storage diseases. *Mol. Ther.* **2006**, *13*, 839–49.

[28] Ballabio, A.; Gieselmann, V. Lysosomal disorders: from storage to cellular damage. *Biochim. Biophys. Acta* **2009**, *1793*, 684–96.

[29] Wraith, J. E. Lysosomal disorders. *Paediatr. Child Health (Oxford).* **2011**, *21*, 76–79.

[30] Muro, S. New Biotechnical and Nanomedicine Strategies for Treatment of Lysosomal Storage Disorders. *Wiley Interdiscip. Rev. Nanomed. Nanobiotechnol.*

2010, *2*, 189–204.

[31] Bley, A. E.; Giannikopoulos, O. A.; Hayden, D.; Kubilus, K.; Tifft, C. J.; Eichler, F. S. Natural History of Infantile GM2 Gangliosidosis. *Pediatrics* **2011**, *128*, e1233–e1241.

[32] Ruiz de Garibay, A. P.; Delgado, D.; del Pozo-Rodríguez, A.; Solinís, M. Á.; Gascón, A. R. Multicomponent nanoparticles as nonviral vectors for the treatment of fabry disease by gene therapy. *Drug Des. Devel. Ther.* **2012**, *6*, 303–310.

[33] Kelly, J. M.; Bradbury, A.; Martin, D. R.; Byrne, M. E. Emerging therapies for neuropathic lysosomal storage disorders. *Prog. Neurobiol.* **2016**.

[34] Condori, J.; Acosta, W.; Ayala, J.; Katta, V.; Flory, A.; Martin, R.; Radin, J.; Cramer, C. L.; Radin, D. N. Enzyme replacement for GM1-gangliosidosis: Uptake, lysosomal activation, and cellular disease correction using a novel β-galactosidase: RTB lectin fusion. *Mol. Genet. Metab.* **2016**, *117*, 199–209.

[35] Weismann, C. M.; Ferreira, J.; Keeler, A. M.; Su, Q.; Qui, L.; Shaffer, S. A.; Xu, Z.; Gao, G.; Sena-Esteves, M. Systemic AAV9 gene transfer in adult GM1 gangliosidosis mice reduces lysosomal storage in CNS and extends lifespan. *Hum. Mol. Genet.* **2015**, *24*, 4353–64.

[36] Utz, J. R. J.; Crutcher, T.; Schneider, J.; Sorgen, P.; Whitley, C. B. Biomarkers of central nervous system inflammation in infantile and juvenile gangliosidoses. *Mol. Genet. Metab.* **2015**, *114*, 274–280.

[37] Sandhoff, K.; Harzer, K. Gangliosides and gangliosidoses: principles of molecular and metabolic pathogenesis. *J. Neurosci.* **2013**, *33*, 10195–208.

[38] Brunetti-Pierri, N.; Scaglia, F. GM1 gangliosidosis: review of clinical, molecular, and therapeutic aspects. *Mol. Genet. Metab.* **2008**, *94*, 391–6.

[39] Betz, A. L.; Goldstein, G. W. Specialized Properties and Solute Transport in Brain Capillaries. *Ann. Rev. Physiol.* **1986**, *48*, 241–250.

[40] Mruk, D. D.; Silvestrini, B.; Cheng, C. Y. A. N.; Council, P.; York, N.; M, N. Y. D. D. Anchoring Junctions As Drug Targets : **2008**, *60*, 146–180.

[41] Simionescu, M.; Simionescu, N.; Palade, G. E. Segmental Differentiations of Cell Junctions in the Vascular Endothelium: The Microvasculature. *J. Cell Biol.* **1975**, *67*, 863–885.

[42] Christ, G. J.; Spray, D. C.; El-Sabban, M.; Moore, L. K.; Brink, P. R. Gap Junctions in Vascular Tissues. *Circ. Res.* **1996**, 631–646.

[43] Ballabh, P.; Braun, A.; Nedergaard, M. The blood-brain barrier: an overview: structure, regulation, and clinical implications. *Neurobiol. Dis.* **2004**, *16*, 1–13.

[44] Pardridge, W. M. Drug Delivery to the Brain. *J. Cereb. Blood Flow Metab.* **1997**, 713–731.

[45] Hirschi, K. K.; D'Amore, P. a Pericytes in the microvasculature. *Cardiovasc. Res.* **1996**, *32*, 687–98.

[46] Armulik, A.; Genové, G.; Mäe, M.; Nisancioglu, M. H.; Wallgard, E.; Niaudet, C.; He, L.; Norlin, J.; Lindblom, P.; Strittmatter, K.; Johansson, B. R.; Betsholtz, C. Pericytes regulate the blood-brain barrier. *Nature* **2010**, *468*, 557–61.

[47] Dehouck, M. P.; Dehouck, B.; Fenart, L.; Cecchelli, R. Blood-Brain Barrier In Vitro: Rapid Evaluation of Strategies for Achieving Drug Targeting to the Central Nervous System. In *Biology and Physiology of the Blood-Brain Barrier: Transport, Cellular Interactions, and Brain Pathologies*; Couraud, P.-O.; Scherman, D., Eds.; Plenum Press: New York, 1996; pp. 143–145.

[48] Krol, S. Challenges in drug delivery to the brain: nature is against us. *J. Control. Release* **2012**, *164*, 145–55.

[49] Davies, K. R.; Richardson, G.; Akmentin, W.; Acuff, V.; Fenstermacher, J. D. The Microarchitecture of Cerebral Vessels. In *Biology and Physiology of the Blood-Brain Barrier: Transport, Cellular Interactions, and Brain Pathologies1*; Couraud, P.-O.; Scherman, D., Eds.; Plenum Press: New York, 1996; pp. 83–90.

[50] Pardridge, W. M. *Peptide Drug Delivery to the Brain*; 1st ed.; Raven Press, Ltd.: New York, 1991.

[51] Tsuji, A.; Tamai, I. Blood-brain barrier transport of drugs. In *Introduction to the Blood-Brain Barrier: Methodology, Biology, and Pathology2*; Pardridge, W. M., Ed.; Cambridge University Press, 2006; pp. 238–245.

[52] Silverberg, G. D.; Heit, G.; Huhn, S.; Jaffe, R. a.; Chang, S. D.; Bronte-Stewart, H.; Rubenstein, E.; Possin, K.; Saul, T. a. The cerebrospinal fluid production rate is reduced in dementia of the Alzheimer's type. *Neurology* **2001**, *57*, 1763–1766.

[53] Miyan, J. A.; Nabiyouni, M.; Zendah, M. Development of the brain: a vital role for cerebrospinal fluid. *Can. J. Physoilogy Pharmacol.* **2003**, *81*, 317–328.

[54] Laterra, J.; Keep, R.; Betz, L. A.; Goldstein, G. W. Blood-Cerebrospinal Fluid Barrier. In *Basic Neurochemistry: Molecular, Cellular and Medical Aspects*; Lippincott-Raven: Philadelphia, 1999.

[55] Saunders, N. R.; Dziegielewska, K. M. Brief Review: Barrier Mechanisms in the Brain, I. Adult Brain. *Clin. Exp. Pharmacol. Physiol.* **1998**, *26*, 11–19.

[56] Veening, J. G.; Barendregt, H. P. The regulation of brain states by neuroactive substances distributed via the cerebrospinal fluid; a review. *Cerebrospinal Fluid Res.* **2010**, *7*, 1.

[57] Sands, M. S.; Haskins, M. E. CNS-directed gene therapy for lysosomal storage disease. *Acta Paediatr.* **2008**, *97*, 22–27.

[58] Cachón-González, M. B.; Wang, S. Z.; McNair, R.; Bradley, J.; Lunn, D.; Ziegler, R.; Cheng, S. H.; Cox, T. M. Gene transfer corrects acute GM2 gangliosidosis--potential therapeutic contribution of perivascular enzyme flow. *Mol. Ther.* **2012**, *20*, 1489–500.

[59] Baek, R. C.; Broekman, M. L. D.; Leroy, S. G.; Tierney, L. a; Sandberg, M. a; d'Azzo, A.; Seyfried, T. N.; Sena-Esteves, M. AAV-mediated gene delivery in adult GM1-gangliosidosis mice corrects lysosomal storage in CNS and improves survival. *PLoS One* **2010**, *5*, e13468.

[60] Bobo, R. H.; Laske, D. W.; Akbasak, a; Morrison, P. F.; Dedrick, R. L.; Oldfield, E. H. Convection-enhanced delivery of macromolecules in the brain. *Proc. Natl. Acad. Sci. U. S. A.* **1994**, *91*, 2076–80.

[61] Allard, E.; Passirani, C.; Benoit, J.-P. Convection-enhanced delivery of nanocarriers for the treatment of brain tumors. *Biomaterials* **2009**, *30*, 2302–18.

[62] Hitt, J. M.; de Leon-Casasola, O. a. Complications of intrathecal drug delivery systems. *Tech. Reg. Anesth. Pain Manag.* **2011**, *15*, 162–166.

[63] Penn, R. D.; York, M. M.; Paice, J. A. Catheter implant systems for intrathecal drug delivery. *J. Neurosurg.* **1995**, *83*, 215–217.

[64] Follett, K. a; Naumann, C. P. A prospective study of catheter-related complications of intrathecal drug delivery systems. *J. Pain Symptom Manage.* **2000**, *19*, 209–15.

[65] Huynh, G. H.; Deen, D. F.; Szoka, F. C. Barriers to carrier mediated drug and gene delivery to brain tumors. *J. Control. Release* **2006**, *110*, 236–59.

[66] Stroobants, S.; Gerlach, D.; Matthes, F.; Hartmann, D.; Fogh, J.; Gieselmann, V.; D'Hooge, R.; Matzner, U. Intracerebroventricular enzyme infusion corrects central nervous system pathology and dysfunction in a mouse model of metachromatic leukodystrophy. *Hum. Mol. Genet.* **2011**, *20*, 2760–2769.

[67] Tsuji, D.; Akeboshi, H.; Matsuoka, K.; Yasuoka, H.; Miyasaki, E.; Kasahara, Y.; Kawashima, I.; Chiba, Y.; Jigami, Y.; Taki, T.; Sakuraba, H.; Itoh, K. Highly phosphomannosylated enzyme replacement therapy for GM2 gangliosidosis. *Ann. Neurol.* **2011**, *69*, 691–701.

[68] Katz, M. L.; Coates, J. R.; Sibigtroth, C. M.; Taylor, J. D.; Carpentier, M.; Young, W. M.; Wininger, F. a.; Kennedy, D.; Vuillemenot, B. R.; O'Neill, C. a. Enzyme replacement therapy attenuates disease progression in a canine model of late-infantile neuronal ceroid lipofuscinosis (CLN2 disease). *J. Neurosci. Res.* **2014**, *92*, 1591–1598.

[69] Cheng, S. H. Gene therapy for the neurological manifestations in lysosomal storage disorders. *Jounal Lipid Res.* **2014**, *55*, 1827–1838.

[70] Kalburgi, S. N.; Khan, N. N.; Gray, S. J. Recent gene therapy advancements for neurological diseases. *Discov. Med.* **2013**, *15*, 111–119.

[71] Yew, N. S.; Cheng, S. H. Gene therapy for lysosomal storage disorders. *Pediatr. Endocrinol. Rev.* **2013**, *11*, 99–109.

[72] Rastall, D. P.; Amalfitano, A. Recent advances in gene therapy for lysosomal storage disorders. *Appl. Clin. Genet.* **2015**, *8*, 157–69.

[73] Bradbury, A. M.; Gurda, B. L.; Casal, M. L.; Ponder, K. P.; Vite, C. H.; Haskins, M. E. A review of gene therapy in canine and feline models of lysosomal storage disorders. *Hum. Gene Ther. Clin. Dev.* **2015**, *26*, 27–37.

[74] Hollak, C. E. M.; Wijburg, F. A. Treatment of lysosomal storage disorders: Successes and challenges. In *Journal of Inherited Metabolic Disease*; 2014; Vol. 37, pp. 587–598.

[75] Ghosh, S.; Thrasher, A. J.; Gaspar, H. B. Gene therapy for monogenic disorders of the bone marrow. *Br. J. Haematol.* **2015**.

[76] Aronovich, E. L.; Hackett, P. B. Lysosomal storage disease: gene therapy on both sides of the blood-brain barrier. *Mol. Genet. Metab.* **2015**, *114*, 83–93.

[77] Byrne, B. J.; Falk, D. J.; Clément, N.; Mah, C. S. Gene Therapy Approaches for Lysosomal Storage Disease: Next-Generation Treatment. *Hum. Gene Ther.* **2012**, *23*, 808–815.

[78] Escolar, M. L.; Poe, M. D.; Provenzale, J. M.; Richards, K. C.; Allison, J.; Wood, S.; Wenger, D. a; Pietryga, D.; Wall, D.; Champagne, M.; Morse, R.; Krivit, W.; Kurtzberg, J. Transplantation of umbilical-cord blood in babies with infantile Krabbe's disease. *N. Engl. J. Med.* **2005**, *352*, 2069–2081.

[79] Aldenhoven, M.; Kurtzberg, J. Cord blood is the optimal graft source for the treatment of pediatric patients with lysosomal storage diseases: clinical outcomes and future directions. *Cytotherapy* **2015**, *17*, 765–774.

[80] Health, U. S. N. I. of ClinicalTrial.gov.

[81] Freeman, B. J.; Roberts, M. S.; Vogler, C. a; Nicholes, a; Hofling, a a; Sands, M. S. Behavior and therapeutic efficacy of beta-glucuronidase-positive mononuclear phagocytes in a murine model of mucopolysaccharidosis type VII. *Blood* **1999**, *94*, 2142–2150.

[82] Daneman, R. The blood-brain barrier in health and disease. *Ann. Neurol.* **2012**, *72*, 648–672.

[83] Gentner, B.; Visigalli, I.; Hiramatsu, H.; Lechman, E.; Ungari, S.; Giustacchini, A.; Schira, G.; Amendola, M.; Quattrini, A.; Martino, S.; Orlacchio, A.; Dick, J. E.; Biffi, A.; Naldini, L. Identification of hematopoietic stem cell-specific miRNAs enables gene therapy of globoid cell leukodystrophy. *Sci. Transl. Med.* **2010**, *2*, 58ra84.

[84] Passini, M. a; Bu, J.; Fidler, J. a; Ziegler, R. J.; Foley, J. W.; Dodge, J. C.; Yang, W. W.; Clarke, J.; Taksir, T. V; Griffiths, D. a; Zhao, M. a; O'Riordan, C. R.; Schuchman, E. H.; Shihabuddin, L. S.; Cheng, S. H. Combination brain and systemic injections of AAV provide maximal functional and survival benefits in the Niemann-Pick mouse. *Proc. Natl. Acad. Sci. U. S. A.* **2007**, *104*, 9505–9510.

[85] Ciron, C.; Desmaris, N.; Colle, M.-A.; Raoul, S.; Joussemet, B.; Vérot, L.; Ausseil, J.; Froissart, R.; Roux, F.; Chérel, Y.; Ferry, N.; Lajat, Y.; Schwartz, B.; Vanier, M.-T.; Maire, I.; Tardieu, M.; Moullier, P.; Heard, J.-M. Gene therapy of the brain in the dog model of Hurler's syndrome. *Ann. Neurol.* **2006**, *60*, 204–13.

[86] Ellinwood, N. M.; Ausseil, J.; Desmaris, N.; Bigou, S.; Liu, S.; Jens, J. K.; Snella, E. M.; Mohammed, E. E. a; Thomson, C. B.; Raoul, S.; Joussemet, B.; Roux, F.; Chérel, Y.; Lajat, Y.; Piraud, M.; Benchaouir, R.; Hermening, S.; Petry, H.; Froissart, R.; Tardieu, M.; Ciron, C.; Moullier, P.; Parkes, J.; Kline, K. L.; Maire, I.; Vanier, M.-T.; Heard, J.-M.; Colle, M.-A. Safe, efficient, and reproducible gene therapy of the brain in the dog models of Sanfilippo and Hurler syndromes. *Mol. Ther.* **2011**, *19*, 251–259.

[87] Ciron, C.; Cressant, A.; Raoul, S.; Cherel, Y.; Hantraye, P.; De, N. Human a - Iduronidase Gene Transfer Mediated of Nonhuman Primates : Vector Diffusion and Biodistribution. *Hum. Gene Ther.* **2009**, *20*, 350–360.

[88] Cachón-González, M. B.; Wang, S. Z.; Lynch, A.; Ziegler, R.; Cheng, S. H.; Cox, T. M. Effective gene therapy in an authentic model of Tay-Sachs-related diseases. *Proc. Natl. Acad. Sci. U. S. A.* **2006**, *103*, 10373–10378.

[89] McCurdy, V. J.; Rockwell, H. E.; Arthur, J. R.; Bradbury, A. M.; Johnson, A. K.; Randle, A. N.; Brunson, B. L.; Hwang, M.; Gray-Edwards, H. L.; Morrison, N. E.; Johnson, J. A.; Baker, H. J.; Cox, N. R.; Seyfried, T. N.; Sena-Esteves, M.; Martin, D. R. Widespread correction of central nervous system disease after intracranial gene therapy in a feline model of Sandhoff disease. *Gene Ther.* **2015**, *22*, 181–9.

[90] Rockwell, H. E.; McCurdy, V. J.; Eaton, S. C.; Wilson, D. U.; Johnson, a. K.; Randle, a. N.; Bradbury, a. M.; Gray-Edwards, H. L.; Baker, H. J.; Hudson, J. a.; Cox, N. R.; Sena-Esteves, M.; Seyfried, T. N.; Martin, D. R. AAV-Mediated Gene Delivery in a Feline Model of Sandhoff Disease Corrects Lysosomal Storage in the Central Nervous System. *ASN Neuro* **2015**, *7*.

[91] Dayton, R. D.; Wang, D. B.; Klein, R. L. The advent of AAV9 expands applications for brain and spinal cord gene delivery. *Expert Opin. Biol. Ther.* **2012**,

12, 757–766.

[92] Miyake, N.; Miyake, K.; Asakawa, N.; Yamamoto, M.; Shimada, T. Long-term correction of biochemical and neurological abnormalities in MLD mice model by neonatal systemic injection of an AAV serotype 9 vector. *Gene Ther.* **2014**, *21*, 427–33.

[93] Yang, B.; Li, S.; Wang, H.; Guo, Y.; Gessler, D. J.; Cao, C.; Su, Q.; Kramer, J.; Zhong, L.; Ahmed, S. S.; Zhang, H.; He, R.; Desrosiers, R. C.; Brown, R.; Xu, Z.; Gao, G. Global CNS Transduction of Adult Mice by Intravenously Delivered rAAVrh.8 and rAAVrh.10 and Nonhuman Primates by rAAVrh.10. *Mol. Ther.* **2014**, *22*, 1299–309.

[94] Ruzo, A.; Marcó, S.; García, M.; Villacampa, P.; Ribera, A.; Ayuso, E.; Maggioni, L.; Mingozzi, F.; Haurigot, V.; Bosch, F. Correction of Pathological Accumulation of Glycosaminoglycans in Central Nervous System and Peripheral Tissues of MPSIIIA Mice Through Systemic AAV9 Gene Transfer. *Hum. Gene Ther.* **2012**, 121017061824000.

[95] Fu, H.; Dirosario, J.; Killedar, S.; Zaraspe, K.; McCarty, D. M. Correction of neurological disease of mucopolysaccharidosis IIIB in adult mice by rAAV9 trans-blood-brain barrier gene delivery. *Mol. Ther.* **2011**, *19*, 1025–1033.

[96] Migeon, B. R.; Sprenkle, J. a; Liebaers, I.; Scott, J. F.; Neufeld, E. F. X-linked Hunter syndrome: the heterozygous phenotype in cell culture. *Am. J. Hum. Genet.* **1977**, *29*, 448–454.

[97] Neufeld, E. F.; Sando, G. N.; Garvin, A. J.; Rome, L. H. The transport of lysosomal enzymes. *J. Supramol. Struct.* **1977**, *6*, 95–101.

[98] Schiffmann, R. Therapeutic approaches for neuronopathic lysosomal storage disorders. *J. Inherit. Metab. Dis.* **2010**, *33*, 373–9.

[99] Beck, M. New therapeutic options for lysosomal storage disorders: enzyme replacement, small molecules and gene therapy. *Hum. Genet.* **2007**, *121*, 1–22.

[100] Byrne, B. J.; Falk, D. J.; Clément, N.; Mah, C. S. Gene therapy approaches for lysosomal storage disease: next-generation treatment. *Hum. Gene Ther.* **2012**, *23*, 808–15.

[101] Harris, J. M.; Chess, R. B. Effect of pegylation on pharmaceuticals. *Nat. Rev. Drug Discov.* **2003**, *2*, 214–21.

[102] Meng, Y.; Sohar, I.; Wang, L.; Sleat, D. E.; Lobel, P. Systemic administration of tripeptidyl peptidase I in a mouse model of late infantile neuronal ceroid lipofuscinosis: effect of glycan modification. *PLoS One* **2012**, *7*, e40509.

[103] Huynh, H. T.; Grubb, J. H.; Vogler, C.; Sly, W. S. Biochemical evidence for

superior correction of neuronal storage by chemically modified enzyme in murine mucopolysaccharidosis VII. *Proc. Natl. Acad. Sci. U. S. A.* **2012**, *109*, 17022–7.

[104] Grubb, J. H.; Vogler, C.; Levy, B.; Galvin, N.; Tan, Y.; Sly, W. S. Chemically modified beta-glucuronidase crosses blood-brain barrier and clears neuronal storage in murine mucopolysaccharidosis VII. *Proc. Natl. Acad. Sci. U. S. A.* **2008**, *105*, 2616–21.

[105] Urayama, A.; Grubb, J. H.; Sly, W. S.; Banks, W. a Developmentally regulated mannose 6-phosphate receptor-mediated transport of a lysosomal enzyme across the blood-brain barrier. *Proc. Natl. Acad. Sci. U. S. A.* **2004**, *101*, 12658–63.

[106] Vogler, C.; Levy, B.; Grubb, J. H.; Galvin, N.; Tan, Y.; Kakkis, E.; Pavloff, N.; Sly, W. S. Overcoming the blood-brain barrier with high-dose enzyme replacement therapy in murine mucopolysaccharidosis VII. *Proc. Natl. Acad. Sci. U. S. A.* **2005**, *102*, 14777–82.

[107] Veronese, F. Peptide and protein PEGylation: a review of problems and solutions. *Biomaterials* **2001**, *22*.

[108] Larsen, J. M.; Martin, D. R.; Byrne, M. E. Recent Advances in Delivery through the Blood-Brain Barrier. *Curr. Top. Med. Chem.* **2014**, 1148–1160.

[109] Zhang, Y.; Pardridge, W. Delivery of β-galactosidase to mouse brain via the blood-brain barrier transferrin receptor. *J. Pharmacol. Exp. Ther.* **2005**, *313*, 1075–1081.

[110] Boado, R. J.; Lu, Z.; Hui, E. K.; Pardridge, W. M. Insulin Receptor Antibody-Sulfamidase Fusion Protein Penetrates the Primate Blood-Brain Barrier and Reduces Glycosoaminoglycans in San fi lippo Type A Cells. *Mol. Pharm.* **2014**, *11*, 2928–2934.

[111] Boado, R. J.; Zhang, Y.; Zhang, Y.; Xia, C.-F.; Wang, Y.; Pardridge, W. M. Genetic engineering of a lysosomal enzyme fusion protein for targeted delivery across the human blood-brain barrier. *Biotechnol. Bioeng.* **2007**, *99*, 475–84.

[112] Mousazadeh, M.; Palizban, A.; Salehi, R.; Salehi, M. Gene delivery to brain cells with apoprotein E derived peptide conjugated to polylysine (apoEdp-PLL). *J. Drug Target.* **2007**, *15*, 226–30.

[113] Kim, H. R.; Gil, S.; Andrieux, K.; Nicolas, V.; Appel, M.; Chacun, H.; Desmaële, D.; Taran, F.; Georgin, D.; Couvreur, P. Low-density lipoprotein receptor-mediated endocytosis of PEGylated nanoparticles in rat brain endothelial cells. *Cell. Mol. life Sci.* **2007**, *64*, 356–64.

[114] Wang, D.; El-Amouri, S. S.; Dai, M.; Kuan, C.-Y.; Hui, D. Y.; Brady, R. O.; Pan, D. Engineering a lysosomal enzyme with a derivative of receptor-binding domain

of apoE enables delivery across the blood-brain barrier. *Proc. Natl. Acad. Sci. U. S. A.* **2013**, *110*, 2999–3004.

[115] Meng, Y.; Sohar, I.; Sleat, D. E.; Richardson, J. R.; Reuhl, K. R.; Jenkins, R. B.; Sarkar, G.; Lobel, P. Effective intravenous therapy for neurodegenerative disease with a therapeutic enzyme and a Peptide that mediates delivery to the brain. *Mol. Ther.* **2014**, *22*, 547–53.

[116] Böckenhoff, A.; Cramer, S.; Wölte, P.; Knieling, S.; Wohlenberg, C.; Gieselmann, V.; Galla, H.-J.; Matzner, U. Comparison of five peptide vectors for improved brain delivery of the lysosomal enzyme arylsulfatase A. *J. Neurosci.* **2014**, *34*, 3122–9.

[117] Lachmann, R. H. Enzyme replacement therapy for lysosomal storage diseases. *Curr. Opin. Pediatr.* **2011**, *23*, 588–93.

[118] National Tay-Sachs and Allied Diseases Association The Diseases. http://ntsad.org/index.php/allied-diseases.

[119] Executive Office of Health and Human Services Table 65: Enzyme Replacement and Substrate Reduction Therapies. https://masshealthdruglist.ehs.state.ma.us/MHDL/pubtheradetail.do?id=193.

[120] Knight, K. H.; Brand, F. M.; Mchaourab, A. S.; Veneziano, G. Implantable intrathecal pumps for chronic pain: highlights and updates. *Croat. Med. J.* **2007**, *48*, 22–34.

[121] Crunkhorn, S. Regulatory watch: enhanced chance of success for protein replacement therapies. *Nat. Rev. Drug Discov.* **2013**, *12*, 414.

[122] Gorzelany, J. A.; de Souza, M. P. Protein replacement therapies for rare diseases: a breeze for regulatory approval? *Sci. Transl. Med.* **2013**, *5*, 178fs10.

[123] Modi, G.; Pillay, V.; Choonara, Y. E.; Ndesendo, V. M. K.; du Toit, L. C.; Naidoo, D. Nanotechnological applications for the treatment of neurodegenerative disorders. *Prog. Neurobiol.* **2009**, *88*, 272–285.

[124] Panyam, J.; Labhasetwar, V. Biodegradable nanoparticles for drug and gene delivery to cells and tissue. *Adv. Drug Deliv. Rev.* **2003**, *55*, 329–347.

[125] Ahmed, F.; Pakunlu, R. I.; Srinivas, G.; Brannan, A.; Bates, F.; Klein, M. L.; Minko, T.; Discher, D. E. Shrinkage of a rapidly growing tumor by drug-loaded polymersomes: pH-triggered release through copolymer degradation. *Mol. Pharm.* **2006**, *3*, 340–350.

[126] Sundaram, P.; Wower, J.; Byrne, M. E. A nanoscale drug delivery carrier using nucleic acid aptamers for extended release of therapeutic. *Nanomedicine Nanotechnology, Biol. Med.* **2012**, *8*, 1143–51.

[127] Huwyler, J.; Wu, D.; Pardridge, W. M. Brain drug delivery of small molecules using immunoliposomes. *Proc. Natl. Acad. Sci. U. S. A.* **1996**, *93*, 14164–14169.

[128] Ko, Y. T.; Bhattacharya, R.; Bickel, U. Liposome encapsulated polyethylenimine/ODN polyplexes for brain targeting. *J. Control. Release* **2009**, *133*, 230–7.

[129] Pardridge, W. M. Gene Targeting In Vivo with Pegylated Immunoliposomes. *Methods Enzymol.* **2003**, *373*, 507–528.

[130] Boado, R. J.; Pardridge, W. M. The Trojan Horse Liposome Technology for Nonviral Gene Transfer across the Blood-Brain Barrier. *J. Drug Deliv.* **2011**, *2011*, 296151.

[131] Pardridge, W. M. Blood-brain barrier delivery of protein and non-viral gene therapeutics with molecular Trojan horses. *J. Control. Release* **2007**, *122*, 345–8.

[132] Pardridge, W. M. shRNA and siRNA delivery to the brain. *Adv. Drug Deliv. Rev.* **2007**, *59*, 141–152.

[133] Kabanov, A. V.; Gendelman, H. E. Nanomedicine in the diagnosis and therapy of neurodegenerative disorders. *Prog. Polym. Sci.* **2007**, *32*, 1054–1082.

[134] Pardridge, W. M. Blood-brain barrier delivery. *Drug Discov. Today* **2007**, *12*, 54–61.

[135] Leamon, C. P. Receptor-Mediated Drug Delivery. In *Drug Delivery: Principles and Applications2*; Wang, B.; Siahaan, T.; Soltero, R., Eds.; John Wiley & Sons, Inc., 2005; pp. 167–185.

[136] Shier, D.; Butler, J. L.; Lewis, R. *Hole's Human Anatomy and Physiology*; McGraw-Hill Higher Education, 2004.

[137] Gabathuler, R. Approaches to transport therapeutic drugs across the blood-brain barrier to treat brain diseases. *Neurobiol. Dis.* **2010**, *37*, 48–57.

[138] Chandra, D.; Karande, P. Transferrin mediated drug delivery to brain. *Bioeng. Conf.* **2011**, 1–2.

[139] Stenehjem, D. D.; Hartz, A. M. S.; Bauer, B.; Anderson, G. W. Novel and emerging strategies in drug delivery for overcoming the blood-brain barrier. *Future Med. Chem.* **2009**, *1*, 1623–41.

[140] Pardridge, W. M. Drug transport across the blood-brain barrier. *J. Cereb. Blood Flow Metab.* **2012**, *32*, 1959–72.

[141] Coloma, M. J.; Lee, H. J.; Kurihara, A.; Landaw, E. M.; Boado, R. J.; Morrison, S. L.; Pardridge, W. M. Transport Across the Primate Blood- Brain Barrier of a

Genetically Engineered Chimeric Monoclonal Antibody to the Human Insulin Receptor. *Pharm. Res.* **2000**, *17*, 266–274.

[142] Boado, R. J.; Zhang, Y.; Zhang, Y.; Pardridge, W. M. Humanization of Anti-Human Insulin Receptor Antibody for Drug Targeting Across the Human. *Biotechnol. Bioeng.* **2007**, *96*, 381–391.

[143] Pardridge, W. M.; Boado, R. J. Reengineering biopharmaceuticals for targeted delivery across the blood-brain barrier. *Methods Enzymol.* **2012**, *503*, 269–92.

[144] Boado, R. J.; Zhang, Y.; Zhang, Y.; Wang, Y.; Pardridge, W. M. GDNF fusion protein for targeted-drug delivery across the human blood-brain barrier. *Biotechnol. Bioeng.* **2008**, *100*, 387–396.

[145] Sorrentino, N. C.; D'Orsi, L.; Sambri, I.; Nusco, E.; Monaco, C.; Spampanato, C.; Polishchuk, E.; Saccone, P.; De Leonibus, E.; Ballabio, A.; Fraldi, A. A highly secreted sulphamidase engineered to cross the blood-brain barrier corrects brain lesions of mice with mucopolysaccharidoses type IIIA. *EMBO Mol. Med.* **2013**, 675–690.

[146] Pan, W.; Kastin, A. J.; Zankel, T. C.; van Kerkhof, P.; Terasaki, T.; Bu, G. Efficient transfer of receptor-associated protein (RAP) across the blood-brain barrier. *J. Cell Sci.* **2004**, *117*, 5071–8.

[147] Rapoport, S. I. Osmotic opening of the blood-brain barrier: principles, mechanism, and therapeutic applications. *Cell. Mol. Neurobiol.* **2000**, *20*, 217–30.

[148] Frank, R. T.; Aboody, K. S.; Najbauer, J. Strategies for enhancing antibody delivery to the brain. *Biochim. Biophys. Acta* **2011**, *1816*, 191–8.

[149] Blanchette, M.; Fortin, D. Chapter 23: Blood-Brain Barrier Disruption in the Treatment of Brain Tumors. In *The Blood-Brain and Other Neural Barriers*; Nag, S., Ed.; Methods in Molecular Biology; Humana Press: Totowa, NJ, 2011; Vol. 686, pp. 447–463.

[150] Obata, Y.; Tajima, S.; Takeoka, S. Evaluation of pH-responsive liposomes containing amino acid-based zwitterionic lipids for improving intracellular drug delivery in vitro and in vivo. *J. Control. Release* **2010**, *142*, 267–76.

[151] Zhang, Y.; Schlachetzki, F.; Pardridge, W. Global non-viral gene transfer to the primate brain following intravenous administration. *Mol. Ther.* **2003**, *7*, 11–18.

[152] Yang, H. Nanoparticle-mediated brain-specific drug delivery, imaging, and diagnosis. *Pharm. Res.* **2010**, *27*, 1759–71.

[153] Immordino, M. L.; Dosio, F.; Cattel, L. Stealth liposomes: review of the basic science, rationale, and clinical applications, existing and potential. *Int. J. Nanomedicine* **2006**, *1*, 297–315.

[154] Gatter, K. C.; Brown, G.; Trowbridge, I. S.; Woolston, R. E.; Mason, D. Y. Transferrin receptors in human tissues: their distribution and possible clinical relevance. *J. Clin. Pathol.* **1983**, *36*, 539–45.

[155] Ponka, P.; Lok, C. N. The transferrin receptor: role in health and disease. *Int. J. Biochem. Cell Biol.* **1999**, *31*, 1111–37.

[156] Qian, Z. M.; Li, H.; Sun, H.; Ho, K. Targeted Drug Delivery via the Transferrin Receptor-. **2002**, *54*, 561–587.

[157] Abdalla, M. Y. Glutathione as Potential Target for Cancer Therapy ; More or Less is Good? *Jordan J. Biol. Sci.* **2011**, *4*, 119–124.

[158] Vashist, S. K.; Zheng, D.; Pastorin, G.; Al-Rubeaan, K.; Luong, J. H. T.; Sheu, F.-S. Delivery of drugs and biomolecules using carbon nanotubes. *Carbon N. Y.* **2011**, *49*, 4077–4097.

[159] Sundaram, P.; Kurniawan, H.; Wower, J.; Byrne, M. E. Controlled and Extended Release of Daunomycin from DNA Aptamer-Programmed Gold Nanoparticles. *Trans. Soc, Biomater.* **2012**, *35*, 542.

[160] Aktaş, Y.; Yemisci, M.; Andrieux, K.; Gürsoy, R. N.; Alonso, M. J.; Fernandez-Megia, E.; Novoa-Carballal, R.; Quiñoá, E.; Riguera, R.; Sargon, M. F.; Celik, H. H.; Demir, A. S.; Hincal, a A.; Dalkara, T.; Capan, Y.; Couvreur, P. Development and brain delivery of chitosan-PEG nanoparticles functionalized with the monoclonal antibody OX26. *Bioconjug. Chem.* **2005**, *16*, 1503–11.

[161] Cole, A. J.; David, A. E.; Wang, J.; Galbán, C. J.; Yang, V. C. Magnetic brain tumor targeting and biodistribution of long-circulating PEG-modified, cross-linked starch-coated iron oxide nanoparticles. *Biomaterials* **2011**, *32*, 6291–301.

[162] Etame, A. B.; Diaz, R. J.; O'Reilly, M. a; Smith, C. a; Mainprize, T. G.; Hynynen, K.; Rutka, J. T. Enhanced delivery of gold nanoparticles with therapeutic potential into the brain using MRI-guided focused ultrasound. *Nanomedicine* **2012**, *8*, 1133–42.

[163] Chertok, B.; David, A. E.; Yang, V. C. Magnetically-enabled and MR-monitored selective brain tumor protein delivery in rats via magnetic nanocarriers. *Biomaterials* **2011**, *32*, 6245–53.

[164] Opsteen, J.; Cornelissen, J.; van Hest, J. C. Block copolymer vesicles. *Pure Appl. Chem.* **2004**, *76*, 1309–1319.

[165] Meng, F.; Hiemstra, C.; Engbers, G. H. M.; Feijen, J. Biodegradable Polymersomes. *Macromolecules* **2003**, *36*, 3004–3006.

[166] Lee, J. S.; Feijen, J. Polymersomes for drug delivery: design, formation and characterization. *J. Control. Release* **2012**, *161*, 473–83.

[167] Ahmed, F.; Discher, D. E. Self-porating polymersomes of PEG-PLA and PEG-PCL: hydrolysis-triggered controlled release vesicles. *J. Control. Release* **2004**, *96*, 37–53.

[168] Li, D.; Li, C.; Wan, G.; Hou, W. Self-assembled vesicles of amphiphilic poly(dimethylsiloxane)-b-poly(ethylene glycol) copolymers as nanotanks for hydrophobic drugs. *Colloids Surfaces A Physicochem. Eng. Asp.* **2010**, *372*, 1–8.

[169] Rutnakornpituk, M.; Ngamdee, P.; Phinyocheep, P. Synthesis, characterization and properties of chitosan modified with poly(ethylene glycol)–polydimethylsiloxane amphiphilic block copolymers. *Polymer (Guildf).* **2005**, *46*, 9742–9752.

[170] Bakkour, Y.; Darcos, V.; Coumes, F.; Li, S.; Coudane, J. Brush-like amphiphilic copolymers based on polylactide and poly(ethylene glycol): Synthesis, self-assembly and evaluation as drug carrier. *Polymer (Guildf).* **2013**, *54*, 1746–1754.

[171] Chécot, F.; Lecommandoux, S.; Klok, H.; Gnanou, Y. From supramolecular polymersomes to stimuli-responsive nano-capsules based on poly(diene-b-peptide) diblock copolymers. *Eur. Phys. J. E. Soft Matter* **2003**, *10*, 25–35.

[172] Pang, Z.; Lu, W.; Gao, H.; Hu, K.; Chen, J.; Zhang, C.; Gao, X.; Jiang, X.; Zhu, C. Preparation and brain delivery property of biodegradable polymersomes conjugated with OX26. *J. Control. Release* **2008**, *128*, 120–7.

[173] Pang, Z.; Gao, H.; Yu, Y.; Chen, J.; Guo, L.; Ren, J.; Wen, Z.; Su, J.; Jiang, X. Brain delivery and cellular internalization mechanisms for transferrin conjugated biodegradable polymersomes. *Int. J. Pharm.* **2011**, *415*, 284–92.

[174] Stojanov, K.; Georgieva, J. V.; Brinkhuis, R. P.; van Hest, J. C.; Rutjes, F. P.; Dierckx, R. A. J. O.; de Vries, E. F. J.; Zunhorn, I. S. In vivo biodistribution of prion-and GM1-targeted polymersomes following intravenous administration in mice. *Mol. Pharm.* **2012**, *9*, 1620–1627.

[175] Popescu, M.-T.; Tsitsilianis, C. Controlled Delivery of Functionalized Gold Nanoparticles by pH-Sensitive Polymersomes. *ACS Macro Lett.* **2013**, *2*, 222–225.

[176] Mühlstein, a.; Gelperina, S.; Kreuter, J. Development of nanoparticle-bound arylsulfatase B for enzyme replacement therapy of mucopolysaccharidosis VI. *Pharmazie* **2013**, *68*, 549–554.

[177] Garnacho, C.; Dhami, R.; Simone, E.; Dziubla, T.; Leferovich, J.; Schuchman, E. H.; Muzykantov, V.; Muro, S. Delivery of acid sphingomyelinase in normal and niemann-pick disease mice using intercellular adhesion molecule-1-targeted polymer nanocarriers. *J. Pharmacol. Exp. Ther.* **2008**, *325*, 400–408.

[178] Mayer, F. Q.; Adorne, M. D.; Bender, E. A.; Carvalho, T. G. De; Dilda, A. C.; Carlos, R.; Beck, R.; Guterres, S. S.; Giugliani, R.; Matte, U.; Pohlmann, A. R.

Laronidase-Fuctionalized Multiple-Wall Lipid-Core Nanocapsules : Promising Formulation for a More Effective Treatment of Mucopolysaccharidosis Type I. *Pharm. Res.* **2014**.

[179] del Pozo-Rodríguez, A.; Delgado, D.; Solinís, M. Á.; Pedraz, J. L.; Echevarría, E.; Rodríguez, J. M.; Gascón, A. R. Solid lipid nanoparticles as potential tools for gene therapy: In vivo protein expression after intravenous administration. *Int. J. Pharm.* **2010**, *385*, 157–162.

[180] Bharali, D. J.; Klejbor, I.; Stachowiak, E. K.; Dutta, P.; Roy, I.; Kaur, N.; Bergey, E. J.; Prasad, P. N.; Stachowiak, M. K. Organically modified silica nanoparticles: a nonviral vector for in vivo gene delivery and expression in the brain. *Proc. Natl. Acad. Sci. U. S. A.* **2005**, *102*, 11539–11544.

[181] Genetics, I. Sandhoff Disease. https://www.labcorp.com/wps/wcm/connect/IntGeneticsLib/integratedgenetics/resources/diseases/sandhoff+disease?Sandhoff Disease.

[182] Genzyme Incidence & Prevalence. http://www.pompe.com/healthcare-professionals/genetics-epidemiology/incidence-prevalence.aspx.

[183] Beck, M. Hurler Syndrome. http://www.orpha.net/consor/cgi-bin/OC_Exp.php?Lng=EN&Expert=93473.

[184] Burton, B. Mucopolysaccharidosis Type 2. http://www.orpha.net/consor/cgi-bin/Disease_Search.php?lng=EN&data_id=131&Disease_Disease_Search_diseaseGroup=hunter-syndrome&Disease_Disease_Search_diseaseType=Pat&Disease(s)/group of diseases=Mucopolysaccharidosis-type-2--Hunter-syndrome-&title=Muco.

[185] Harmatz, P.; Nicely, H.; Turbeville, S.; Valayannopoulos, V. Mucopolysaccharidosis Type 6. http://www.orpha.net/consor/cgi-bin/Disease_Search.php?lng=EN&data_id=24&Disease_Disease_Search_diseaseGroup=MPS-VI&Disease_Disease_Search_diseaseType=Pat&Disease(s)/group of diseases=Mucopolysaccharidosis-type-6--MPSVI-&title=Mucopolysaccharidosis-ty.

[186] Schuchman, E. H. The pathogenesis and treatment of acid sphingomyelinase-deficient Niemann-Pick disease. *J. Inherit. Metab. Dis.* **2007**, *30*, 654–63.

[187] National Institute of Health Mucopolysaccharidosis Type VII. http://ghr.nlm.nih.gov/condition/mucopolysaccharidosis-type-vii.

[188] Froissart, R.; Maire, I. Mucopolysaccharidosis Type 7. http://www.orpha.net/consor/cgi-bin/OC_Exp.php?Lng=GB&Expert=584.0.

[189] National Institute of Health Metachromatic Leukodystrophy.

http://ghr.nlm.nih.gov/condition/metachromatic-leukodystrophy.

[190] Baumann, N.; Turpin, J. Metachromatic Leukodystrophy. http://www.orpha.net/consor/cgi-bin/OC_Exp.php?Expert=512.

[191] Luzi, P.; Wenger, D. Krabbe Disease. http://www.orpha.net/consor/cgi-bin/OC_Exp.php?Expert=487.

[192] Froissart, R.; Maire, I. Aspartylglucosaminuria. http://www.orpha.net/consor/cgi-bin/OC_Exp.php?Expert=93.

[193] U.S. National Library of Medicine Aspartylglucosaminuria. http://ghr.nlm.nih.gov/condition/aspartylglucosaminuria (accessed February 9, 2015).

[194] Betanzos, A.; Nava, P.; Jaramillo, B. E.; Gonz, L. Tight junction proteins. *Prog. Biophys. Mol. Biol.* **2003**, *81*, 1–44.

[195] Huber, O. Structure and function of desmosomal proteins and their role in development and disease. *Cell. Mol. Life Sci.* **2003**, *60*, 1872–90.

[196] Sorensson, J. Glomerular Endothelial Fenestrae In Vivo Are Not Formed from Caveolae. *J. Am. Soc. Nephrol.* **2002**, *13*, 2639–2647.

[197] Tkachenko, E.; Tse, D.; Sideleva, O.; Deharvengt, S. J.; Luciano, M. R.; Xu, Y.; McGarry, C. L.; Chidlow, J.; Pilch, P. F.; Sessa, W. C.; Toomre, D. K.; Stan, R. V Caveolae, fenestrae and transendothelial channels retain PV1 on the surface of endothelial cells. *PLoS One* **2012**, *7*, e32655.

[198] Dermietzel, R.; Traub, O.; Hwang, T. K.; Beyer, E.; Bennett, M. V; Spray, D. C.; Willecke, K. Differential expression of three gap junction proteins in developing and mature brain tissues. *Proc. Natl. Acad. Sci. U. S. A.* **1989**, *86*, 10148–52.

[199] Fauci, A.; Braunwald, E.; Isselbacher, K.; Wilson, J.; Marin, J.; Kasper, D.; Hauser, S.; Longo, D. *Harrison's principles of internal medicine*; 14th ed.; McGraw-Hill Health Professions Division: New York, 1998.

[200] Bickel, U. Intravenous Injection/Pharmacokinetics. In *Introduction to the Blood-Brain Barrier: Methodology, Biology, and Pathology*; Pardridge, W. M., Ed.; Cambridge University Press, 2006; pp. 41–47.

[201] Bickel, U.; Yoshikawa, T.; Pardridge, W. Delivery of peptides and proteins through the blood–brain barrier. *Adv. Drug Deliv. Rev.* **2001**, *46*, 247–279.

[202] Haselbacher, G. K.; Schwab, M. E.; Pasi, a; Humbel, R. E. Insulin-like growth factor II (IGF II) in human brain: regional distribution of IGF II and of higher molecular mass forms. *Proc. Natl. Acad. Sci. U. S. A.* **1985**, *82*, 2153–7.

[203] Acerini, C. L.; Clayton, K. L.; Hintz, R.; Baker, B.; Watts, a; Holly, J. M.; Dunger, D. B. Serum insulin-like growth factor II levels in normal adolescents and those with insulin dependent diabetes mellitus. *Clin. Endocrinol. (Oxf).* **1996**, *45*, 13–9.

[204] Golden, P. Human blood-brain barrier leptin receptor. Binding and endocytosis in isolated human brain microvessels. *J. Clin. Invest.* **1997**, *99*, 14–18.

[205] Klein, S.; Coppack, S. W.; Mohamed-Ali, V.; Landt, M. Adipose tissue leptin production and plasma leptin kinetics in humans. *Diabetes* **1996**, *45*, 984–7.

[206] Considine, R. V; Sinha, M. K.; Heiman, M. L.; Kriauciunas, a; Stephens, T. W.; Nyce, M. R.; Ohannesian, J. P.; Marco, C. C.; McKee, L. J.; Bauer, T. L. Serum immunoreactive-leptin concentrations in normal-weight and obese humans. *N. Engl. J. Med.* **1996**, *334*, 292–5.

[207] Mankarious, S.; Lee, M.; Fischer, S.; Pyun, K.; Ochs, H.; Oxelius, V.; Wedgwood, R. The half-lives of IgG subclasses and specific antibodies in patients with primary immunodeficiency who are receiving intravenously administered. *J. Lab. Clin. Med.* **1988**, *112*, 634–40.

[208] Ulbrich, K.; Hekmatara, T.; Herbert, E.; Kreuter, J. Transferrin- and transferrin-receptor-antibody-modified nanoparticles enable drug delivery across the blood-brain barrier (BBB). *Eur. J. Pharm. Biopharm.* **2009**, *71*, 251–6.

[209] Prades, R.; Guerrero, S.; Araya, E.; Molina, C.; Salas, E.; Zurita, E.; Selva, J.; Egea, G.; López-Iglesias, C.; Teixidó, M.; Kogan, M. J.; Giralt, E. Delivery of gold nanoparticles to the brain by conjugation with a peptide that recognizes the transferrin receptor. *Biomaterials* **2012**, *33*, 7194–205.

[210] Hu, K.; Li, J.; Shen, Y.; Lu, W.; Gao, X.; Zhang, Q.; Jiang, X. Lactoferrin-conjugated PEG-PLA nanoparticles with improved brain delivery: in vitro and in vivo evaluations. *J. Control. Release* **2009**, *134*, 55–61.

[211] Jain, J. P.; Kumar, N. Self assembly of amphiphilic (PEG)(3)-PLA copolymer as polymersomes: preparation, characterization, and their evaluation as drug carrier. *Biomacromolecules* **2010**, *11*, 1027–35.

[212] Yildiz, M.; Prud'homme, R. Formation and characterization of polymersomes made by a solvent injection method. *Polym.* … **2007**, 427–432.

[213] Yin, H.; Kang, S.-W.; Bae, Y. H. Polymersome Formation from AB 2 Type 3-Miktoarm Star Copolymers. *Macromolecules* **2009**, *42*, 7456–7464.

[214] Kim, H.-O.; Kim, E.; An, Y.; Choi, J.; Jang, E.; Choi, E. B.; Kukreja, A.; Kim, M.-H.; Kang, B.; Kim, D.-J.; Suh, J.-S.; Huh, Y.-M.; Haam, S. A Biodegradable Polymersome Containing Bcl-xL siRNA and Doxorubicin as a Dual Delivery

Vehicle for a Synergistic Anticancer Effect. *Macromol. Biosci.* **2013**, 1–10.

[215] Ayen, W. Y.; Garkhal, K.; Kumar, N. Doxorubicin-loaded $(PEG)_3$-PLA nanopolymersomes: effect of solvents and process parameters on formulation development and in vitro study. *Mol. Pharm.* **2011**, *8*, 466–78.

[216] Ho, C. S.; Kim, J. W.; Weitz, D. A. Microfluidic fabrication of monodisperse biocompatible and biodegradable polymersomes with controlled permeability. *J. Am. Chem. Soc.* **2008**, *130*, 9543–9549.

[217] Kamat, N. P.; Katz, J. S.; Hammer, D. A. Engineering Polymersome Protocells. *J. Phys. Chem. Lett.* **2012**, *2*, 1612–1623.

[218] Perro, A.; Nicolet, C.; Angly, J.; Lecommandoux, S.; Le Meins, J. F.; Colin, A. Mastering a double emulsion in a simple co-flow microfluidic to generate complex polymersomes. *Langmuir* **2011**, *27*, 9034–9042.

[219] Xu, J.; Zhao, Q.; Jin, Y.; Qiu, L. High loading of hydrophilic/hydrophobic doxorubicin into polyphosphazene polymersome for breast cancer therapy. *Nanomedicine* **2014**, *10*, 349–58.

[220] Ayen, W. Y.; Kumar, N. A systematic study on lyophilization process of polymersomes for long-term storage using doxorubicin-loaded $(PEG)_3$-PLA nanopolymersomes. *Eur. J. Pharm. Sci.* **2012**, *46*, 405–14.

[221] Roy, I.; Gupta, M. N. Freeze-drying of proteins: some emerging concerns. *Biotechnol. Appl. Biochem.* **2004**, *39*, 165–77.

[222] van Winden, E. C.; Crommelin, D. J. Short term stability of freeze-dried, lyoprotected liposomes. *J. Control. Release* **1999**, *58*, 69–86.

[223] Kulkarni, S. a; Feng, S.-S. Effects of Particle Size and Surface Modification on Cellular Uptake and Biodistribution of Polymeric Nanoparticles for Drug Delivery. *Pharm. Res.* **2013**.

[224] Williams, N. A.; Polli, G. P. The Lyophilization of Pharmaceuticals : A Literature Review. *PDA J. Pharm. Sci. Technol.* **1984**, *38*, 48–60.

[225] Chandler, D. Interfaces and the driving force of hydrophobic assembly. *Nature* **2005**, *437*, 640–647.

[226] Luo, L.; Eisenberg, A. Thermodynamic size control of block copolymer vesicles in solution. *Langmuir* **2001**, 6804–6811.

[227] Westfall, B.; Landis, E. The molecular weight of inulin. *J. Biol. Chem.* **1936**, 727–734.

[228] Skrabanja, A. T. P.; De Meere, A. L. J.; Ruiter, R. A.; Van Den Oetelaar, P. J. M.

Lyophilization of biotechnology products. *PDA J. Pharm. Sci. Technol.* **1994**, *48*, 311–317.

[229] Lu, X.; Pikal, M. J. Freeze-drying of mannitol-trehalose-sodium chloride-based formulations: the impact of annealing on dry layer resistance to mass transfer and cake structure. *Pharm. Dev. Technol.* **2004**, *9*, 85–95.

[230] Discher, D. E.; Ortiz, V.; Srinivas, G.; Klein, M. L.; Kim, Y.; Christian, D.; Cai, S.; Photos, P.; Ahmed, F. Emerging applications of polymersomes in delivery: From molecular dynamics to shrinkage of tumors. *Prog. Polym. Sci.* **2007**, *32*, 838–857.

[231] Christian, D. a; Cai, S.; Bowen, D. M.; Kim, Y.; Pajerowski, J. D.; Discher, D. E. Polymersome carriers: from self-assembly to siRNA and protein therapeutics. *Eur. J. Pharm. Biopharm.* **2009**, *71*, 463–74.

[232] Rodriguez-Hernandez, J.; Checot, F.; Gnanou, Y.; Lecommandoux, S. Toward "smart" nano-objects by self-assembly of block copolymers in solution. *Prog. Polym. Sci.* **2005**, *30*, 691–724.

[233] Samoylova, T. I.; Martin, D. R.; Morrison, N. E.; Hwang, M.; Cochran, A. M.; Samoylov, A. M.; Baker, H. J.; Cox, N. R. Generation and characterization of recombinant feline beta-galactosidase for preclinical enzyme replacement therapy studies in GM1 gangliosidosis. *Metab. Brain Dis.* **2008**, *23*, 161–73.

[234] Ohto, U.; Usui, K.; Ochi, T.; Yuki, K.; Satow, Y.; Shimizu, T. Crystal structure of human β-galactosidase: Structural basis of G M1 gangliosidosis and morquio B diseases. *J. Biol. Chem.* **2012**, *287*, 1801–1812.

[235] Distler, J. J.; Jourdian, G. W. The Purification and from Bovine Testes * Properties of P-Galactosidase. **1973**, 6772–6781.

[236] Jiang Schwendeman SP, W. Stabilization and controlled release of bovine serum albumin encapsulated in poly(D,L-lactide) and poly(ethylene glycol) microsphere blends. *Pharm. Res.* **2001**, *18*, 878–885.

[237] Jamshidian, M.; Tehrany, E. A.; Imran, M.; Jacquot, M.; Desobry, S. Poly-Lactic Acid: Production, applications, nanocomposites, and release studies. *Compr. Rev. Food Sci. Food Saf.* **2010**, *9*, 552–571.

[238] Gill, S. C.; von Hippel, P. H. Calculation of protein extinction coefficients from amino acid sequence data. *Anal. Biochem.* **1989**, *182*, 319–326.

[239] Suelter, C. H.; DeLuca, M. How to prevent losses of protein by adsorption to glass and plastic. *Anal. Biochem.* **1983**, *135*, 112–119.

[240] Kelly, J. M.; Martin, D. R.; Byrne, M. E. Polyethylene glycol-b-Poly(lactic acid) Polymersomes as Vehicles for Enzyme Replacement Therapy. *Nanomedicine*

Nanotechnology, Biol. Med. **2017**, *Submitted*.

[241] Saudubray, J. M.; Nassogne, M. C.; De Lonlay, P.; Touati, G. Clinical approach to inherited metabolic disorders in neonates: An overview. *Semin. Neonatol.* **2002**, *7*, 3–15.

[242] Neufeld, E. Lysosomal storage diseases. *Annu. Rev. Biochem.* **1991**, *60*, 257–280.

[243] Kelly, J. M.; Bradbury, A.; Martin, D. R.; Byrne, M. E. Emerging Therapies for Neuropathic Lysosomal Storage Disorders. *Prog. Neurobiol.* **2016**.

[244] Salvalaio, M.; Rigon, L.; Belletti, D.; D'Avanzo, F.; Pederzoli, F.; Ruozi, B.; Marin, O.; Vandelli, M. A.; Forni, F.; Scarpa, M.; Tomanin, R.; Tosi, G. Targeted Polymeric Nanoparticles for Brain Delivery of High Molecular Weight Molecules in Lysosomal Storage Disorders. *PLoS One* **2016**, *11*, e0156452.

[245] Vila, A.; Sánchez, A.; Évora, C.; Soriano, I.; McCallion, O.; Alonso, M. J. PLA-PEG particles as nasal protein carriers: The influence of the particle size. *Int. J. Pharm.* **2005**, *292*, 43–52.

[246] Vila, A.; Sánchez, A.; Tobío, M.; Calvo, P.; Alonso, M. J. Design of biodegradable particles for protein delivery. *J. Control. Release* **2002**, *78*, 15–24.

[247] Zhao, H.; Lin, Z. Y.; Yildirimer, L.; Dhinakar, A.; Zhao, X.; Wu, J. Polymer-based nanoparticles for protein delivery: design, strategies and applications. *J. Mater. Chem. B* **2016**, *4*, 4060–4071.

[248] Kan, S. -h.; Aoyagi-Scharber, M.; Le, S. Q.; Vincelette, J.; Ohmi, K.; Bullens, S.; Wendt, D. J.; Christianson, T. M.; Tiger, P. M. N.; Brown, J. R.; Lawrence, R.; Yip, B. K.; Holtzinger, J.; Bagri, a.; Crippen-Harmon, D.; Vondrak, K. N.; Chen, Z.; Hague, C. M.; Woloszynek, J. C.; Cheung, D. S.; Webster, K. a.; Adintori, E. G.; Lo, M. J.; Wong, W.; Fitzpatrick, P. a.; LeBowitz, J. H.; Crawford, B. E.; Bunting, S.; Dickson, P. I.; Neufeld, E. F. Delivery of an enzyme-IGFII fusion protein to the mouse brain is therapeutic for mucopolysaccharidosis type IIIB. *Proc. Natl. Acad. Sci.* **2014**, 1–6.

[249] Spencer, B. J.; Verma, I. M. Targeted delivery of proteins across the blood-brain barrier. *Proc. Natl. Acad. Sci. U. S. A.* **2007**, *104*, 7594–9.

[250] Cohen, F. E.; Kelly, J. W. Therapeutic approaches to protein-misfolding diseases. *Nature* **2003**, *426*, 905–9.

[251] Balasubramanian, V.; Herranz-Blanco, B.; Almeida, P. V.; Hirvonen, J.; Santos, H. A. Multifaceted Polymersome Platforms: Spanning from Self-assembly To Drug Delivery and Protocells. *Prog. Polym. Sci.* **2016**.

[252] Schöttler, S.; Becker, G.; Winzen, S.; Steinbach, T.; Mohr, K.; Landfester, K.; Mailänder, V.; Wurm, F. R. Protein adsorption is required for stealth effect of

poly(ethylene glycol)- and poly(phosphoester)-coated nanocarriers. *Nat. Nanotechnol.* **2016**.

[253] Photos, P. J.; Bacakova, L.; Discher, B.; Bates, F. S.; Discher, D. E. Polymer vesicles in vivo: Correlations with PEG molecular weight. *J. Control. Release* **2003**, *90*, 323–334.

[254] U.S. Department of Health and Human Services Drugs @ FDA: FDA Approved Drug Products. http://www.accessdata.fda.gov/scripts/cder/drugsatfda/index.cfm (accessed July 28, 2016).

[255] Kelly, J. M.; Pearce, E. E.; Martin, D. R.; Byrne, M. E. Lyoprotectants modify and stabilize self-assembly of polymersomes. *Polym. (United Kingdom)* **2016**, *87*.

[256] Martin, D. R.; Cox, N. R.; Morrison, N. E.; Kennamer, D. M.; Peck, S. L.; Dodson, A. N.; Gentry, A. S.; Griffin, B.; Rolsma, M. D.; Baker, H. J. Mutation of the GM2 activator protein in a feline model of GM2 gangliosidosis. *Acta Neuropathol.* **2005**, *110*, 443–450.

[257] Discher, B. M.; Won, Y. Y.; Ege, D. S.; Lee, J. C.; Bates, F. S.; Discher, D. E.; Hammer, D. a Polymersomes: tough vesicles made from diblock copolymers. *Science* **1999**, *284*, 1143–6.

[258] Lu, W.; Zhang, Y.; Tan, Y. Z.; Hu, K. L.; Jiang, X. G.; Fu, S. K. Cationic albumin-conjugated pegylated nanoparticles as novel drug carrier for brain delivery. *J. Control. Release* **2005**, *107*, 428–448.

[259] Panyam, J.; Sahoo, S. K.; Prabha, S.; Bargar, T.; Labhasetwar, V. Fluorescence and electron microscopy probes for cellular and tissue uptake of poly(D,L-lactide-co-glycolide) nanoparticles. *Int. J. Pharm.* **2003**, *262*, 1–11.

[260] Ali, M.; Horikawa, S.; Venkatesh, S.; Saha, J.; Hong, J. W.; Byrne, M. E. Zero-order therapeutic release from imprinted hydrogel contact lenses within in vitro physiological ocular tear flow. *J. Control. Release* **2007**, *124*, 154–162.

[261] DiCioccio, R. A.; Barlow, J. J.; Matta, K. L. Purification of a beta-D-galactosidase from bovine liver by affinity chromatography. *Carbohydr. Res.* **1984**, *127*, 109–20.

[262] Hiraiwa, M.; Uda, Y. GM1 ganglioside beta-galactosidases from bovine liver. *Jpn. J. Exp. Med.* **1988**, *58*, 129–38.

[263] Atthoff, B.; Hilborn, J. Protein adsorption onto polyester surfaces: Is there a need for surface activation? *J. Biomed. Mater. Res. Part B Appl. Biomater.* **2007**, *80B*, 121–130.

[264] Popa, C.; Netea, M. G.; van Riel, P. L. C. M.; van der Meer, J. W. M.; Stalenhoef, A. F. H. The role of TNF-alpha in chronic inflammatory conditions, intermediary metabolism, and cardiovascular risk. *J. Lipid Res.* **2007**, *48*, 751–762.

[265] Stopeck, A. T.; Nicholson, A. C.; Mancini, F. P.; Hajjars, D. P. Cytokine Regulation of Low Density Lipoprotein Receptor. *J. Biol. Chem.* **1993**, *268*, 17489–94.

[266] Wang, D.; El-Amouri, S. S.; Dai, M.; Kuan, C.-Y.; Hui, D. Y.; Brady, R. O.; Pan, D. Engineering a lysosomal enzyme with a derivative of receptor-binding domain of apoE enables delivery across the blood-brain barrier. *Proc. Natl. Acad. Sci. U. S. A.* **2013**, *110*, 2999–3004.

[267] Lowry, O. H.; Rosebrough, N. J.; Farr, A. L.; Randall, R. J. Protein measurement with the Folin-Phenol Reagent. *J. Biol. Cemistry* **1951**, *193*, 265–275.

[268] Martin, D. R.; Cox, N. R.; Morrison, N. E.; Kennamer, D. M.; Peck, S. L.; Dodson, A. N.; Gentry, A. S.; Griffin, B.; Rolsma, M. D.; Baker, H. J. Mutation of the GM2 activator protein in a feline model of GM2 gangliosidosis. *Acta Neuropathol.* **2005**, *110*, 443–450.

[269] Martens, T. F.; Remaut, K.; Demeester, J.; De Smedt, S. C.; Braeckmans, K. Intracellular delivery of nanomaterials: How to catch endosomal escape in the act. *Nano Today* **2014**, *9*, 344–364.

[270] Rejman, J.; Oberle, V.; Zuhorn, I. S.; Hoekstra, D. Size-dependent internalization of particles via the pathways of clathrin- and caveolae-mediated endocytosis. *Biochem. J.* **2004**, *377*, 159–69.

[271] Mulik, R. S.; Monkkonen, J.; Juvonen, R. O.; Mahadik, K. R.; Paradkar, A. R. ApoE3 Mediated Poly(butyl) Cyanoacrylate Nanoparticles Containing Curcumin: Study of Enhanced Activity of Curcumin against Beta Amyloid Induced Cytotoxicity Using In Vitro Cell Culture Model. *Mol. Ph* **2010**, *7*, 815–825.

[272] Panyam, J.; Zhou, W.-Z.; Prabha, S.; Sahoo, S. K.; Labhasetwar, V. Rapid endo-lysosomal escape of poly(DL-lactide-co-glycolide) nanoparticles: implications for drug and gene delivery. *FASEB J.* **2002**, *16*, 1217–26.

[273] Biffi, A.; Montini, E.; Lorioli, L.; Cesani, M.; Fumagalli, F.; Plati, T.; Baldoli, C.; Martino, S.; Calabria, A.; Canale, S.; Benedicenti, F.; Vallanti, G.; Biasco, L.; Leo, S.; Kabbara, N.; Zanetti, G.; Rizzo, W. B.; Mehta, N. A.; Cicalese, M. P.; Casiraghi, M.; Boelens, J. J.; Del Carro, U.; Dow, D. J.; Schmidt, M.; Assanelli, A.; Neduva, V.; Di Serio, C.; Stupka, E.; Gardner, J.; von Kalle, C.; Bordignon, C.; Ciceri, F.; Rovelli, A.; Roncarolo, M. G.; Aiuti, A.; Sessa, M.; Naldini, L. Lentiviral Hematopoietic Stem Cell Gene Therapy Benefits Metachromatic Leukodystrophy. *Science (80-.).* **2013**, *341*, 1233158.

Appendix A: Additional Data and Figures

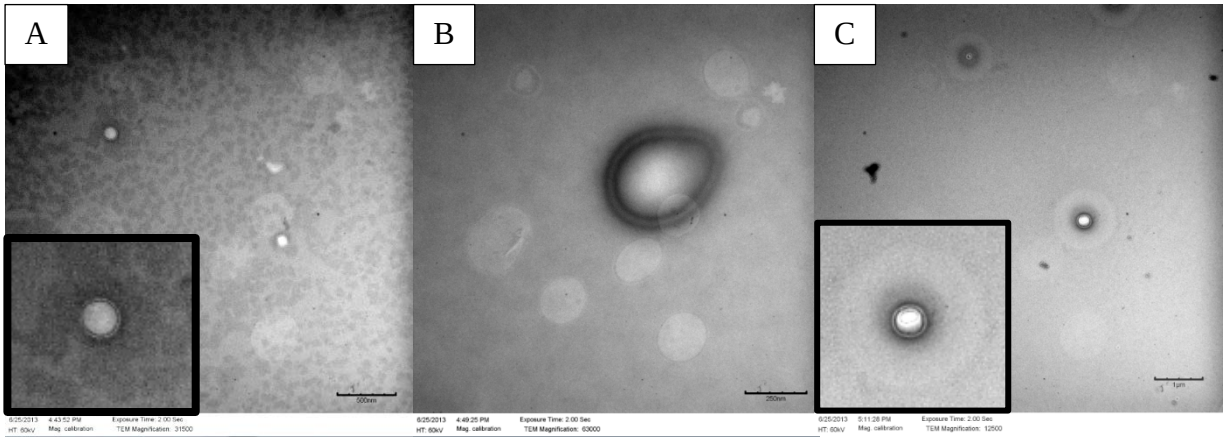

Figure A.1. Low density TEM images from polymersomes that were visualized after being cryogenically frozen prior to lyophilization (Procedure 3). *In Chapter 3, a representative high density image is presented. Here, low density images are presented where you can clearly see membrane integrity and minimal aggregation. Insets are zoomed in cropped images from the larger image. A has a scale bar of 500 nm, B has a scale bar of 250 nm, and C has a scale bar of 1 µm.*

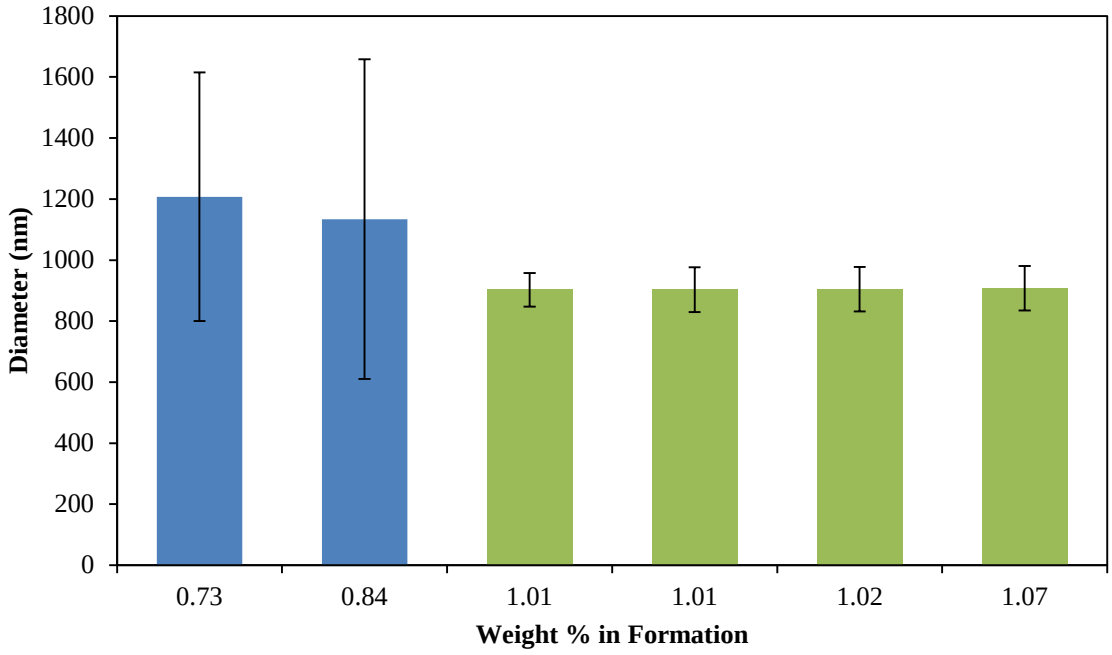

Figure A.25. Effect of concentration of co-Polymer in solution on particle size diameter. *Blue bars denote concentrations of less than one weight%, while green bars denote concentrations of greater than one weight%. Samples with less than one weight percent show statistically higher diameters (p value of 0.0434 from 1 tailed t-test) and an increased deviation denoting a wider spread of shapes.*

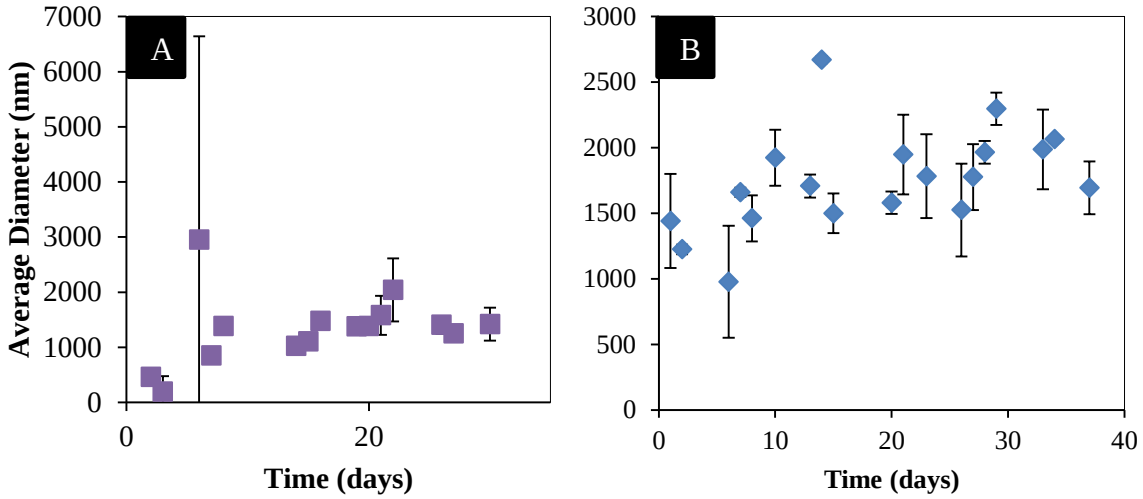

Figure A.3. Long –term PEG-b-PLA polymersome diameters with incorporation of 2 wt%/v Mannitol (A) and 2 wt%/v Inulin (B). *For chapter 4, initial studies were done analyzing the stability of particles with lyoprotectants in water over a one month period. The water with lyoprotectant and polymer was continually stirred throughout the study. In general, polymersomes maintain an average diameter after a period of 20 days. However, some variation was apparent. (A) PEG-b-PLA polymersomes formed with mannitol at an average diameter around 500 nm, which increases over 30 days to ~1300 nm, with around a 2x increase in size. (B) PEG-b-PLA polymersomes formed with inulin ar an average diameter around 1500 nm, which increases slightly to 1700 nm in diameter. The smallest PEG-b-PLA diameter was ~1000 nm at day 8.*

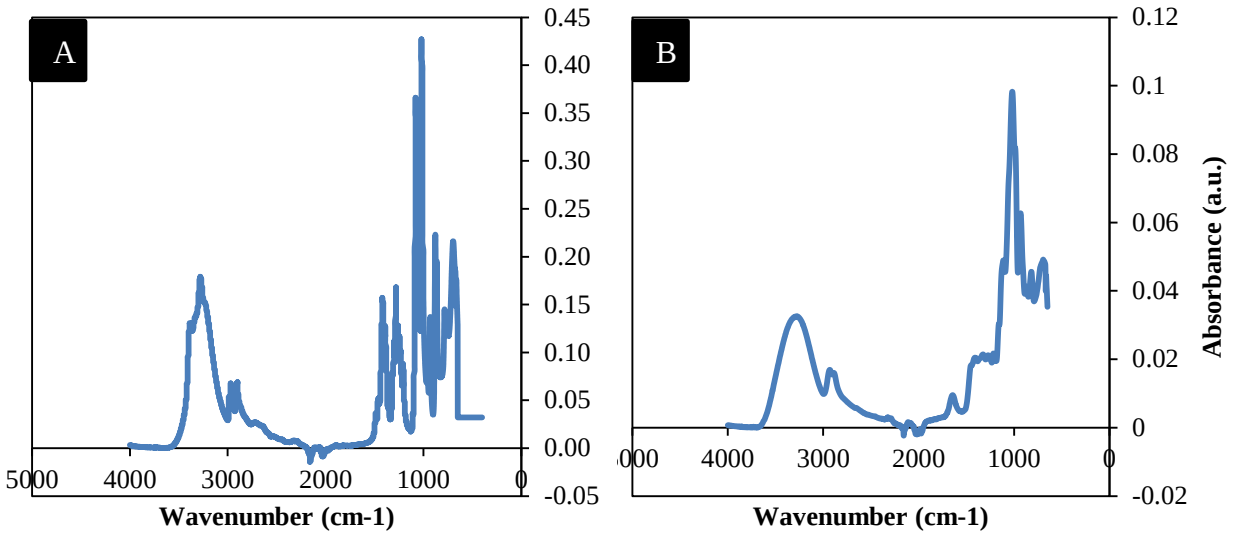

Figure A.4. Control Spectra for Mannitol (A) and Inulin (B). *(A) Mannitol presents with a large broad peak around 3300 cm^{-1}, which denotes O-H bonds. The cluster of peaks around 3000 – 2850 cm^{-1} denotes regular alkyl chain carbons. (B) Inulin presents with a broader peak than mannitol around 3300 cm^{-1},which denotes O-H bonds. The small weak peak between 2100 and 2200 cm^{-1} represents C-C triple bond and the peak at 1650 cm^{-1} denotes a C-C- double bond.*

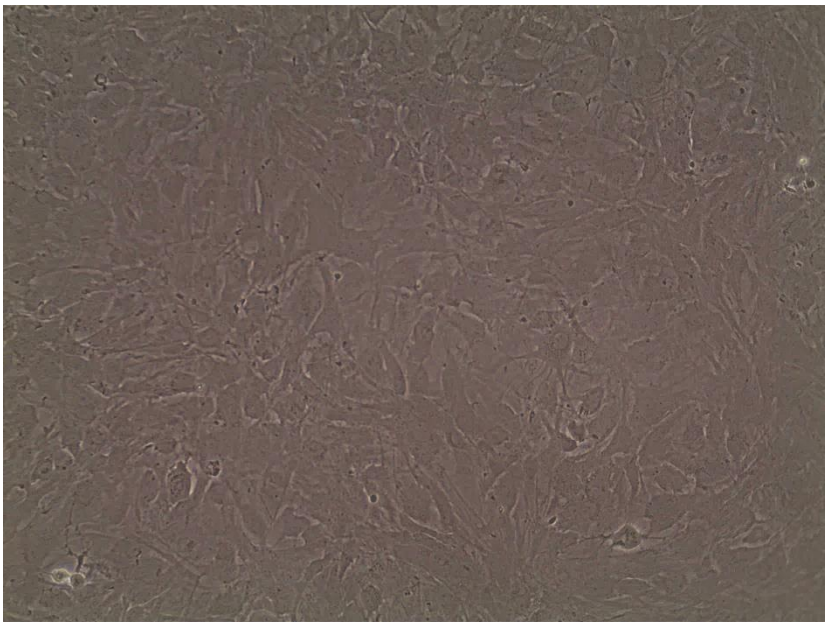

Figure A.56. Primary Rat Cortical Astrocytes at Passage 1. *An in vitro blood-brain barrier culture was attempted, which would involve the culture of primary rat cortical astrocytes on the bottom of a well plate and the culture of bovine brain endothelial cells on a transwell insert. Although rat cortical astrocytes were easily cultured, bovine brain endothelial cells never preseted with appropriate morphology, or reached confluency. Because of this, the in vitro blood-brain barrier project was discontinued.*

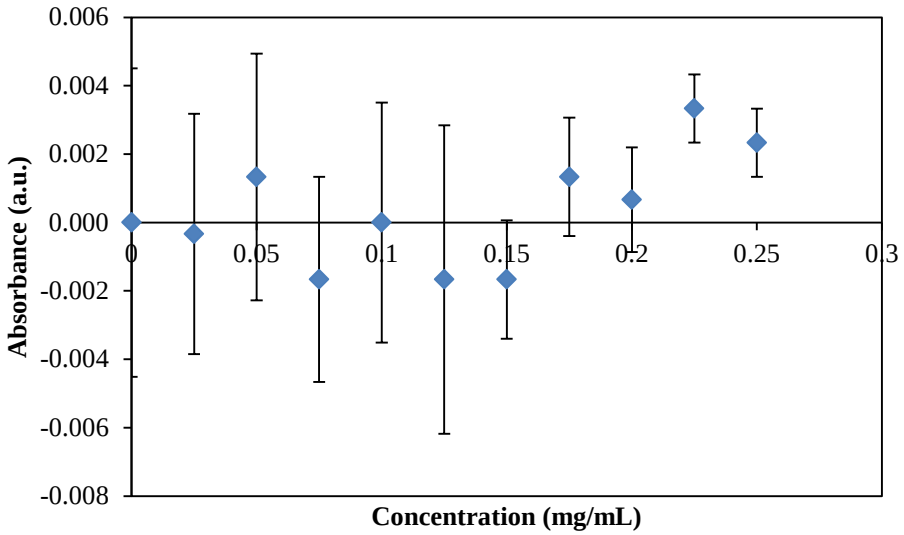

Figure A.6. PEG-Assay on PEG-b-PLA at various concentrations. *A PEG assay was performed using 2% $BaCl_2$ and 0.002 N iodine and comparing results to a calibration curve of PEG1000. As PEG-b-PLA degrades with in the PLA block, PEG alone was not available for binding in this colorimetric assay. Therefore, the assay was unsuccessful and discontinued.*

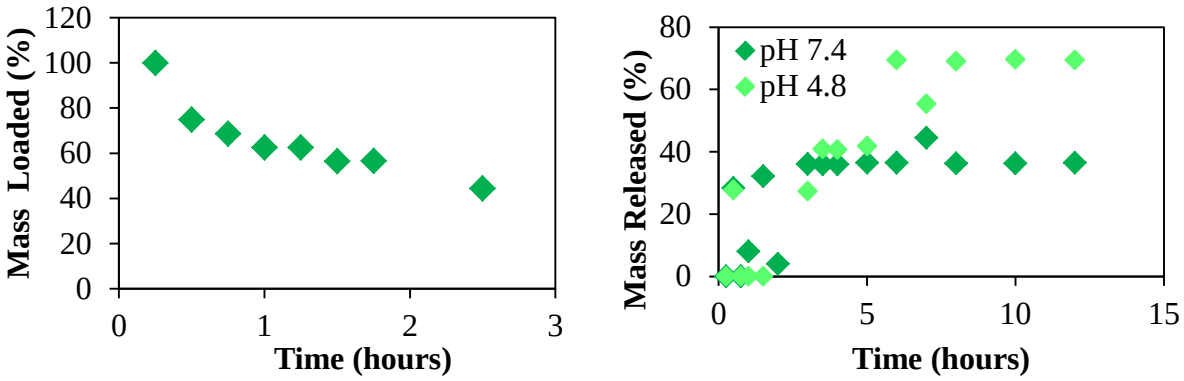

Figure A.7 . Loading (left) and Release (right) of AF488. *AF488 was loaded at a ~40% efficiency. Release of ~40% occurred in 0.1M tris buffer at pH 7.4 over a period of 12 hours. Release of ~70% occurred in 0.1M sodium acetate buffer at pH 4.8 over a period of 12 hours.*

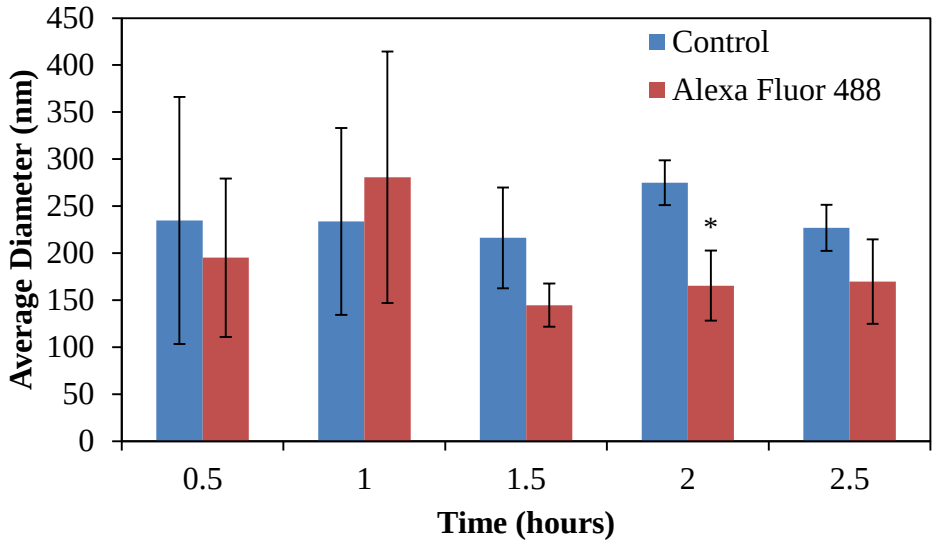

Figure A.8. Particle Size Distributions of PEG-b-PLA polymersomes loaded with AF488. *Hydrodynamic diameters of unloaded PEG-b-PLA polymersomes (blue) and AF488-loaded PEG-b-PLA polymersomes (red) are measured via dynamic light scattering. The addition of AF488 into the PEG-b-PLA polymersomes causes no increase in diameter over the 2.5-hour formation. At hour 2, AF488 loaded polymersomes are statistically smaller than unloaded polymersomes.*

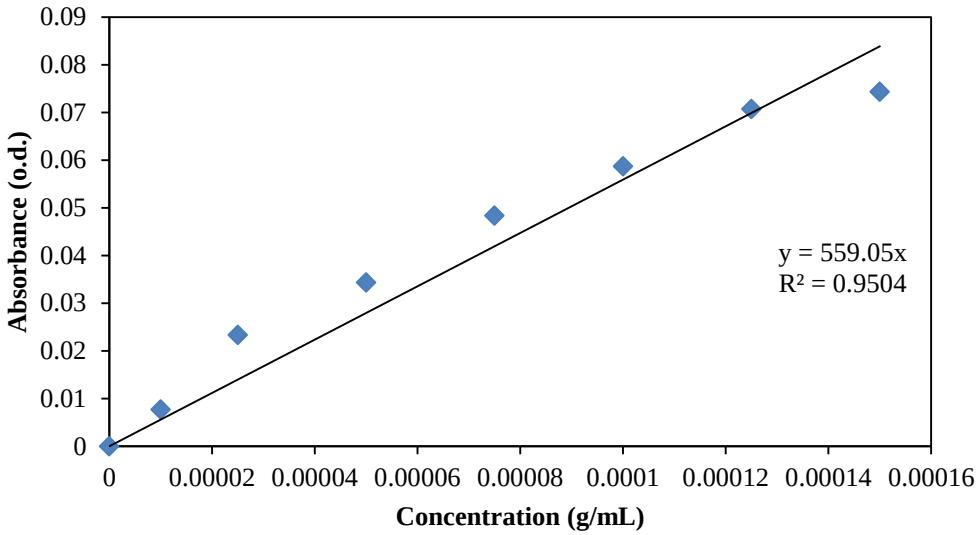

Figure A.9. Absorbance of NHS-PEG(2000)-NHS in Water at 200 nm. *Initially, ligand attachment was monitored by measuring NHS leaving groups after amide bond formation, which show an absorbance at 200 nm. NHS groups rapidly leave in water, which is easily visualized in the above curve, demonstrating increased absorbance (a.u.) with increased NHS-PEG(2000)-NHS concentration (g/mL).*

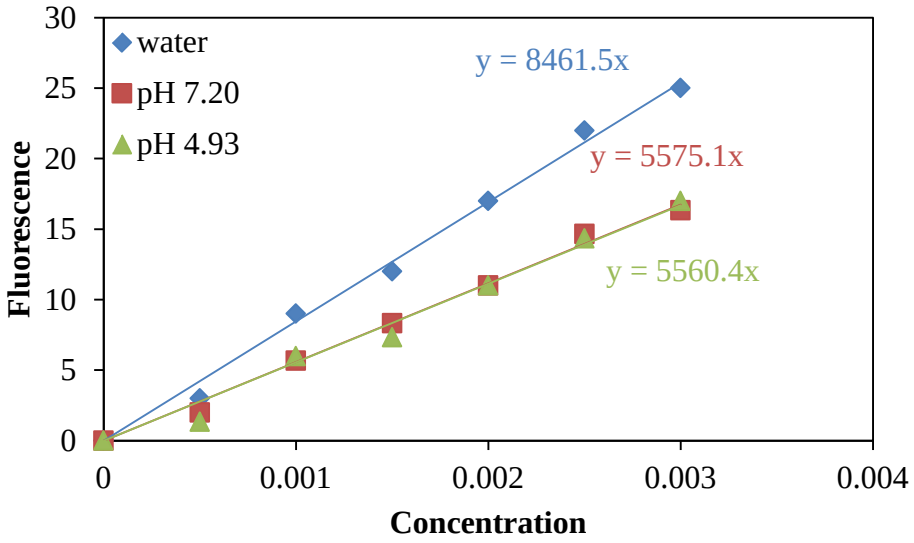

Figure A.10. Calibration Curve of AF488 under Various pH Conditions. *AF488 has different fluorescence under different pH conditions, as is shown by different calibration curves in water (blue), 0.1 M tris buffer at pH 7.2 (red), and 0.1 M acetate buffer at pH 4.93 (green).*

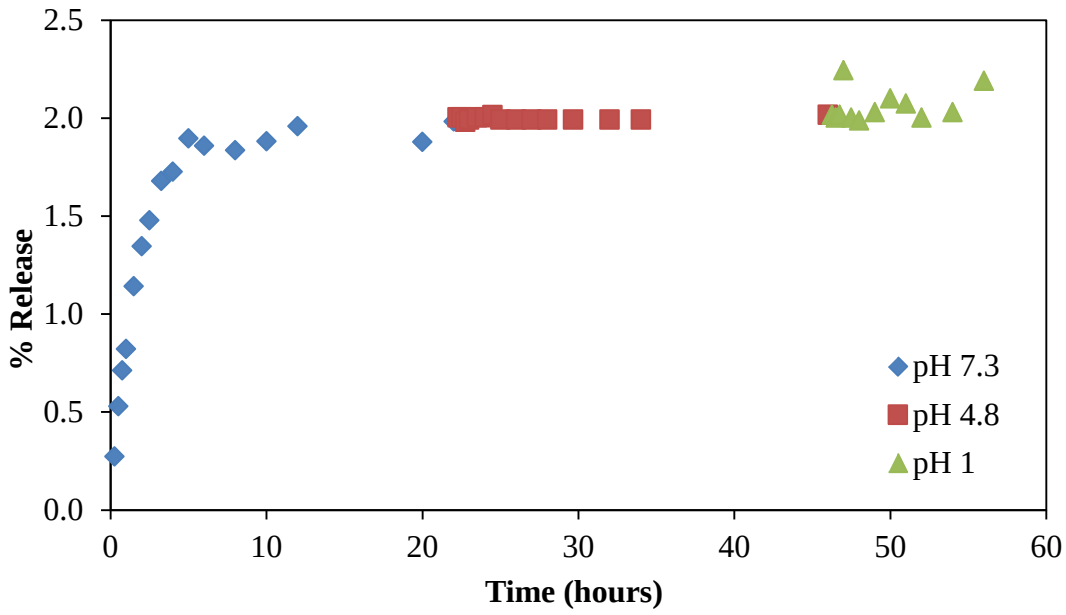

Figure A.11. Release of Acetaminophen from PEG-b-PLA Polymersomes. *After extensive difficulty calculating acetaminophen loading, release of acetaminophen was extremely limited under neutral pH, as expected. However, release under lysosomal, pH 4.8, conditions was also limited which was not expected. After seeing limited release in pH 4.8 over 24 hours, PEG-b-PLA polymersomes were inserted in pH 1to attempt to increase acetaminophen release. However, release continued to be stunted. Limited release measurements may be due to the difficulty associated with acetaminophen solubility and detection.*

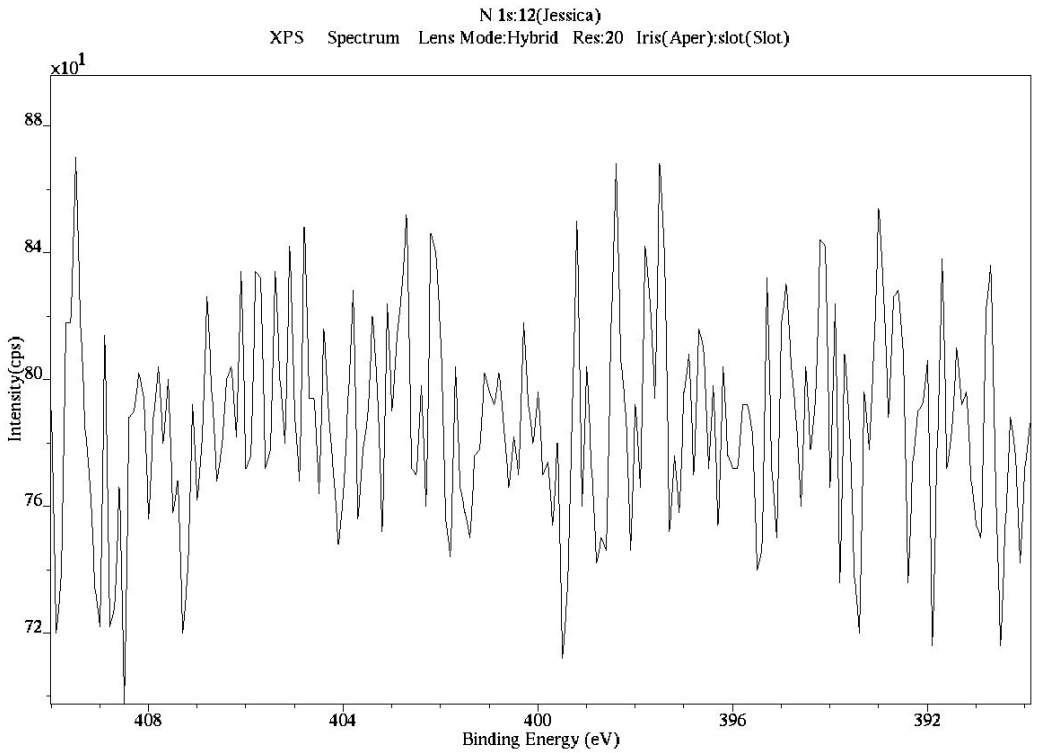

Figure A.12. Surface Analysis of Nitrogen Content in CF350-Tagged PEG-b-PLA polymersomes. *X-ray photoelectron spectroscopy (XPS) was attempted on lyophilized polymersomes after being attached to CF350 via NHS-PEG(2000)-NHS. Nitrogen analysis was done, since nitrogen was added to the system via amide bond. However, because the theoretical N:C ratio was only 1:50, the nitrogen peak could not be resolved and XPS was no longer attempted.*

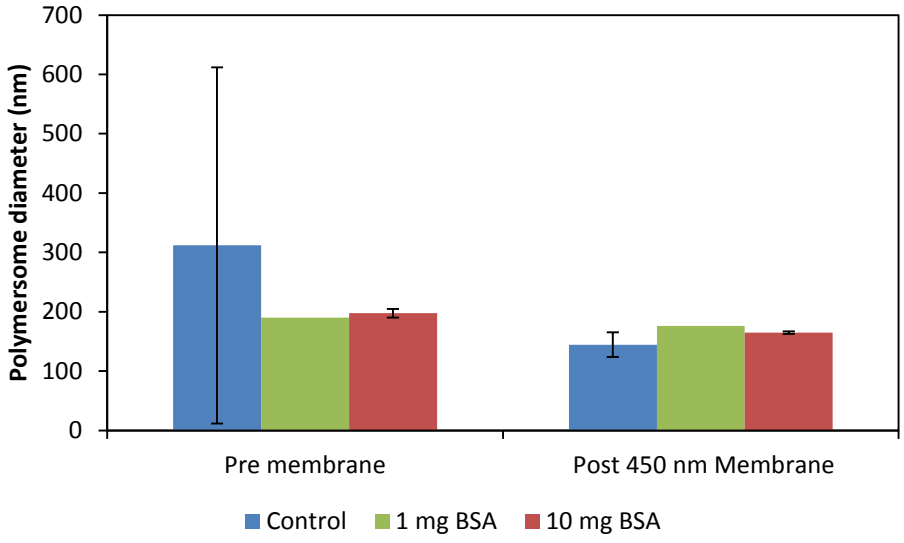

Figure A.13. Average Hydrodynamic Diameter of PEG-b-PLA Polymersomes Loaded with Bovine Serum Albumin. *PEG-b-PLA polymersomes were loaded with both 1 mg (green) and 10 mg (red) of BSA. The addition of BSA at both masses did not cause a statistical change in polymersome diameter.*

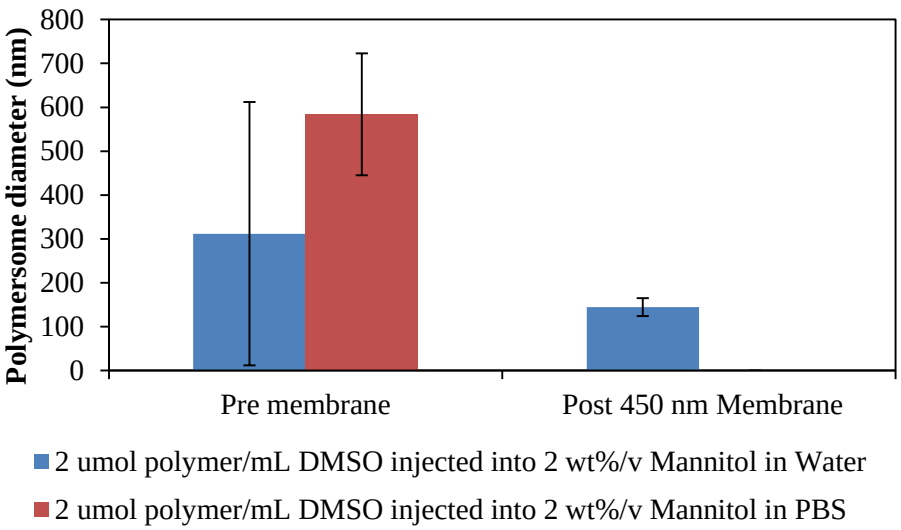

Figure A.14. Average Hydrodynamic Diameter of PEG-b-PLA Polymersomes formed in PBS. *PEG-b-PLA polymersomes formed in PBS (red) are not statistically larger than when formed in water (blue). However, they appear to be trending towards an increased size. Although this wasn't further explored in this dissertation work, this may be important to explore prior to moving towards clinically relevant treatments.*

Table A.1. Enzyme Activity of Loaded Polymersomes. *4MU enzyme assays were performed on polymersomes before and after loading. The most important data from this is the activity of βgal per milligram loaded at 651 ± 193. In all cases, βgal activity was maintained after encapsulation, meaning that PEG-b-PLA polymersomes are able to encapsulate an effective treatment for GM1 gangliosidosis.*

	Average
Loading Measured Via Enzyme Activity	106 ± 83 %
Initial βgal Activity	993 ± 1204 a.u.
Final βgal Activity	452 ± 81 a.u.
βgal Activity/mg Loaded	651 ± 193 a.u.

Figure A.15. X-Gal Staining on NSV3 (1-2) and GM1SV3 (3-4) Cells. *As a baseline, NSV3 and GM1SV3 cells were stained for βgal activity (blue) using X-gal. It is clear that NSV3, which are the normal feline fibroblasts, stain blue for βgal activity while GM1SV3, which are the GM1 gangliosidosis-derived feline fibroblasts, do not present with any blue color.*

Table A.2. Doses for Determination of Free Bgal Treatment Threshold. *Free βgal was added to both NSV3 and GM1SV3 cell lines at various doses, presented in the last column of the table. The lowest possible total volume of 380 µL was used for dosing in 24 well plates.*

Wells	Cells	mg bgal	vol stock (uL)	vol 1 mg/mL βgal in Media (uL)	Dose (mg/cm^2)
A1	NSV3	0	0	380	0
A2	NSV3	2	0	380	1.052631579
A3	NSV3	2.5	188	192	1.315789474
A4	NSV3	3	225	155	1.578947368
A5	NSV3	4	300	80	2.105263158
A6	NSV3	5	375	5	2.631578947
B1	GM1SV3	0	0	380	0
B2	GM1SV3	0	0	380	0
B3	GM1SV3	0	0	380	0
B4	GM1SV3	0	0	380	0
B5	GM1SV3	0	0	380	0
B6	GM1SV3	0	0	380	0
C1	GM1SV3	1.5	113	267	0.789473684
C2	GM1SV3	2	150	230	1.052631579
C3	GM1SV3	2.25	169	211	1.184210526
C4	GM1SV3	2.5	188	192	1.315789474
C5	GM1SV3	2.75	206	174	1.447368421
C6	GM1SV3	3	225	155	1.578947368
D1	GM1SV3	3.25	244	136	1.710526316
D2	GM1SV3	3.5	263	117	1.842105263
D3	GM1SV3	3.75	281	99	1.973684211
D4	GM1SV3	4	300	80	2.105263158
D5	GM1SV3	4.5	338	42	2.368421053
D6	GM1SV3	5	375	5	2.631578947

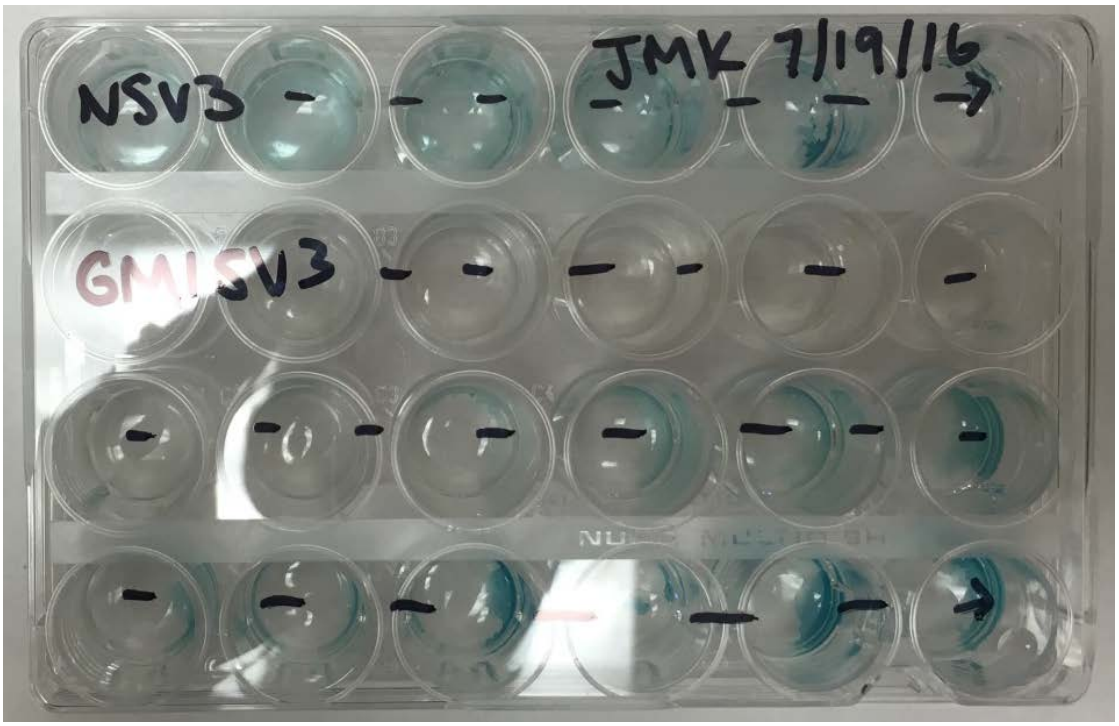

Figure A.16. X-Gal Staining after Free βgal Dosing. *X-gal staining was performed on both NSV3 and GM1SV3 cells after dosing via Table A.2. X-gal was capable of detecting βgal activity in NSV3 cells prior to any βgal dose (A1). However, it appears as if βgal activity increased with increasing dose from A1 to A6. GM1SV3 cells in Row 2 were not treated with free βgal and therefore do not have any blue color. Based on results, it appears as if free βgal treatment became effective at cell C3, which corresponded to a dose of approximately 1.18 mg/cm^2. Blue color continued to increase with increasing dose from cell C3 through D6.*

Table A.3. AF488 Labeling of βgal. *After AF488 labeling, measurements were taken via UV/Vis absorbance to determine protein content, degree of labeling, and labeling efficiency (n=9). AF488 decreased the activity of βgal to around 24 ± 13% of unlabeled βgal, as measured by a 4MU enzyme assay.*

	Average
Protein Content	0.42 ± 0.39 mg/mL
Degree of Labeling	23 ± 11 dye molecules/protein molecule
Labeling Efficiency	21 ± 19%
Activity Compared to Unlabeled Control	24 ± 13%